

# Variations on a theme of nuclear matter\*

V. R. Pandharipande and R. B. Wiringa†

Department of Physics, University of Illinois at Urbana-Champaign, Urbana, Illinois 61801

The authors review new techniques developed to apply the variational method to the nuclear matter problem. The variational wave function is taken to be  $(S\Pi_{i<j}F_{ij})\Phi$ ; the correlation operators  $F_{ij}$  can in principle induce central, backflow, spin isospin, tensor, etc. correlations, and  $\Phi$  is the ideal Fermi gas wave function. The application of diagrammatic cluster expansion and chain summation techniques to calculate expectation values with such wave functions is discussed in detail. The authors also give a brief overview of various other approaches to the calculation of the binding energies of quantum fluids, and a comparison of results for simple systems such as helium liquids. Results obtained by various methods for simplified models of nuclear matter, which include central, spin, isospin, and tensor forces, have converged significantly in recent months. Results obtained with more realistic models which include the spin-orbit potentials are also discussed. The potential models considered so far either give too little binding or too high equilibrium density.

## CONTENTS

Glossary of Symbols in Variational Calculations with Correlation Operators	821
I. Introduction	822
A. Properties of nuclear matter	822
B. Nucleon-nucleon potentials	822
C. The nuclear matter problem	824
II. Overview of Theoretical Methods	824
A. History of the many-body problem	824
B. Brueckner-Bethe-Goldstone expansion	824
C. Jastrow theory	825
D. Green's function Monte Carlo method	825
E. Correlated basis perturbation theory	826
F. Correlation operator method	826
G. Comparison of results for simple systems	827
III. Calculation of $F$	829
IV. Diagrammatic Cluster Expansion	831
A. Expectation values and diagram rules	831
B. Cluster expansion	833
C. Examples of diagrams	834
D. Other cluster expansions	835
V. Calculation of $C$ Parts	835
A. Operator diagrams	835
B. Single-operator rings	836
C. Multiple-operator diagrams	837
VI. FHNC/SOC Equations	840
A. Single and hypernetted chains in Bose systems	840
B. Modifications for Fermi systems	840
C. Operator chains	841
VII. Calculation of Energy	844
A. Calculation of $W$	844
B. Calculation of $U$	847
C. Calculation of $W_F + U_F$	848
VIII. Further Variations of the Theme	848
A. Hypernetted operator chain equations	848
B. Calculations with independent-pair wave function	849
IX. Results	850
A. Neutron matter model $v_3$	850
B. Nuclear matter $v_6$ model	851
C. Convergence of FHNC/SOC calculations	852
D. The $v_8$ problem	854
X. Outlook	855
A. Variational method	856
B. Brueckner-Bethe-Goldstone expansion	857
C. The nuclear Hamiltonian	857

## Acknowledgments

858

## References

858

## GLOSSARY OF SYMBOLS IN VARIATIONAL CALCULATIONS WITH CORRELATION OPERATORS

$A^p$	Matrix defined by Eq. (5.1).
$[Aa], [\bar{A}][a]$	Notation for separable diagrams.
$D^{pq}$	Matrix defined by Eq. (5.22).
$F_{ij}, F_{ij}^{H(N)}$	The correlation operator for pair $ij$ ; superscripts $H$ and $N$ denote the specific forms used in liquid helium [Eq. (2.20)] and nuclear matter [Eq. (2.24)] calculations.
$F_{ij}^p$	Functions used to expand $(\Pi F_{ij}^2)$ [Eq. (4.2)]; the superscript $p$ denotes the associated operator.
$f_J, f_{JO}$	Jastrow and optimized Jastrow correlation functions.
$f_{ij}^p$	Correlation function associated with operator $O_{ij}^p$ .
$f_{T,S}, f_{t,T}$ and $f_{\delta,T}$	Correlations in two-body channels having isospin $T$ and spin $S$ .
$G_{xy,ij}^p$	Chain function associated with operator $O_{ij}^p$ . The subscripts $x$ and $y$ denote the nature of vertices $i$ and $j$ at the ends of the chains.
$g_{ij}$	Two-particle distribution function.
$H_{ij}^p$	Part of the Hamiltonian associated with $O_{ij}^p$ .
$J^p(x_y, x_z, x_q)$	Single operator ring integrals [Eqs. (6.29)–(6.33)].
$K^{par}$	Matrix defined by Eq. (5.2).
$L^{par}$	Matrix defined by Eq. (5.15).
$L(r)$	Generalized Slater function.
$M(t_p, x_t, x_y)$ or $M_x^p$	Vertex correction factors [Eq. (6.28)].
$m(x_t, x_y, x_z, x_q)$	Probability factors (Sec. V.C).
$O_{ij}^p$	Operator labeled by superscript $p$ .
$T_F$	Fermi gas kinetic energy [Eq. (7.1)].
$U, U_F$	Parts of "three-body" kinetic energy [Eq. (7.1)].

\*Supported by NSF PHYS 76-22147

†Current address: Los Alamos Scientific Laboratory, Los Alamos, New Mexico 87545.

$v_{ij}^p$	Part of the two-body potential associated with $O_{ij}^p$ .
$v_{T,S}, v_{t,T}$ and $v_{b,T}$	Potentials in two-body channels with isospin $T$ and spin $S$ .
$W, W_o, W_c, W_s,$ $W_{cs}$ and $W_F$	Parts of "two-body" interaction energy.
$X_{xy,ij}^p$	Link functions associated with $O_{ij}^p$ ; $x$ and $y$ denote the type of vertices $i$ and $j$ .
$\alpha(A, B)$	Generalizations of the tensor operator [Eq. (9.1)].
$\beta(A)$	Generalizations of the $L \cdot S$ operator [Eq. (9.2)].
$\Delta^p$	Matrix whose $p=1-4$ elements equal unity and the rest are zero.
$\eta_{ij}$	Backflow correlation function [Eq. (2.20)].
$\theta_{ijk}^{par}$	Integral operator in the chain equations.
$\xi_{ijk}^{par}$	Angle functions in the coupling of $O_{ij}^p$ and $O_{jk}^q$ [Eq. (5.5)].
$\Phi$	Uncorrelated wave function.
$\Psi_{IP}, \Psi_J$ and $\Psi_{SP}$	Variational wave functions of the independent pair [Eq. (2.26)], Jastrow [Eq. (2.6)], and symmetrized product [Eq. (2.19)] form.

## I. INTRODUCTION

Nuclear matter is a hypothetical system of nucleons interacting without Coulomb forces. It is translationally invariant with a fixed ratio of protons and neutrons, and can be thought of as an idealization of matter inside a large nucleus. The goal of nuclear matter theory is to obtain empirically known bulk properties, such as the binding energy, equilibrium density, symmetry energy, incompressibility, etc., starting from the underlying two-body interactions.

A good many-body theory for nuclear matter may be used to study the details of nucleon-nucleon interactions. The observed phase shifts from scattering experiments plus the properties of the only bound two-nucleon system, the deuteron, are insufficient to pick out a unique nucleon-nucleon potential. Nuclear matter studies can help us understand better exactly how the different elements of a potential affect the matter properties, and what sorts of features are required to produce the observed saturation. It is also conceivable that a potential model for nuclear forces is simply not workable; nuclear matter studies may indicate whether or not this is true.

A solution of the infinite matter problem would also be useful as the starting point for a microscopic theory of finite nuclei. It is the first step in obtaining the equation of state for dense matter, which is essential in the study of neutron stars. Finally it is simply a very interesting many-body problem in its own right. Methods developed for it should be useful in other dense quantum fluids such as liquid helium.

## A. Properties of nuclear matter

Symmetric nuclear matter is characterized by its binding energy and equilibrium density  $\rho_0$ . The binding energy is given by the volume term  $\alpha$  in the semi-empirical mass formula for nuclei:

$$M(A, Z) = NM_n + ZM_H - \frac{1}{c^2} \left[ \alpha A - \frac{\beta(N-Z)^2}{A} - \gamma A^{2/3} - \frac{3e^2 Z^2}{5r_0 A^{1/3}} \right. \\ \left. + \text{pairing term} + \text{shell corrections} + \dots \right]. \quad (1.1)$$

The original mass formula is due to von Weizsäcker (1935) and Bethe and Bacher (1936). Today there are many competing versions which add higher-order terms in the symmetry, surface, and Coulomb effects, and use different methods for calculating the shell corrections. Values for  $\alpha$ , the symmetry term  $\beta$ , the surface term  $\gamma$ , the unit radius  $r_0$  defined by

$$\frac{4}{3} \pi r_0^3 \rho = 1, \quad (1.2)$$

and other parameters are obtained by fitting over one thousand experimentally known nuclear masses, and the fission barriers for several dozen heavy nuclei. A collection of contemporary mass formulas by many different authors can be found in At. Data and Nucl. Data Tables 17 5-6, (1976). Typical values for  $\alpha$  are 15 to 16 MeV;  $r_0$  varies from 1.16 to 1.22 fm, corresponding to densities of 0.15 to 0.13 nucleons/fm<sup>3</sup> or a  $k_F$  between 1.31 and 1.25 fm<sup>-1</sup>. The values for  $\beta$  and  $\gamma$  are in the ranges 30-40 MeV and 20-21 MeV, respectively.

Also of interest is the incompressibility of nuclear matter,  $K$ ,

$$K = k_F^2 \frac{\partial(E/A)}{\partial k_F^2}, \quad (1.3)$$

which appears as a parameter in some of the more sophisticated mass formulas, but is not well determined by them; the values given range from 240 to 300 MeV, with large error bars. Recent experimental observations of an isoscalar breathing mode in nuclei by Youngblood *et al.* (1977, 1978) provide a better estimate of  $K$  than ever before. They have measured an  $E_{0^+}$  resonance in <sup>208</sup>Pb at 13.7 MeV, in <sup>144</sup>Sm at 15.1 MeV, and in <sup>90</sup>Zr at 17 MeV. This energy is related to the incompressibility of a finite nucleus  $k_A$  in the liquid drop model by

$$E_{0^+} = (\pi/3 r_0 A^{1/3}) \sqrt{(\hbar^2/m) k_A}. \quad (1.4)$$

If we insert the simple semiempirical mass formula (1.1) into Eq. (1.3), we get an expansion for  $k_A$ ,

$$k_A = K + K_\beta \left( \frac{N-Z}{A} \right)^2 + K_\gamma A^{-1/3} + \frac{6e^2 Z^2}{5r_0 A^{4/3}}, \quad (1.5)$$

where  $K_\beta$  and  $K_\gamma$  are symmetry and surface incompressibilities, respectively. A simple calculation indicates  $K \approx 260$  MeV,  $K_\beta \approx 3$  MeV, and  $K_\gamma \approx -405$  MeV. There is a question as to how valid the liquid drop model expression (1.4) is for extracting  $k_A$  from  $E_{0^+}$ . An RPA calculation by Blaizot *et al.* (1976) suggests that  $K \approx 210$  MeV will reproduce the observed data.

A good theory should be able to calculate the ground-state  $E(\rho)$  curve for any given potential. The occur-

rence of a minimum will indicate both the equilibrium density  $\rho_0$  and binding energy  $E(\rho_0)$ . The curvature of  $E(\rho)$  at  $\rho_0$  will give us  $K$ . To calculate  $\beta$ , we can allow the number of neutrons and protons to differ slightly and measure the curvature of  $E(N, Z)$  at the point  $N=Z$ . A somewhat more difficult problem is the calculation of  $\gamma$ , which would obviously require the introduction of a surface of some kind. Additional quantities of interest that might be obtained by functional differentiation of  $E(\rho)$  include the effective mass and Landau parameters. In principle we may deduce their values by analyzing the spectra of near closed-shell nuclei with the Landau-Migdal theory of finite Fermi systems (Speth *et al.*, 1977; Brown, 1971; Bäckman *et al.*, 1979).

## B. Nucleon-nucleon potentials

The starting point for any nuclear matter calculation is a two-body potential that models the nucleon-nucleon interaction. A more fundamental viewpoint would be a meson theory of nuclear forces (Brown and Jackson, 1976), or even a quark model for the strong interaction. The former has not been quantitatively successful, however, while the latter is still in its infancy. At present it is necessary to resort to phenomenological potentials that fit the experimental data, and incorporate elements that are consistent with our fundamental knowledge of strong interactions. The potentials used are generally nonrelativistic, and of course cannot take into account many-body forces, about which very little is known.

"Realistic" potentials are those that give good fits to the low-energy ( $\leq 300$  MeV) two-body scattering data, and get the binding energy and quadrupole moment of the deuteron correct. The phase-shift data varies greatly from channel to channel, indicating a very complicated potential. To fit the phase shifts in channels with  $J \leq 2$  a potential requires at least ten operator components:

$$\begin{aligned} v_{ij} = & v^c + v^s(\sigma_i \cdot \sigma_j) + v^t(\tau_i \cdot \tau_j) + v^{\sigma t}(\sigma_i \cdot \sigma_j)(\tau_i \cdot \tau_j) \\ & + v^t S_{ij} + v^t S_{ij}(\tau_i \cdot \tau_j) + v^b(\mathbf{L} \cdot \mathbf{S})_{ij} + v^{bt}(\mathbf{L} \cdot \mathbf{S})_{ij}(\tau_i \cdot \tau_j) \\ & + v^q L_{ij} + v^{qt} L_{ij}(\tau_i \cdot \tau_j), \end{aligned} \quad (1.6)$$

where  $S_{ij} = 3(\sigma_i \cdot \hat{r})(\sigma_j \cdot \hat{r}) - \sigma_i \cdot \sigma_j$  is the tensor operator,  $(\mathbf{L} \cdot \mathbf{S})_{ij}$  is the spin-orbit operator, and  $L_{ij} = (\sigma_i \cdot \sigma_j) \mathbf{L}^2 - \frac{1}{2}[(\sigma_i \cdot \mathbf{L})(\sigma_j \cdot \mathbf{L}) + (\sigma_j \cdot \mathbf{L})(\sigma_i \cdot \mathbf{L})]$  is the quadratic spin-orbit operator. The  $v^i$  are then simple functions of the radial distance  $|\mathbf{r}_i - \mathbf{r}_j|$ . Even greater operator dependence might be called for in (1.6) if the lesser studied phase shifts in  $J > 2$  channels were to be fitted.

All realistic nucleon-nucleon potentials exhibit some common features. These include a very strong repulsion at short distances, an intermediate-range attraction, and a long-range behavior that is well described by the one-pion exchange potential (OPEP):

$$v_\pi = \frac{1}{3} \frac{f^2}{\hbar c} m_\pi c^2 (\tau_i \cdot \tau_j) \left[ (\sigma_i \cdot \sigma_j) + S_{ij} \left( 1 + \frac{3}{\mu r} + \frac{3}{(\mu r)^2} \right) \right] \frac{e^{-\mu r}}{\mu r}. \quad (1.7)$$

Here  $\mu = m_\pi c / \hbar = 0.7 \text{ fm}^{-1}$  is the inverse Compton wavelength of the pion, and  $f^2 / \hbar c = 0.08$  is the coupling

strength in  $\pi N$  interactions. All  $NN$  potentials contain the OPEP but the treatment of the intermediate-range attraction, which is probably due to multiple  $\pi$  exchange, and the short-range repulsion, which comes from  $\omega$ - and  $\rho$ -meson exchange, is highly varied. One choice is a superposition of Yukawa forces:

$$(v - v_\pi)^i = \sum_n y_n^i \frac{e^{-n\mu r}}{\mu r}. \quad (1.8)$$

Here  $n$  may take on a series of integer values, as in the potential of Reid (1968) ( $n=2, 3, 4, 6, 7$ ), or it may have noninteger values to represent the actual  $\omega$ - $\rho$  range ( $n=5.5$ ), as in some of the models of Bethe and Johnson (1974). These soft-core potentials may be contrasted to the earlier hard-core potentials such as those of Hamada and Johnston (1962), which use Yukawa forces as in Eq. (1.8) at intermediate distances, but an infinite hard core at short distances, i.e.,  $v = +\infty$  for  $r < r_c$ ,  $r_c \approx 0.5$  fm. The hard core was originally used because of its simplicity, although it is not physically reasonable.

The  $v^p$  obtained from the Reid potentials in the singlet states  $^1S_0$  and  $^1P_1$ , and the triplet states  $^3S_1$ - $^3D_1$  and  $^3P_2$ - $^3F_2$ , are shown in Fig. 1. The strong operator dependence is quite evident, particularly the  $\mathbf{L} \cdot \mathbf{S}$  force at short distances and the pion part ( $\sigma\tau$  and  $t\tau$ ) at large distances. There are many other types of potentials that can be used to adequately explain the low-energy ( $< 300$  MeV) scattering data and deuteron properties, as reviewed by Bethe (1971). The onset of inelastic processes at higher energies makes it difficult to predict the correct potential behavior inside  $\approx 0.5$  fm.

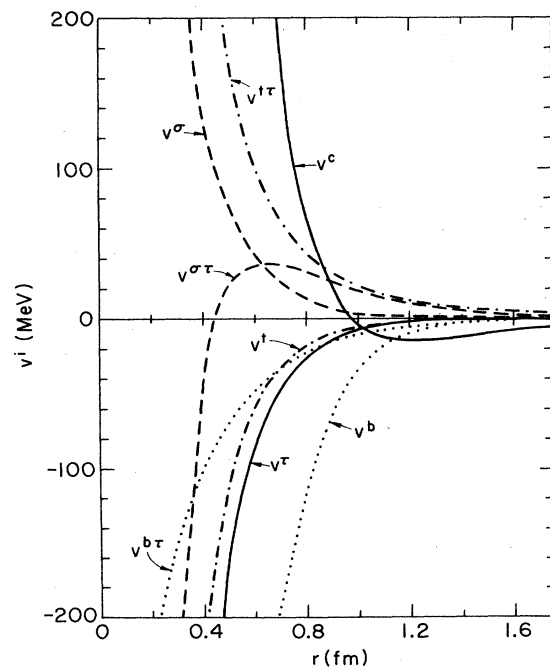


FIG. 1. The  $v^i(r)$  in models  $v_6$  and  $v_8$  based on the Reid potentials.

### C. Nuclear matter problem

The problem to be solved may be summarized as follows. A large box of volume  $\Omega$  contains  $A$  nucleons which interact via a two-body potential  $v_{ij}$ ,

$$H = \sum_i \left( \frac{-\hbar^2}{2m} \nabla_i^2 \right) + \sum_{i < j} v_{ij}. \quad (1.9)$$

We wish to calculate the ground-state energy  $AE(\rho)$  of this system in the limit  $A, \Omega \rightarrow \infty$ , while the density  $\rho = A/\Omega$  is kept constant. The minimum in the curve  $E(\rho)$  will give both the binding energy and equilibrium density for the given potential.

At present it is very difficult to do a good many-body calculation for the full operator-dependent potential (1.6). Bethe (1977) has suggested that the many-body theory could be developed in a series of steps by considering homework potentials that successively incorporate more and more sophistication. Starting from any full potential, one may define a sequence of homework potentials which have successively more of the operator dependences given in Eq. (1.6). At present it appears that the so-called  $v_6$  problem, which includes central, spin, isospin, and tensor forces, can be treated with reasonable accuracy. Some preliminary work on the  $v_6$  problem which incorporates spin-orbit forces is also available. It may not be profitable to calculate anything beyond the  $E(\rho)$  curve until many-body calculations can be done for a full realistic potential.

## II. OVERVIEW OF THEORETICAL METHODS

### A. History of the many-body problem

Just two years after the semiempirical mass formula was first suggested, the first nuclear matter calculations were performed by Euler (1937). Very little was known about the interaction of nucleons at that time, however, and only a nonsingular potential was studied. The modern studies began after the need for a strong repulsive core in the potential was realized. The specialized perturbation methods required were pioneered by Brueckner [Brueckner (1954), Brueckner and Levinson (1955)], Bethe (1956), and Goldstone (1957); this approach is called the BBG expansion. It is a low-density expansion, whose convergence properties are still not fully understood. It may be useful at nuclear matter density, but its application to denser quantum fluids like liquid helium or neutron star matter is thought to be very difficult.

At the same time the perturbation theory of Brueckner was first being formulated, Jastrow (1955) suggested an alternate variational approach for treating the strong repulsive core. Jastrow recommended the use of a trial wave function where the unperturbed wave function is modified by a product of two-body correlation functions. However, it was thought that the spin, isospin, tensor, etc., correlations would be difficult to handle in this way. The discovery of pulsars and their identification as neutron stars in 1968 revived the interest in the variational approach, because the method does not have the density limitations of the BBG expansion. The study of astronomical objects whose central densities could be several times that of nuclear matter

would clearly require the development of such an alternate approach.

Nuclear matter calculations in lowest-order versions of both the variational and BBG methods were in substantial agreement by 1972 (Pandharipande, 1972), but disturbingly no realistic potentials had been found that could explain the energy and density saturation; typical potentials either gave too little binding or too high a density (Day and Coester, 1976). More advanced variational studies by Bäckman *et al.* (1972) and Pandharipande *et al.* (1975) indicated a considerable discrepancy with the lowest-order results for some simple model potentials. It has since become clear that much more careful calculations are required, particularly for a weakly bound system like nuclear matter, where the kinetic and potential energies cancel to a large extent.

In the following pages we give a brief review of the approaches being actively pursued at present. Whether the previous failure to achieve the correct matter properties is attributable solely to the inadequacy of the many-body theory is not yet clear. In the future when the various theories are developed to a point where we have confidence in them, we must still examine the question of whether a satisfactory nucleon-nucleon potential can be found. At present we can only speculate on that subject.

### B. Brueckner-Bethe-Goldstone expansion

The BBG theory has been reviewed by Day (1967, 1978a) and Bethe (1971). It is based on the Goldstone (1957) linked-cluster expansion for the ground state  $E(\rho)$ . The Hamiltonian is broken into two parts,  $H_0$  and  $H_1$ :

$$H_0 = \sum_i \left[ \frac{-\hbar^2}{2m} \nabla_i^2 + U(k_i) \right],$$

$$H_1 = \sum_{i < j} v_{ij} - \sum_i U(k_i). \quad (2.1)$$

Here the single-particle potential  $U$  is introduced for ease of calculation; it is chosen so that the perturbation expansion for  $H_1$  is rapidly convergent. The singular matrix elements of  $v$  are replaced by the reaction matrix  $G$ ,

$$G = v - v(Q/e)G, \quad (2.2)$$

where  $Q$  is the Pauli operator and  $e$  is an energy denominator. The nonsingular  $G$  sums the interaction between two particles to all orders. It is obtained by calculating the perturbed wave function  $\Psi$  from the ideal gas wave function  $\Phi$ ,

$$\Psi = \Phi - (Q/e)v\Psi, \quad (2.3)$$

which implies

$$v\Psi = G\Phi. \quad (2.4)$$

A perturbation expansion in powers of  $G$  is not convergent, but the cluster diagrams can be grouped instead according to the number of independent hole lines. Formal arguments for the convergence of the hole-line expansion have been advanced by Brandow

(1966) which indicate an  $n$ -hole-line diagram should be proportional to  $\kappa^{n-1}$ , where  $\kappa$  measures the probability that there is an unoccupied state below the Fermi surface. If we neglect many-body clusters,  $\kappa$  is given by

$$\kappa \approx \rho \int |\phi - \psi|^2 d\tau, \quad (2.5)$$

where  $\psi$  and  $\phi$  are two-body correlated and uncorrelated wave functions. This estimate of  $\kappa$ , however, depends critically on the choice of  $U$ , a topic of much discussion in the recent literature. The standard choice in the past has been to set  $U$  to zero for particle states, and to the self-consistent Hartree-Fock potential in hole states. For this choice and the Reid potential,  $\kappa \approx 0.15$  near the saturation density. However, the standard choice has an unphysical gap at the Fermi surface, and several recent calculations use what is called the "continuous choice" advocated by Jeukenne *et al.* (1975).

The hole-line expansion seems to be valid, i.e., obeys the  $\kappa^{n-1}$  prescription, for the short-range correlations induced by the strong repulsive core. A number of internal checks have been performed by Day (1978a) without any inconsistencies being found. However, Friman and Nyman (1978) point out that the pion exchange ring diagrams may need to be summed to all orders. Recent three-body cluster calculations of Day go up to twice nuclear matter density. Even at these densities, which are below those expected for neutron star interiors, the necessity of calculating through at least four-body clusters to get within 10% of the binding energy is indicated. This is a very difficult task, which has not yet been accomplished.

### C. Jastrow theory

The variational wave function in Jastrow theory,  $\Psi_J$ , is taken as

$$\Psi_J = \prod_{i < j} f_{ij}(r_{ij}) \Phi. \quad (2.6)$$

Jastrow (1955) anticipated that the two-body correlation  $f_{ij}$  could be an operator in general, but for our nomenclature we shall use it to designate the case of simple radial dependence,  $r_{ij} = |\mathbf{r}_i - \mathbf{r}_j|$ . The  $f_{ij}$  is usually parametrized in some form, and the parameters are varied so as to minimize the variational energy  $E_J$ ,

$$E_J = \frac{\langle \Psi_J | H | \Psi_J \rangle}{\langle \Psi_J | \Psi_J \rangle}, \quad (2.7)$$

which should give an upper bound for  $E(\rho)$ .

The  $E_J$  can be evaluated exactly with a Monte Carlo integration, or approximately by means of cluster expansions. The most popular expansion uses the method of hypernetted chains (HNC), which is based on the Mayer cluster expansion of statistical mechanics. This chain summation method was developed by van Leeuwen, Groeneveld, and de Boer (1959) for Bose systems, and extended to Fermi systems (FHNC) by Fantoni and Rosati (1975). There is a hierarchy of approximations in the method, the simplest being called (F)HNC, followed by (F)HNC/4, (F)HNC/5, etc. HNC calculations in a wide variety of simple Bose systems by Pandharipande and Schmidt (1977) and simple Fermi systems by Zabolitzky (1977) show excellent agreement

with the exact Monte Carlo integrations.

Calculations designed to solve the variational problem  $\partial E_J / \partial f_{ij} = 0$  exactly are called optimized Jastrow calculations. The optimum correlation  $f_{JO}$  has a long-range tail, i.e.,  $[f_{JO}(r) - 1] \propto r^{-2}$  as  $r \rightarrow \infty$ , for which the energy calculation is very difficult (Smith *et al.*, 1978). Lantto and Siemens (1977, 1979) have devised a method of minimizing the (F)HNC energy to obtain  $f_{JO}$ , but the long tail  $f_{JO}$  does not seem to lower the energy significantly.

The basic shortcomings of the choice of Eq. (2.6) for  $\Psi_J$  are that it does not allow for momentum dependence appropriate to interacting systems, or the complicated operator dependence indicated by the nucleon-nucleon potential (1.6). Nor does it allow for three-body or higher correlations. The simple Jastrow studies have been useful, however, as a starting point for the more sophisticated methods we describe below.

### D. Green's function Monte Carlo method

The GFMC method developed by Kalos *et al.* (Kalos, 1970; Kalos *et al.*, 1974) and reviewed by Ceperley and Kalos (1978) gives an exact solution for the energy of an  $A$ -body system in a box of volume  $\Omega$ . It has not been extended to nuclear matter or even to Fermi systems at present, but it is useful as a standard of comparison in Bose systems, and requires a good solution for the Jastrow  $\Psi_J$  as input.

Let  $\mathbf{R}$  denote a multidimensional vector representing the coordinates  $\mathbf{r}_1, \mathbf{r}_2, \dots, \mathbf{r}_A$  of the  $A$  particles. The Schrödinger equation for the ground-state energy  $E_0$  is

$$H\Psi_0(\mathbf{R}) = E_0\Psi_0(\mathbf{R}). \quad (2.8)$$

Let  $\Psi_n$  denote the  $n$ th eigenstate corresponding to  $E_n$ , and  $G(\mathbf{R}, \mathbf{R}')$  be the Green's function

$$G(\mathbf{R}, \mathbf{R}') = \sum_n \frac{|\Psi_n(\mathbf{R})\rangle \langle \Psi_n(\mathbf{R}')|}{E_n}. \quad (2.9)$$

An initial guess for  $\Psi_0$  is labeled  $\Psi(0, \mathbf{R})$ ; the  $\Psi_J$  is used here. A series of successive improved guesses  $\Psi(i, \mathbf{R})$  is calculated by iterating the equation

$$\Psi(i+1, \mathbf{R}) = E(i) \int G(\mathbf{R}, \mathbf{R}') \Psi(i, \mathbf{R}') d^3\mathbf{R}', \quad (2.10)$$

where  $E(i)$  is a normalization constant for  $\Psi(i+1, \mathbf{R})$ , and all the  $\Psi(i, \mathbf{R})$  are assumed to be normalized. In the limit  $i \rightarrow \infty$ ,

$$\Psi(i \rightarrow \infty, \mathbf{R}) = \Psi_0(\mathbf{R}), \quad (2.11)$$

$$E(i \rightarrow \infty) = E_0. \quad (2.12)$$

The  $G(\mathbf{R}, \mathbf{R}')$  is actually not known, and it is not practical to solve Eq. (2.10) directly. However, one can again use the  $\Psi_J$  from the Jastrow problem to define a  $\tilde{\Psi}$ ,

$$\Psi(i, \mathbf{R}) = \tilde{\Psi}(i, \mathbf{R}) \Psi_J^{-1}(\mathbf{R}), \quad (2.13)$$

and corresponding Green's function  $\tilde{G}$ ,

$$\tilde{G}(\mathbf{R}, \mathbf{R}') = \Psi_J(\mathbf{R}) G(\mathbf{R}, \mathbf{R}') \Psi_J^{-1}(\mathbf{R}'). \quad (2.14)$$

so that Eq. (2.10) becomes

$$\tilde{\Psi}(i+1, \mathbf{R}) = E(i) \int \tilde{G}(\mathbf{R}, \mathbf{R}') \tilde{\Psi}(i, \mathbf{R}') d^3\mathbf{R}'. \quad (2.15)$$

The  $\tilde{G}(\mathbf{R}, \mathbf{R}')$  is still not known, but it can be sampled in a Monte Carlo fashion, and very accurate energies are obtained after about forty iterations of Eq. (2.15). The practical necessity of using  $\tilde{\Psi}, \tilde{G}$  is where the limitation to Bose systems comes in. Whereas  $\Psi_J$  will always be positive definite in a Bose system, it can have nodes in a Fermi system causing  $\Psi_J^{-1}$  in Eqs. (2.13) and (2.14) to blow up. Whether or not this difficulty can be overcome in the future is not clear.

### E. Correlated basis perturbation theory

A perturbation theory has been developed by Feenberg (1969) and collaborators [see the recent review by Clark (1978)] that gives a prescription for improving on the Jastrow  $E_J$ . If  $\mathcal{G}$  is a suitable many-body correlation operator and  $|\Phi_m\rangle$  is the complete set of ideal gas states, then the set  $|\Psi_m\rangle$ ,

$$|\Psi_m\rangle = \mathcal{G} |\Phi_m\rangle \langle \Phi_m | \mathcal{G}^\dagger \mathcal{G} |\Phi_m\rangle^{-1/2}, \quad (2.16)$$

is a normalized, complete, but nonorthogonal set of "correlated basis functions." A formal perturbation expansion can be made for the exact ground-state energy  $E$ , which to second order is given by

$$E = \langle \Psi_0 | H | \Psi_0 \rangle - \sum_{m \neq 0} \frac{|\langle \Psi_m | H | \Psi_0 \rangle - \langle \Psi_0 | H | \Psi_m \rangle \langle \Psi_m | \Psi_0 \rangle|^2}{\langle \Psi_m | H | \Psi_m \rangle - \langle \Psi_0 | H | \Psi_0 \rangle}. \quad (2.17)$$

Here the subtracted part in the numerator of the second term corrects for the nonorthogonality of  $|\Psi_m\rangle$ . If  $\mathcal{G}$  is just the usual Jastrow choice (2.6) then  $\langle \Psi_0 | H | \Psi_0 \rangle = E_J$ . We also see that the second-order perturbation correction in Eq. (2.17) always lowers the energy below the variational result.

The disadvantage of this treatment is that its convergence is difficult to establish; no third-order perturbation terms have ever been calculated, and the second-order terms must be approximated at a small-cluster level. The most extensive calculations to date have been done on the Bose liquid  $^4\text{He}$  by Chang and Campbell (1977) where the only  $\Psi_m$  used are

$$\Psi_0 = \Psi(0) = N(0) \prod_{i < j} f_J(r_{ij}),$$

$$\begin{aligned} \Psi_2 = \Psi(m, -m) = N(m, -m) \prod_{i < j} f_J(r_{ij}) \\ \times \sum_{i, j} \exp(i\mathbf{k}_m \cdot \mathbf{r}_i - i\mathbf{k}_m \cdot \mathbf{r}_j), \end{aligned}$$

$$\begin{aligned} \Psi_3 = \Psi[m, n, -(m+n)] = N[m, n, -(m+n)] \prod_{i < j} f_J(r_{ij}) \\ \times \sum_{i, j, k} \exp(i\mathbf{k}_m \cdot \mathbf{r}_i + i\mathbf{k}_n \cdot \mathbf{r}_j - i(\mathbf{k}_m + \mathbf{k}_n) \cdot \mathbf{r}_k). \end{aligned} \quad (2.18)$$

The  $N$  functions are normalization constants,  $\Psi_2$  is a "two-phonon" state with zero total momentum, and  $\Psi_3$  is a "three-phonon" state. (The corresponding "one-phonon" state  $\Psi_1$  is not used because it cannot conserve momentum.) When placed in Eq. (2.17) the perturbation correction due to  $\Psi_2$  can be used to optimize

the  $f_J$ ; in fact its contribution is zero when  $f_{JO}$  is used. The three-phonon term  $\Psi_3$  essentially introduces three-body correlations, which are of course absent in  $\Psi_J$ . In nuclear matter the perturbation correction in Eq. (2.17) to date has only been evaluated at the two-phonon level (Kürten *et al.*, 1978, 1979).

### F. Correlation operator method

Let  $F_{ij}$  be a general operator that acts on the degrees of freedom of particles  $i$  and  $j$ . The variational wave function is then of a generalized Jastrow form,

$$\Psi_{SF} = \left\{ S \prod_{i < j} F_{ij} \right\} \Phi, \quad (2.19)$$

where a symmetrized product is required because  $F_{ij}$  and  $F_{ik}$  may not commute. The  $F_{ij}$  includes the Jastrow  $f_J(r_{ij})$  plus other terms that help to overcome the limitations of the simple Jastrow choice.

Pandharipande (1978) has found that a very good choice for  $F$  in liquid helium is

$$F_{ij}^H = f_J(r_{ij}) + \eta(r_{ij}) \mathbf{r}_{ij} \cdot \nabla_{ij}. \quad (2.20)$$

The  $\nabla_{ij}$  in Eq. (2.20) can operate either on other  $F_{ik}$  or on  $\Phi$ . This is a generalization of the wave function used by Pandharipande and Itoh (1973) to explain the effective mass of a  $^3\text{He}$  impurity in liquid  $^4\text{He}$ . For this case the conventional Jastrow choice would be

$$\Psi(k_j) = \prod_m f_J(r_{jm}) \prod_{m < n} f_J(r_{mn}) \exp[i\mathbf{k}_j \cdot \mathbf{r}_j], \quad (2.21)$$

where  $j$  specifies the  $^3\text{He}$  impurity. The effective mass  $m^*$  of the impurity is defined by

$$\lim_{k_j \rightarrow 0} \frac{\partial}{\partial k_j} \frac{\langle \Psi(k_j) | H | \Psi(k_j) \rangle}{\langle \Psi(k_j) | \Psi(k_j) \rangle} = \frac{\hbar^2}{m^*} k_j, \quad (2.22)$$

and experimentally is found to be  $m^* = 2.34m_3$ . The two terms involving  $k_j$  in the energy expectation value are  $\nabla_j f_J(r_{jm}) \cdot \nabla_j \exp[i\mathbf{k}_j \cdot \mathbf{r}_j]$  and  $\nabla_j^2 \exp[i\mathbf{k}_j \cdot \mathbf{r}_j]$ ; the first gives zero contribution because  $f_J$  is spherically symmetric, while the latter gives only  $\hbar^2 k_j^2 / 2m_3$ , which obviously implies  $m^* = m_3$ . If instead we use the  $F^H$  of Eq. (2.20) and let the  $\nabla_{ij}$  operate only on the  $\exp[i\mathbf{k}_j \cdot \mathbf{r}_j]$ , the variational wave function becomes

$$\Psi(k_j) = \prod_m [f_J(r_{jm}) + i\mathbf{k}_j \cdot \mathbf{r}_{jm} \eta(r_{jm})] \prod_{m < n} f_J(r_{mn}) \exp[i\mathbf{k}_j \cdot \mathbf{r}_j]. \quad (2.23)$$

This is essentially the backflow wave function of Feynman and Cohen (1956), which describes mathematically the physical flow of  $^4\text{He}$  atoms around the  $^3\text{He}$  impurity. The backflow term boosts  $m^*$  to near its correct value (2.1 to 2.25  $m_3$  according to the potential used) through the extra kinetic piece  $\nabla_j [i\mathbf{k}_j \cdot \mathbf{r}_{jm} \eta(r_{jm}) f_J(r_{jm})] \cdot \nabla_j \exp[i\mathbf{k}_j \cdot \mathbf{r}_j]$ . The general behavior of  $m^*$  as the liquid  $^4\text{He}$  density is changed is also explained.

In addition to the generation of backflow terms, the form (2.20) for  $F_{ij}$  also allows for many-body correlations by letting the  $\nabla_{ij}$  operate on other  $F_{ik}$ . To date, only three-body correlations of the type  $\eta(r_{ij}) \mathbf{r}_{ij} \cdot \nabla_{ij} f_J(r_{ik})$  have been used, but they provide

a significant improvement over the simple Jastrow choice in liquid helium.

It has long been recognized that the  $F_{ij}$  used to describe the correlations induced by the nucleon-nucleon potential (1.6) must contain several operators, for example,

$$F_{ij}^N = \sum_p f^p(r_{ij}) O_{ij}^p, \quad (2.24)$$

where  $O_{ij}^p = 1, (\sigma_i \cdot \sigma_j), (\tau_i \cdot \tau_j)$ , etc.

At small relative momenta the  $F^H$  reduces to a correlation that is different in  $l=0$  and 1 partial waves. Interestingly this difference can also be simulated by the spin-isospin correlations  $f^\sigma, f^\tau$ , and  $f^{\sigma\tau}$  in  $F^N$ . Thus  $F^N$  provides an approximate method of including the backflow effects contained in  $F^H$  at low densities.

The symmetrization of the product of  $F_{ij}$  in the wave function (2.19) increases substantially the complexity of calculating energy expectation values. The two-body correlation operator (2.24) can as well be written in the form  $f_{ij}^c(1+u_{ij})$ , where

$$u_{ij} = \sum_{p>1} \frac{f_{ij}^p}{f_{ij}^c} O_{ij}^p. \quad (2.25)$$

An alternative approach is the independent-pair approximation suggested by Owen (1979a), where the many-body variational wave function is taken to be

$$\Psi_{IP} = \prod_{i<j} f_{ij}^c \left[ 1 + \sum_{i<j} u_{ij} + \sum_{i<j,k} u_{ij} u_{kl} + \dots \right] \Phi, \quad (2.26)$$

so that no products of noncommuting operators are included. The wave functions (2.19) and (2.26) are identical in linear terms of  $u_{ij}$ , but the former contains higher-order terms, such as  $\frac{1}{2} \sum_{i,j,k} \{u_{ij}, u_{jk}\}$ , which are absent in (2.26).

The chief disadvantage of the correlation operators is in the difficulty of evaluating accurately the energy expectation value or other quantities. Much of the work on this problem has gone into the generalization of the chain summation techniques developed for the simple Jastrow  $f_J$ , so that expectation values with  $F^N$  can be calculated. While the convergence of (F)HNC methods has been checked against accurate Monte Carlo integrations in the Jastrow case, there are no such checks at present for operator-dependent correlations. The advantages of the method are its simplicity and wide range of applicability. The method is easily applied to both Bose and Fermi systems, and can be used over a wide range of densities. It has been used successfully in studying many systems in a relatively short period of development and still has much room for improvement. The computational facilities required are miniscule compared to present-day BBG or GFMC calculations.

### G. Comparison of results for simple systems

Before beginning our detailed discussion of the theory for nuclear matter, it would be worthwhile to compare the results of the various methods in simpler systems. This will point out some of the relative merits and

limitations of the different approaches. We shall look at liquid  $^4\text{He}$  and  $^3\text{He}$  and a simple model potential,  $v_2$ , which has been widely studied.

There has been very little success in applying the BBG theory to liquid helium because of the large value of  $\kappa (>0.5$  in  $^3\text{He}$ ), which makes convergence practically impossible. The Bose liquid  $^4\text{He}$  has been studied in simple Jastrow, GFMC, CBPT, and correlation operator approaches. The results are shown in Fig. 2 for the Lennard-Jones potential due to de Boer and Michaels (1938):

$$v_{LJ}(r) = 4\epsilon[(\sigma/r)^{12} - (\sigma/r)^6], \quad (2.27)$$

where  $\epsilon = 10.22^\circ\text{K}$ ,  $\sigma = 2.556 \text{ \AA}$ . The experimental equilibrium density is  $\rho_0 = 0.365\sigma^{-3}$  and the binding energy is  $E(\rho_0) = -7.14^\circ\text{K}$ . The GFMC curve of Kalos (1977) has a minimum at  $\rho_0 = 0.375\sigma^{-3}$  with  $E(\rho_0) = -6.85^\circ\text{K}$ . The GFMC results may be considered exact for  $v_{LJ}$ , and the discrepancy with experiment can be attributed to the inaccuracy of the potential.

Many variational calculations in the simple Jastrow approximation have been made; the results of Pandharipande and Schmidt (1977) are typical, yielding  $\rho_0 = 0.35\sigma^{-3}$  and  $E(\rho_0) = -5.9^\circ\text{K}$ . The exact choice of  $f_J$  does not seem to be too critical; with reasonable but different choices of  $f_J$  Kalos *et al.* (1974), Pandharipande and Schmidt (1977), and Smith *et al.* (1978) seem to get very similar  $E(\rho)$ . The  $f_J$  used by Smith *et al.* should be very close to the  $f_{JO}$ . The fact that the Jastrow results lie  $\approx 1^\circ\text{K}$  above the exact GFMC value is attributable largely to the lack of three-body or higher correlations in  $\Psi_J$ .

Both the CBPT and correlation operator (CO) methods include three-body effects, and their results agree quite well with the GFMC curve. The CBPT calculation of Chang and Campbell (1977) gives  $\rho_0 = 0.36\sigma^{-3}$  and  $E(\rho_0) = -6.6^\circ\text{K}$ , while the correlation operator calculation of Pandharipande (1978) gives  $\rho_0 = 0.375\sigma^{-3}$  and  $E(\rho_0) = -6.7^\circ\text{K}$ . There are approximations in both

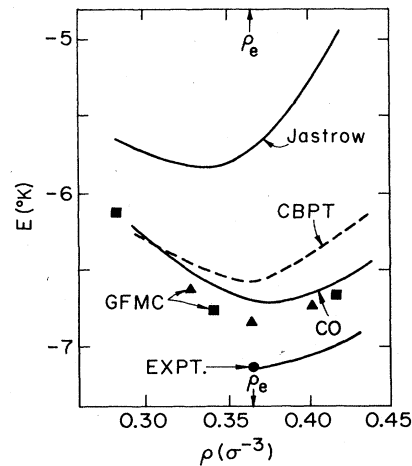


FIG. 2. The curves labeled Jastrow, CBPT, CO, GFMC, and EXPT, respectively, show the  $E(\rho)$  of liquid  $^4\text{He}$  obtained with Jastrow, correlated-basis perturbation theory, correlation operator, and Green's function Monte Carlo calculations with Lennard-Jones potential, and the experimental data.

of these advanced variational calculations, but the energies are probably correct to within  $\approx 0.2^\circ\text{K}$ . It is clear that the simple inclusion of three-body correlations makes up for most of the deficiency of the simple Jastrow  $\Psi_J$ .

In liquid  $^3\text{He}$  there are fewer calculations available. Jastrow and correlation operator results are shown in Fig. 3, along with the experimental  $E(\rho)$  curve which has  $\rho_0 = 0.277\sigma^{-3}$  and  $E(\rho_0) = -2.52^\circ\text{K}$ . The GFMC method cannot be used in Fermi systems, but since the potential for  $^3\text{He}$  should be the same as in  $^4\text{He}$ , we can estimate from the Bose results that  $v_{LJ}$  should underbind  $^3\text{He}$  by  $\approx 0.3^\circ\text{K}$ , and get approximately the correct density.

The Jastrow calculation has been done with an FHNC/4 energy evaluation by Zabolitzky (1977) and by Monte Carlo integrations by Ceperley *et al.* (1977) with various kinds of parametrization for the  $f_J$ . Again the two methods agree closely, the exact choice for  $f_J$  is not critical, and the typical Jastrow results have too little binding with  $E(\rho_0) = -1.2^\circ\text{K}$  at a density  $\rho_0 = 0.24\sigma^{-3}$  that is too low.

The correlation operator method has been applied recently by Schmidt and Pandharipande (1979a) with a wave function of the form

$$\Psi = \left\{ \sum_{i < j} (f_J(r_{ij}) + \eta(r_{ij}) \mathbf{r}_{ij} \cdot \nabla_{ij}^R) \sum_{i < j < k} f_3(r_{ij}, r_{jk}, r_{ki}) \right\} \Phi, \quad (2.28)$$

where the  $\nabla_{ij}^R$  is only allowed to operate on  $\Phi$ . The inclusion of backflow and three-body correlations lowers the  $E(\rho)$  curve to near its expected value:  $E(\rho_0) = -2.2^\circ\text{K}$ ,  $\rho_0 = 0.29\sigma^{-3}$ . However, it should be noted that the  $E(\rho)$  obtained with the CO method is much too flat. This is a reflection of the difficulties associated with the calculation of the energy expectation value with the wave function (2.28). The CBPT calculations have not been done with comparable sophistication in  $^3\text{He}$ .

From the liquid helium studies, it is clear that the

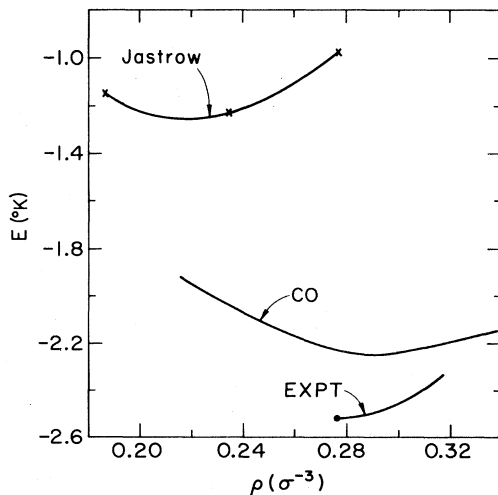


FIG. 3. The curves labeled Jastrow, CO, and EXPT, respectively, show the  $E(\rho)$  of liquid  $^3\text{He}$  obtained with Jastrow calculations, correlation operator calculations with Lennard-Jones potential, and the experimental data.

correlation operator  $F^H$  of Eq. (2.20) is a significant improvement over the Jastrow  $f_J$ , and does a reasonable job of predicting the binding energy and density for simple systems. In the  $v_2$  model of nuclear matter the potential is assumed to be the central part of the Reid ( $^3S_1$ - $^3D_1$ ) potential. It is thus similar to helium liquids, and was first studied by Pandharipande, Wiringa, and Day (1975) to compare lowest-order BBG and variational methods. It has since been studied more extensively by many authors utilizing different methods. In Fig. 4 we show Jastrow results for both Monte Carlo and FHNC energy evaluations, correlation operator results for  $F^H$  and  $F^N$ , and more recent BBG results.

The Monte Carlo evaluation of Ceperley *et al.* (1977), labeled  $E_J(\text{MC})$ , was done with an  $f_J$  of the form:

$$f_J = A \exp[-Br](1 - \exp[-r/D])/r, \quad (2.29)$$

the parameters  $A$ ,  $B$ , and  $D$  being varied to minimize the energy. Zabolitzky (1977) has carried out FHNC-FHNC/4 calculations with this  $f_J$ . He found the convergence to be very good up to more than twice nuclear matter density, the exact FHNC/4 energy being  $\approx 2$  MeV higher than FHNC at  $\rho = 0.39 \text{ fm}^{-3}$ , and in agreement with the Monte Carlo evaluation. The Jastrow results, labeled  $J$ , and the  $F^H$  results are due to Schmidt and Pandharipande (1978), who use correlation functions parametrized by a healing distance. They use an approximate FHNC/4 calculation, whose error estimates are shown in Fig. 4. The  $F^H$  values are several MeV lower than the Jastrow ones throughout the density range, and indicate that  $v_2$  is a bound system. This is a very subtle feature to pick out in view of the fact that the small energies shown in Fig. 4 are the result of a very large cancellation between kinetic and potential energy terms ( $\approx -98$  MeV potential and  $+97$  MeV kinetic at  $\rho = 0.39 \text{ fm}^{-3}$ ). The lower  $F^H$  values are almost totally attributable to the  $\eta \mathbf{r} \cdot \nabla$  terms rather than three-body effects.

The  $F^N$  of Eq. (2.24) has no three-body terms, but can simulate backflow at low momenta through the non-central correlations. In this case  $F^N$ , as calculated in Sec. III, takes the simple form

$$F_{ij}^N = f_{ij}^c + f_{ij}^s(\sigma_i \cdot \sigma_j) + f_{ij}^T(\tau_i \cdot \tau_j) + f_{ij}^{sT}(\sigma_i \cdot \sigma_j)(\tau_i \cdot \tau_j), \quad (2.30)$$

and  $f^s = f^T = f^{sT}$ . The  $F^N$  results lie between the Jastrow and  $F^H$  values, with roughly half the energy lowering due to the  $k$ -dependent backflow terms being picked up by  $F^N$  at nuclear matter densities. This fraction decreases as  $\rho$  increases, as would be expected. Nevertheless, the  $F^N$  is a sufficient improvement over  $f_J$  to pick out the bound feature of the  $v_2$  model. The FHNC/SOC equations discussed in subsequent sections are used to calculate the energies with  $F^N$ , and the error in these could be comparable to that in the Jastrow calculation.

Finally there are recent calculations of Day (1978b) in which a complete three-body cluster BBG evaluation has been done. The points in Fig. 4 labeled BBG include the three-body cluster plus an estimate of the four-body cluster; the assigned error bar is  $\pm$  the estimated magnitude of the four-body cluster. These results are in close agreement with the advanced vari-



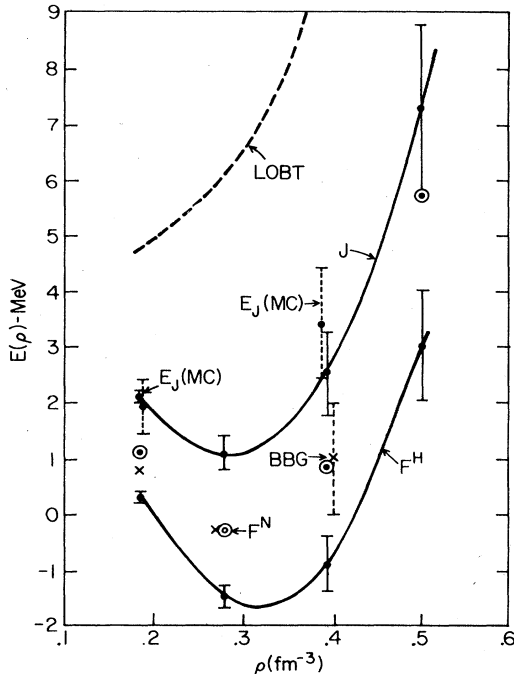


FIG. 4. The  $E(\rho)$  of nuclear matter model  $v_2$ . Curves/points labeled  $J$ ,  $F^N$ , and  $F^H$  show results of variational calculations with the Jastrow,  $F^N$ , and  $F^H$  correlation operators and FHNC, FHNC/4 integral equations. The  $E_J(\text{MC})$  show exact Monte Carlo results with the Jastrow wave function. Results of lowest-order Brueckner calculations with standard spectrum are labeled LOBT, while BBG is the sum of two-, three-, and (approximate) four-hole line terms of the Brueckner-Bethe-Goldstone expansion.

ational results  $F^H$  and  $F^N$ . Also shown is the lowest-order BBG result (curve labeled LOBT), which includes only the two-body cluster contribution with the standard dispersion correction.

From the results in these simple systems, we draw the following conclusions. Variational calculations of the Jastrow type, with energy evaluated by means of chain summation techniques, give reliable upper bounds to the energy in simple Bose and Fermi systems. The use of correlation operators, which include backflow and/or three-body effects, gives lower energies than the simple Jastrow correlation, and good agreement with experiment in the liquid helium. It has not been proved that the upper bound property is maintained when the more elaborate chain summation techniques needed for evaluation of operator-dependent correlations are used. The results in simpler systems are encouraging, however, and we believe the energy calculation can be made with reasonable accuracy.

### III. CALCULATION OF $F$

The first step in the variational theory for nuclear matter is the selection of the correlation operator  $F$ . We discuss here a commonly used method for obtaining a reasonable correlation operator for the  $v_8$  problem, in which  $v_{ij}$  is given by the first eight terms of Eq. (1.6). The  $F$  is assumed to be

$$F_{ij} = \sum_{p=1,8} f^p(r_{ij}) O_{ij}^p, \quad (3.1)$$

where the  $f^p(r_{ij})$  are to be determined by minimizing the energy. This complicated variational problem is often simplified somewhat as follows. The two-body cluster contribution,  $C_2$ , is minimized subject to the constraint that the correlated wave function "heal" smoothly at some distance  $d$ . This constraint implies  $f^c(r > d) = 1$ , and  $f^{p>1}(r > d) = 0$ , and the variation gives a series of Schrödinger-type equations that include Lagrange multipliers  $\lambda^p$  chosen so that the  $\partial f^p / \partial r$  are continuous at  $r = d$ . The solutions of these equations gives a set of  $f^p(r_{ij}, d)$  characterized by the healing distance  $d$ .

The general approach for obtaining correlation functions parametrized by the healing distance was originally developed by Pandharipande (1971, 1972) for a lowest-order constrained-variation method, and its physical assumptions have been studied by Pandharipande and Schmidt (1977). Briefly, this approach assumes that the long-range part of the potential,  $v(r > d)$ , only contributes to the average one-body potential, and should not be used in calculating  $F$ . It thus neglects the long-range  $r^{-2}$  component of optimal two-body correlations, which we believe is relatively unimportant in nuclear matter. The nature of  $F$  is primarily determined by  $v(r < d)$ , a smooth part of which must also contribute to the average field. The Lagrange multipliers  $\lambda^p$  essentially approximate this part by a constant. The  $\lambda^p$  and  $d$  are related by the requirement that  $\Psi$  be continuous.

The one-parameter family  $f^p(d)$ , obtained from the Schrödinger-type equations, can be generalized by multiplying each  $f^p$  by a constant factor  $\beta_p$ , to produce a variational  $F_{ij}$  with parameters  $d$  and  $\beta_p$ :

$$F_{ij}(d, \beta_p) = \sum_{p=1,8} \beta_p f^p(r_{ij}, d) O_{ij}^p. \quad (3.2)$$

Normalization requires that  $\beta_c = \beta_1 = 1$ , but the  $\beta_{p>1}$  may be arbitrary. The full energy  $E(\rho, d, \beta_{p>1})$  is calculated and minimized with respect to variations in  $d$  and  $\beta_{p>1}$  at each density.

It is convenient here to use the eight channel functions  $f_{T,S}$ ,  $f_{t,T}$ , and  $f_{b,T}$ , where the subscripts  $T$  and  $S$  give the total isospin and spin of the pair, while  $t$  and  $b$  denote the tensor and spin-orbit parts. The potentials in the  $T, S$  channels are denoted by  $v_{T,S}$ ,  $v_{t,T}$ ,  $v_{b,T}$ . The channel functions are related to the  $f^p$  and  $v^p$  by the general equations

$$x_{T,S} = x^c + (4S - 3)x^s + (4T - 3)x^r + (4S - 3)(4T - 3)x^{\sigma r}, \quad (3.3)$$

$$x_{t,T} = x^t + (4T - 3)x^{tr}, \quad (3.4)$$

$$x_{b,T} = x^b + (4T - 3)x^{br}, \quad (3.5)$$

where  $x$  may be  $f$  or  $v$ . The two-body cluster energy  $C_2$  in the van Kampen cluster expansion (1961) can also be broken into its  $T$  and  $S$  channels,

$$C_2 = \sum_{T,S} C_{2,T,S}, \quad (3.6)$$

with

$$C_{2,T,S} = \frac{(2S+1)(2T+1)}{2A\Omega^2} \sum_{\mathbf{k}_m, \mathbf{k}_n < k_F} \int d^3r_m d^3r_n \{ \exp[-i(\mathbf{k}_m \cdot \mathbf{r}_m + \mathbf{k}_n \cdot \mathbf{r}_n)] - (-1)^{T+S} \exp[-i(\mathbf{k}_m \cdot \mathbf{r}_n + \mathbf{k}_n \cdot \mathbf{r}_m)] \} \\ \times [f_{T,S} + \delta_{S1}(f_{t,T} S_{mn} + f_{b,T}(\mathbf{L} \cdot \mathbf{S})_{mn})] [(-\hbar^2/m)(\nabla_{mn}^2 + k_{mn}^2) + v_{T,S} + \delta_{S1} \\ \times (v_{t,T} S_{mn} + v_{b,T}(\mathbf{L} \cdot \mathbf{S})_{mn})] \\ \times [f_{T,S} + \delta_{S1}(f_{t,T} S_{mn} + f_{b,T}(\mathbf{L} \cdot \mathbf{S})_{mn})] \exp[i(\mathbf{k}_m \cdot \mathbf{r}_m + \mathbf{k}_n \cdot \mathbf{r}_n)]. \quad (3.7)$$

The  $\nabla_{mn}^2$  operates only on the relative coordinate  $\mathbf{r}_{mn} = (\mathbf{r}_m - \mathbf{r}_n)$ , and  $\mathbf{k}_{mn}$  is the relative momentum  $\frac{1}{2}(\mathbf{k}_m - \mathbf{k}_n)$ ;  $k_{mn}^2$  is subtracted here to eliminate the one-body contribution from  $\nabla_{mn}^2$  operating on the plane waves.

In the  $S=0$  channels the tensor and spin-orbit potentials and correlations do not contribute. In this case we find, after doing the  $k$  summations and integrating over  $\mathbf{R}_{mn} = \frac{1}{2}(\mathbf{r}_m + \mathbf{r}_n)$ , that

$$C_{2,T,0} = \frac{(2T+1)}{32} \rho \int d^3r_{mn} \phi_{T,0} f_{T,0} \\ \times (-\hbar^2/m) [\phi_{T,0} \nabla^2 f_{T,0} + 2\nabla \phi_{T,0} \cdot \nabla f_{T,0}] \\ + v_{T,0} f_{T,0} \phi_{T,0}, \quad (3.8)$$

where

$$\phi_{T,S} = [1 - (-1)^{T+S} l^2(k_F r)]^{1/2}. \quad (3.9)$$

The  $l(x)$  is the familiar Slater function,

$$l(x) = 3[\sin(x) - x \cos(x)]/x^3. \quad (3.10)$$

Minimization of Eq. (3.8) with the healing constraint

$$f_{T,0}(r \geq d) = 1, \quad (3.11)$$

gives the Euler-Lagrange equation

$$-(\hbar^2/m) [\phi_{T,0} \nabla^2 f_{T,0} + 2\nabla \phi_{T,0} \cdot \nabla f_{T,0}] \\ + (v_{T,0} - \lambda_{T,0}) f_{T,0} \phi_{T,0} = 0 \quad (3.12)$$

where  $\lambda_{T,0}$  is adjusted so that

$$\left. \frac{\partial f_{T,0}}{\partial r} \right|_{r=d} = 0. \quad (3.13)$$

The  $S=1$  channels are more complicated because of the tensor and spin-orbit potentials and correlations. A study of the possible operator products shows that the only terms with nonzero contributions in the integral (3.7) are accompanied by either the unit operator or  $\mathbf{L}^2$ . A procedure similar to that for  $S=0$  states leads to three coupled equations for  $f_{T,1}, f_{t,T}, f_{b,T}$ :

$$\frac{-\hbar^2}{m} [\phi_{T,1} \nabla^2 f_{T,1} + 2\nabla \phi_{T,1} \cdot \nabla f_{T,1}] + (v_{T,1} - \lambda_{T,1}) f_{T,1} \phi_{T,1} \\ + 8(v_{t,T} - \lambda_{t,T}) f_{t,T} \phi_{t,T} + \frac{2}{3} (v_{b,T} - \lambda_{b,T}) \frac{\phi_{b,T}}{\phi_{T,1}} f_{b,T} \phi_{b,T} = 0, \quad (3.14)$$

$$\frac{-\hbar^2}{m} \left[ \phi_{t,T} \nabla^2 f_{t,T} + 2\nabla \phi_{t,T} \cdot \nabla f_{t,T} - \frac{6}{r^2} f_{t,T} \phi_{t,T} \right] \\ + [v_{T,1} - \lambda_{T,1} - 2(v_{t,T} - \lambda_{t,T}) - 3(v_{b,T} - \lambda_{b,T})] f_{t,T} \phi_{t,T} \\ + (v_{t,T} - \lambda_{t,T}) f_{T,1} \phi_{T,1} - \frac{1}{12} \frac{\phi_{b,T}}{\phi_{t,T}} (v_{b,T} - \lambda_{b,T}) f_{b,T} \phi_{b,T} = 0, \quad (3.15)$$

$$\frac{-\hbar^2}{m} [\phi_{b,T} \nabla^2 f_{b,T} + 2\nabla \phi_{b,T} \cdot \nabla f_{b,T}] + [v_{T,1} - \lambda_{T,1} - (v_{t,T} - \lambda_{t,T}) \\ - \frac{1}{2} (v_{b,T} - \lambda_{b,T})] f_{b,T} \phi_{b,T} + (v_{b,T} - \lambda_{b,T}) (f_{T,1} - f_{t,T}) \phi_{b,T} = 0, \quad (3.16)$$

where

$$\phi_{t,T} = \phi_{T,S=1}, \quad (3.17)$$

$$\phi_{b,T} = [(k_F^2 r^2/5) + (-1)^T r l']^{1/2}. \quad (3.18)$$

The  $\lambda_{T,1}$ ,  $\lambda_{t,T}$ , and  $\lambda_{b,T}$  are chosen so that  $f_{T,1}$  heals smoothly to unity and  $f_{t,T}$  and  $f_{b,T}$  go smoothly to zero at  $r=d$ .

If, as in most of the work described below, the  $v_{b,T}$  is set to zero, i.e., the  $v_6$  problem, then there is no  $f_{b,T}$  correlation. Similarly if  $v_{t,T}=0$ , then there is no  $f_{t,T}$ . However, if a pure central potential is taken, there is still a  $(-1)^{T+S}$  dependence in Eq. (3.9) which will give different  $f_{T,S}$  in different  $T,S$  channels. The projected  $F$  will then have  $f^s$ ,  $f^t$ , and  $f^{st}$  terms, even though the potential is purely central. These terms approximately simulate the backflow discussed in Secs. II.F and II.G. In the  $k \rightarrow 0$  limit the correlation operator (2.20) just gives  $f$  in  $l=0$  states to be  $f_s$  and that in  $l=1$  states to be  $(f_s + \eta)$ . For a pure central potential, the  $f^s = f^t = f^{st} \equiv f^x$ , so that  $f$  is  $f^c + 3f^x$  in odd  $l$  and  $f^c - 5f^x$  in even  $l$  states. Thus at small  $k$  the operator correlation  $f^x$  can be used to get backflow effects. However, at large  $k$  the correlation operator (2.20) implies an explicit  $k$  dependence and differences between correlations in  $l=0, 2, 4$  states, etc., which the  $f^x$  cannot simulate (see Schmidt and Pandharipande, 1978).

The projected  $f^p$  in models  $v_6$  and  $v_8$  of the Reid potential are shown in Figs. 5 and 6. The inclusion of  $\mathbf{L} \cdot \mathbf{S}$  forces changes all the  $f^p$  because of the couplings in Eqs. (3.14)–(3.16). We note that  $f^c$  is large and infinite ranged, but the  $f^{p>1}$  tend to be small and of course are of range  $d$  only. It is dangerous to draw conclusions from the magnitudes of  $f_{ij}^{p>1}$  without considering the contribution of accompanying  $O_{ij}^p$ .

The chain summation methods [(F)HNC, (F)HNC/4, etc.] commonly used to calculate  $E$  in simple systems have a better convergence when used with correlations obtained from a Schrödinger equation such as (3.12) (Zabolitzky, 1977). These methods are least accurate at short distances, but since the large bare interaction is mostly canceled by the  $\nabla^2 f$  term in the Schrödinger equation, this deficiency in the chain summations becomes relatively unimportant. We expect that this will also be true for the more complicated correlations in nuclear matter.

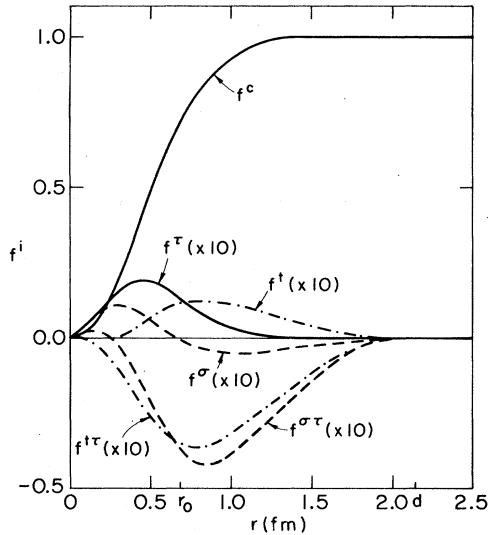


FIG. 5. The correlation functions  $f^b(r, d)$  in the Reid  $v_8$  model at  $k_F = 1.6 \text{ fm}^{-1}$  and  $d = 2.25r_0$ .

A simpler but less sophisticated method for calculating  $E$  is by direct cluster expansion in the number of particles. Generally the expansion does not converge with the number of particles in the cluster, and so only a much more restricted class of  $F$  can be used with this method. Hoping to obtain  $F$  for which the cluster expansion is convergent, Kürten, Ristig, and Clark (1978) have introduced an additional Pauli constraint

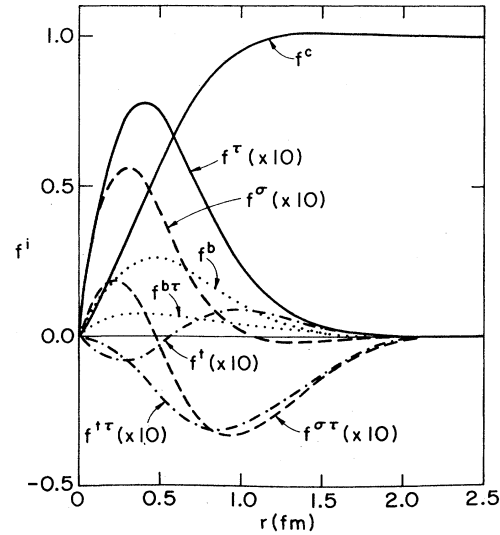


FIG. 6. The correlation functions  $f^b(r, d)$  in the Reid  $v_8$  model at  $k_F = 1.6 \text{ fm}^{-1}$  and  $d = 2.25r_0$ .

in the equations for  $F$ . Their equations are slightly more complicated than those given above.

#### IV. DIAGRAMMATIC CLUSTER EXPANSION

##### A. Expectation values and diagram rules

The many-body expectation value for any two-body operator  $X_{mn}$  is given by

$$\langle X \rangle = \sum_{m < n} \frac{\int A \left( \prod_a \phi_a^* \right) S \left( \prod_{a < b} F_{ab}^\dagger \right) X_{mn} S \left( \prod_{a < b} F_{ab} \right) \prod_a \phi_a d\tau}{\int A \left( \prod_a \phi_a^* \right) S \left( \prod_{a < b} F_{ab}^\dagger \right) S \left( \sum_{a < b} F_{ab} \right) \prod_a \phi_a d\tau}, \quad (4.1)$$

where for simplicity we antisymmetrize only the left-hand side  $\Psi^*$ . The  $\Pi F_{ab}$  is of course symmetrized because the  $F_{ab}$  do not commute. It is impossible to evaluate Eq. (4.1) exactly for an infinite system, so the expression is approximated by expanding the  $\Pi F^2$  in the integrals for both numerator and denominator in powers of the short-ranged functions,  $F_{ab}^c, F_{ab}^{b>1}, f_{ab}^{b>1} f_{ab}^{a>1}$ , where

$$F_{ab}^c = F_{ab}^1 = f_{ab}^{c2} - 1, \quad F_{ab}^{b>1} = 2f_{ab}^c f_{ab}^{b>1}. \quad (4.2)$$

(From this point on we assume each  $f_{ab}^{b>1}$  has an implicit factor of  $\beta_{b>1}$  associated with it.) This expansion is conveniently represented by generalized Mayer diagrams, and a very general diagrammatic cluster expansion is given in Wiringa and Pandharipande (1978). The expansion is valid for noncommuting operators of the type used in nuclear matter or others such as those used in helium [Eq. (2.20)]. We first give the diagram rules, and then the derivation of the expansion.

A typical diagram representing one of the integrals in the expansion will have  $i$  points, each standing for the coordinates  $r_i$  of particle  $i$ . An integration over all  $r_i$  is implied. The points are connected by the various lines shown in Fig. 7, that represent the  $f^b$ , exchange effects due to the antisymmetrized  $\Psi^*$ , and the effects

of the two-body operator  $X_{mn}$ . The operator of primary interest will of course be the Hamiltonian (1.9). Any  $F_{ab}$  not operated on by  $X_{mn}$  is called a passive correlation, and all passive  $f_{ab}^{c2}$  are replaced by  $1 + F_{ab}^c$ . The  $f_{mn}^c$  is not treated this way because  $X_{mn}$  may be singular, as in the case of the potential. The  $F_{ab}^c$  are represented by dashed lines, the  $F_{ab}^{b>1}$  by single wavy lines, and the  $f_{ab}^{b>1} f_{ab}^{a>1}$  by doubly wavy lines. The single (double) wavy lines are labeled with the operator index  $p(q)$  associated with them. Thus every wavy line indicates the presence of an operator-dependent link.

The  $F$  that are operated on by  $X_{mn}$  are called interacting correlations. This generally includes  $F_{mn}$ , and perhaps  $F_{ma}$  or  $F_{na}$  as in the case of a  $\nabla_m^2$  or  $\nabla_n^2$  in the Hamiltonian. We separate out those terms where  $X_{mn}$  only operates on  $F_{mn}$ , and represent the quantity  $F_{mn} X_{mn} F_{mn}$  by a thick solid line, called an interaction line, with indices  $i, j, k$  where  $j$  is associated with the operator dependence of  $X_{mn}$ , and  $i$  and  $k$  with the operator dependence of the  $F_{mn}^\dagger$  and  $F_{mn}$ , respectively. Those terms where  $X_{mn}$  operates on quantities other than  $F_{mn}$  are treated separately. In particular, the  $\nabla_m^2$  term in the Hamiltonian can operate to give  $\nabla_m F_{mn} \cdot \nabla_m \phi_m$  or  $\nabla_m F_{mn} \cdot \nabla_m F_{ma}$ . In this case the  $\nabla_m F$  are represented

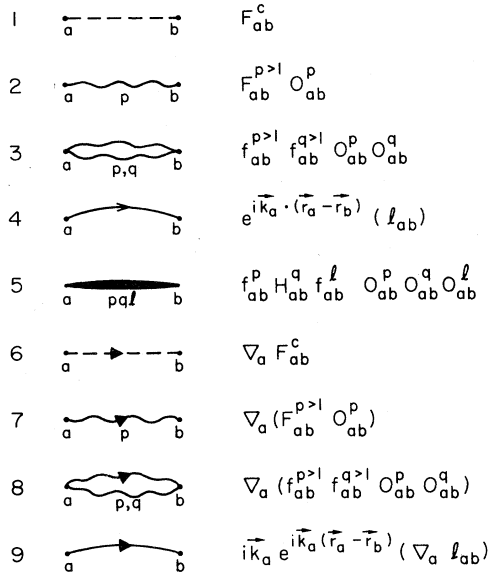


FIG. 7. The elements in the diagrams giving the energy expectation value. On summation over  $\mathbf{k}_a$  the elements 4 and 9, respectively, give  $\ell_{ab}$  and  $\nabla_a \ell_{ab}$ .

by the appropriate dashed, single wavy, or double wavy lines, with a superposed solid directional arrow pointing away from point  $m$ , and we shall refer to them as derivative lines.

Since the  $\Psi^*$  is antisymmetrized, we need to keep track of the plane-wave states occupied by the particles in  $\Psi^*$ . For this we use solid lines with directions (open arrows) which are called exchange or state lines. By convention the particles 1, 2, ...,  $A$  occupy states  $\mathbf{k}_1, \mathbf{k}_2, \dots, \mathbf{k}_A$  in the  $\Psi$ . Those terms in the Slater determinant  $\Delta \Pi_a \exp[-i\mathbf{k}_a \cdot \mathbf{r}_a]$  of  $\Psi^*$  where the particles remain in the same states are called direct, and their diagrams contain no exchange lines. An exchange line going from  $a$  to  $b$  represents the contribution of a term in  $\Psi^*$  where particle  $b$  occupies state  $\mathbf{k}_a$ . Since each particle must end up in a definite state, all exchange lines must join to form closed loops, and only one exchange line may pass through any point. The total exchange pattern in any exchange diagram will consist of one or more nontouching exchange loops.

$$\frac{1}{\Omega^3} \sum_{m \neq n \neq 1} \int e^{i\mathbf{k}_n \cdot \mathbf{r}_{n1}} e^{i\mathbf{k}_1 \cdot \mathbf{r}_{1n}} F_{m1}^c f_{mn}^i H_{mn}^j f_{mn}^k \left\{ -\frac{1}{4} \sum_{p=1,4} O_{n1}^p \right\} O_{mn}^i O_{mn}^j O_{mn}^k d^3\mathbf{r}_m d^3\mathbf{r}_n d^3\mathbf{r}_1.$$

We may sum over  $m, n$ , and 1, ignoring the restriction  $m \neq n \neq 1$  because the error is of order  $1/\Omega$ , and obtain

$$\rho^3 \int \int F_{m1}^c f_{mn}^i H_{mn}^j f_{mn}^k \left\{ -\frac{1}{4} \sum_{p=1,4} O_{n1}^p \right\} O_{mn}^i O_{mn}^j O_{mn}^k d^3\mathbf{r}_m d^3\mathbf{r}_n d^3\mathbf{r}_1,$$

for diagram 8.4. The exchange lines in "proper" diagrams simply become Slater functions on particle summation. Note that all "improper" exchange diagrams must be discarded before replacing exchange lines by Slater functions.

The  $\nabla_m \phi_m \cdot \nabla_m F_{ma}$  terms in the energy expectation value give zero contribution, unless particle  $m$  is exchanged, provided  $F$  is independent of  $\mathbf{k}$ . When the particle  $m$  is

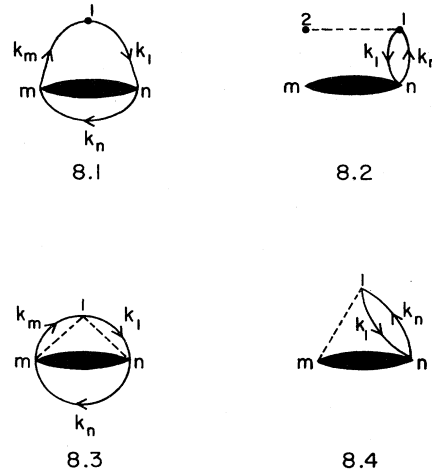


FIG. 8. Examples of proper (8.3, 8.4) and improper (8.1, 8.2) exchange diagrams.

The exchange of particles also involves operator-dependent terms. The exchange of particles  $a$  and  $b$  can be represented by an operator  $e_{ab}$ :

$$e_{ab} = -\frac{1}{4} \exp[i(\mathbf{k}_a - \mathbf{k}_b) \cdot \mathbf{r}_{ab}] [1 + \sigma_a \cdot \sigma_b + \tau_a \cdot \tau_b + (\sigma_a \cdot \sigma_b)(\tau_a \cdot \tau_b)]. \quad (4.3)$$

An  $n$ -particle exchange loop is equivalent to a series of  $(n-1)$  two-body exchanges. Thus every such loop has an associated factor of  $(-1/4)^{n-1}$ , and all but one of the exchange lines has an operator label  $n$  to represent  $O_{ab}^n$ . Every exchange line also has the  $\exp[i\mathbf{k}_a \cdot \mathbf{r}_{ab}]$  factor.

Diagrams like 8.1, 8.2, etc. of Fig. 8, in which uncorrelated particles are exchanged, give zero contribution due to the orthogonality of plane waves. We shall refer to these as "improper" exchange diagrams. In "proper" exchange diagrams only correlated or interacting particles are exchanged; the correlations could be through other particles, as in diagram 8.4.

The summation over  $\mathbf{k}$ 's can be carried out independently for every exchange line in a "proper" exchange diagram. For example, the contribution of diagram 8.4 is given by:

exchanged, the  $\exp[i\mathbf{k}_m \cdot \mathbf{r}_{mb}] i\mathbf{k}_m \cdot \nabla F_{ma}$  leads to  $\nabla_m l(\mathbf{k}_F \mathbf{r}_{mb}) \cdot \nabla_m F_{ma}$ , and we mark the exchange line from  $m$  to  $b$  with a solid arrow to differentiate it from the regular exchange line. In this notation, derivative exchange and correlation lines appear in pairs, and there is an implied  $\cos \theta$  dependence between the directions of the solid arrows.

The contribution of any diagram can be separated into

two factors. One is the spatial integral that contains all the functions  $F^c$ ,  $F^{p>1}$ ,  $X^p$ ,  $\exp[i\mathbf{k}\cdot\mathbf{r}]$ , etc., represented in the diagram. The other is the operator-dependent part which we may write as  $\sum_i w^i \Pi^i O_{ab}^p$  where  $w^i$  is a weight factor giving the probability that the operator product will appear in the specific order  $i$ , denoted by  $\Pi^i O_{ab}^p$ . The Pauli identity

$$(\sigma_1 \cdot \mathbf{A})(\sigma_1 \cdot \mathbf{B}) = \mathbf{A} \cdot \mathbf{B} + i\sigma_1 \cdot (\mathbf{A} \times \mathbf{B}), \quad (4.4)$$

can be used to express the operator product as

$$\Pi^i O_{ab}^p = C^i + \text{rest}, \quad (4.5)$$

where  $C^i$  is a constant independent of spin or isospin operators, and the rest contains terms in which each  $\sigma_a$  or  $\tau_a$  occurs at most once. Since the expectation value requires a sum over all spin-isospin states, the contribution of  $\Pi^i O_{ab}^p$  is just given by  $C^i$ . In general  $C^i$  depends on the ordering of operators in  $\Pi^i O_{ab}^p$ , so that all possible orderings allowed by the  $\Pi F_{ab}$  must be considered in any given evaluation. We note also that any operator product due to the exchange of particles must be kept in the order indicated by the direction of the exchange. Some useful rules for calculating  $C$  parts will be given in the next section.

If there were no operator dependence in the problem then only irreducible numerator diagrams would need to be evaluated to obtain the expectation value (4.1). An irreducible diagram is a connected diagram that cannot be sliced into two disconnected pieces by cutting at a single point. It is found (see Pandharipande and Bethe, 1973) that reducible and disconnected diagrams from the numerator cancel with the denominator terms to within factors of order  $A^{-1}$ , which are negligible for infinite systems. When operators are present, however, this cancellation of diagrams which have one or more articulation points at which the diagram is separable into different pieces is not exact. The more general diagrammatic cluster expansion for use when operators are present is given below.

## B. Cluster expansion

Let us divide all possible connected diagrams into two classes: interacting and noninteracting. Interacting diagrams can occur only in the numerator; they contain the interaction line  $X_{mn}$  (or two derivative lines), and an arbitrary number of correlation lines. Noninteracting diagrams can contain only correlation lines, and may appear either in the numerator or the denominator. Diagrams of both classes may have any number of "proper" exchange loops. There is a countably infinite number of diagrams in each class. Let  $[I]$  denote the  $I$ th connected diagram in the interacting class, and  $[i]$  the  $i$ th connected diagram in the noninteracting class.

The expectation value is given by

$$\frac{N}{D} = \frac{[I] + [I][i] + \frac{1}{2}[I][i][j] + \dots}{1 + [i] + \frac{1}{2}[i][j] + \dots} = \frac{\sum_p N_p}{1 + \sum_p D_p} \equiv \sum_p E_p, \quad (4.6)$$

where we have assumed normalization  $\Omega^{-1/2}$  for the plane-wave states, so that the first term of the denom-

inator is unity, and ordered the  $N$ ,  $D-1$ , and  $E$  in the series such that the  $p$ th term contains diagrams having  $p$  disconnected pieces. Thus  $N_p$  contains diagrams represented by  $[I][i][j]$ ; it is the sum of the products of diagrams  $I$ ,  $i$ , and  $j$ , the summation over these being restricted so that  $I$ ,  $i$ , and  $j$  do not have a common particle. Similar restrictions occur in the summation over  $i_1, i_2, \dots, i_p$  in  $D_p$ :

$$D_p = \frac{1}{p!} [i_1][i_2] \dots [i_p] \\ = \sum_{\substack{i_1, i_2, \dots, i_p \\ \text{no common particles}}} \frac{1}{p!} \text{product of diagrams } i_1, i_2, \dots, i_p; \quad (4.7)$$

the  $1/p!$  takes care of the overcounting when  $i_1 \dots i_p$  are independently summed.

In contrast a product  $N_p D_q$ , for example, is also a sum of diagrams having  $p+q$  disconnected pieces, but the above restrictions do not occur. We represent such products by a multiplication symbol  $\times$ ; for example,

$$N_1 D_1 = [I] \times [i] = [I][i] + [\overline{I}][i] + [\overline{I}][i] + \dots \quad (4.8)$$

where the number of overhead lines denotes the number of common particles,

$$[\overline{I}][i] = \sum_{\substack{i, i' \\ \text{one common particle}}} \text{product of diagrams } I \text{ and } i. \quad (4.9)$$

In a general term shown as  $[\overline{I}][i][j][k] \dots$  a summation over  $I, i, j, k \dots$  is implied, with the restriction that  $I, i, j, k \dots$  do not have any common particles other than those indicated by the overhead bars. The  $E_p$  are obtained by solving the set of equations

$$E_p = N_p - \sum_{q,r} D_q E_r \delta(p-r-q), \quad (4.10)$$

starting from  $p=1$ . This gives

$$E_1 = [I], \\ E_2 = [I][i] - [I] \times [i] = -[\overline{I}][i] - [\overline{I}][i] - \dots, \\ E_3 = \frac{1}{2}[I][i][j] - \frac{1}{2}[\overline{I}][i] \times [j] + [i] \times ([\overline{I}][j] + [\overline{I}][j] + \dots) \\ = [\overline{I}][i][j] + \frac{1}{2}[\overline{I}][i][j] + [\overline{I}][i][j] + [\overline{I}][i][j] + \dots \quad (4.11)$$

The first term in  $E_3$  represents diagrams in which one common particle occurs in all the three pieces  $I$ ,  $i$ , and  $j$ . The second term in  $E_3$  is the sum of  $-\frac{1}{2}[\overline{I}][i][j]$  coming from  $D_2 E_1$  and  $+\frac{1}{2}[\overline{I}][i][j]$  from  $D_1 E_2$ . Giving a general expression for  $E_p$  is a combinatorial problem beyond the scope of this work. However, it is clear that  $E_p$  consists of terms of type

$$[\overline{I}][i_1][i_2] \dots [i_{p-1}],$$

which are completely connected with overhead bars and have no gaps of the type shown between  $i_2$  and  $i_3$ :

$$[\overline{I}][i_1][i_2][i_3] \dots [i_{p-1}].$$

A connected diagram having  $n$  particles has a con-

tribution proportional to  $\Omega^{-n+1}$ . However, there exist  $\approx A^n$  such diagrams which have the same topology and differ only in particle labels. Thus all connected diagrams of a given topology have a contribution  $\propto A\rho^{n-1}$ . Disconnected diagrams of a given topology and  $p$  pieces have a contribution  $\propto A^p$ . An overhead line restricts the summation over one particle index, however, and reduces the contribution by a factor  $A^{-1}$ ; we consider  $\overline{\quad}$  indicating a common particle in three pieces as two overhead lines, etc. The contributions of  $E_p$  diagrams are proportional to  $A^{p-q}$  where  $q$  is the number of overhead lines. Since at least  $p-1$  lines are needed to completely connect  $p$  pieces,  $E$  cannot have contributions  $\propto A^{r>1}$ , and in the limit  $A \rightarrow \infty$  we need to consider only those terms in  $E_p$  that have  $p-1$  overhead lines. This gives

$$E_{A \rightarrow \infty} = [I] - [I][i] + \frac{1}{2}[\overline{I}][\overline{i}][j] + [I][\overline{i}][j] + [\overline{I}][i][j] \\ + \text{four-piece terms} + \dots \quad (4.12)$$

Now there is a countably infinite set of inseparable diagrams containing no articulation points. The  $A$ th ( $a$ th) inseparable interacting (noninteracting) diagram is denoted by  $[A]$  ( $[a]$ ). A connected diagram that is separable into  $s$  inseparable pieces  $[I_s]$  or  $[i_s]$  may be represented as

$$[I_s] = [\overline{A}a_1\overline{a_2} \dots \overline{a_{s-1}}], \quad (4.13)$$

where the overhead lines (which all appear inside a square bracket) now denote the articulation points at which the diagram  $[I_s]$  is separable. For example, diagram 9.3 of Fig. 9 is represented by the expression  $[\overline{A}a]$ , where the  $A$  and  $a$  denote the disconnected inseparable diagrams of 9.4. The overhead line specifies the connection of these two pieces, which yields the connected diagram. We obviously have

$$[I] = [A] + [\overline{A}a] + [\overline{A}ab] + \frac{1}{2}[\overline{A}ab] + \frac{1}{2}[\overline{A}ab] + \dots, \quad (4.14)$$

$$[i] = [a] + \frac{1}{2}[\overline{a}b] + \dots, \quad (4.15)$$

with which we may now order  $E$  according to the number of inseparable pieces it contains:

$$E = [A] + \{[\overline{A}a] - [\overline{A}][a]\} \\ + \{[\overline{A}ab] - [\overline{A}][\overline{a}b] - [\overline{A}][a][b] + [\overline{A}][a][b]\} \\ + \{\frac{1}{2}[\overline{A}ab] - [\overline{A}][\overline{a}b] + \frac{1}{2}[\overline{A}][a][b]\} \\ + \{\frac{1}{2}[\overline{A}ab] - [\overline{A}][\overline{a}b] - \frac{1}{2}[\overline{A}][a][b] + [\overline{A}][a][b]\} \\ + \text{terms having } \geq 4 \text{ inseparable pieces.} \quad (4.16)$$

The first term in  $E$  is just  $[A]$ , which represents the sum of all connected inseparable interacting diagrams. The second term is the difference between the expectation value of all connected diagrams  $[\overline{A}a]$  that could be separated at one point into two inseparable pieces, and the product of expectation values of the two corresponding disconnected diagrams  $[\overline{A}][a]$ .

The thrice-separable terms have been grouped into three categories where (i)  $a$  and  $b$  share one point in common, while  $A$  shares a different point with  $a$ ; (ii)  $a$  and  $b$  have no points in common, but each shares one point with  $A$ ; and (iii)  $a$ ,  $b$ , and  $A$  all share one common point.

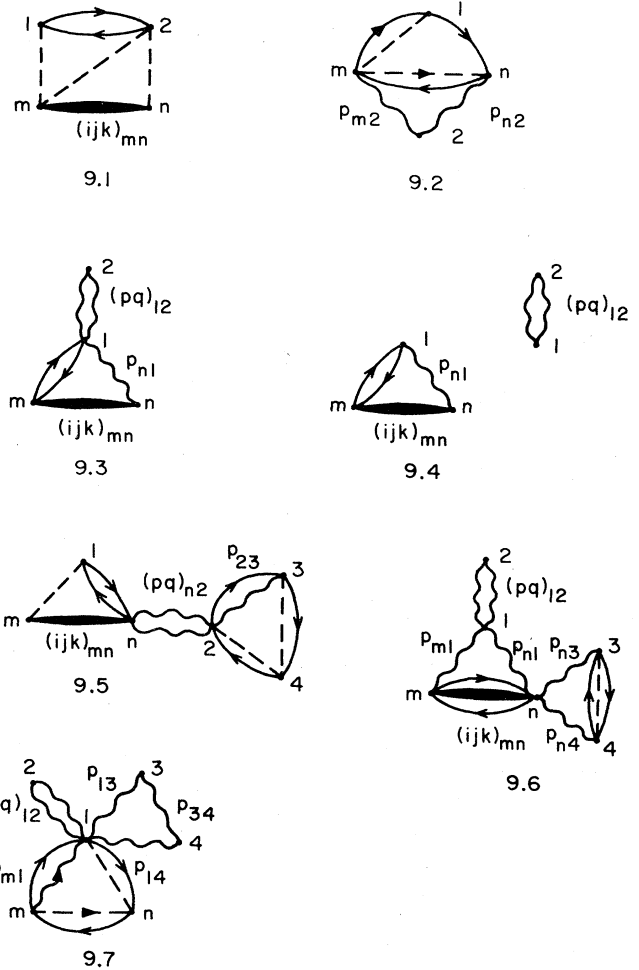


FIG. 9. Examples of diagrams in the cluster expansion of the energy expectation value.

The radial integrals of a separable diagram factorize, and thus are identical in both the separated and connected cases. When no operators are present then all terms in curly brackets are zero, and only the irreducible diagrams  $[A]$  contribute to  $E$ . In this case the expansion reduces to the well-known irreducible cluster expansion. When operators are present, the additional terms may be nonzero due to the dependence of  $C$  parts on the ordering of operators in the products, which is in general different for the connected and separated cases.

### C. Examples of diagrams

We discuss here some examples of different diagrams, as shown in Fig. 9, to illustrate the cluster expansion. Diagram 9.1 is a typical irreducible interacting diagram. The interaction between particles  $m$  and  $n$  is labeled with its operator dependence  $(ijk)_{mn}$ , while particles 1 and 2 are correlated to  $m$  and  $n$  by a number of central correlations, and exchanged with each other. Diagram 9.2 is also an irreducible interacting diagram representing a  $\nabla_m F_{mn}^c \cdot ik_m$  term. The operator correlations  $F_{m2}^{p>1}$ ,  $F_{n2}^{p>1}$  are also present and

labeled  $p_{m2}, p_{n2}$ , respectively. Both diagrams 9.1 and 9.2 are included in the class  $[A]$  of Eq. (4.16).

Diagram 9.3 is a connected, separable diagram of the type  $[\bar{A}\bar{a}]$ . Point 1 is an articulation point at which the diagram could be broken into two parts, so it is reducible. The correlation  $f_{12}^{p>1} f_{12}^{q>1}$  is labeled by  $(pq)_{12}$ , and the other operator-dependent correlations are labeled as usual; although the exchange carries operator dependence, often we do not label it. Diagram 9.3 arises strictly from the numerator of Eq. (4.1). The separated counterpart of 9.3 is shown in diagram 9.4 and is of type  $[\bar{A}][\bar{a}]$ . The interacting portion containing particles  $m, n, 1$  comes from the numerator of Eq. (4.1), but the separated portion with particles 1, 2 comes from the denominator. The  $C$  parts of the two separate pieces in diagram 9.4 are calculated independently, while the  $C$  part of 9.3 must be calculated all at once. In general these are different and thus the difference between  $[\bar{A}\bar{a}]$  and  $[\bar{A}][\bar{a}]$  is nonzero.

Some further examples of connected separable diagrams are shown in 9.5, 9.6, and 9.7. They are, respectively, of type  $[\bar{A}\bar{a}\bar{b}]$ ,  $[\bar{A}\bar{a}\bar{b}]$ , and  $[\bar{A}\bar{a}\bar{b}]$ .

#### D. Other cluster expansions

There are a number of other methods for obtaining the cluster expansion with noncommuting operators. Some of these are the power-series (PS) method of Fantoni and Rosati (1978), Owen's (1979a) generalization of the method of Gaudin, Gillespie and Ripka (GGR) (1971), and factorized cluster expansions such as those of Iwamoto and Yamada (1957) and van Kampen (1961). All these are presumably equivalent, as can be easily verified at the three-body cluster level.

The Iwamoto and Yamada and van Kampen methods are not diagrammatic, and it is much more laborious to obtain many-body cluster contributions with them than with the other methods. The method presented above is applicable to Bose, Fermi, or Boltzmann systems, whereas the PS and the GGR methods are primarily developed for Fermi systems.

In Fermi systems we may consider diagrams having two or more particles in the same momentum state. On considering all exchanges these will add up to zero; for example, the two diagrams 10.1 and 10.2 of Fig. 10 having two particles  $n$  and  $n'$  in state  $k_n$ , obviously cancel each other. The diagram 10.1 is essentially of type  $[\bar{I}][\bar{i}]$ , since  $n'$  is indistinguishable from  $n$ . When all diagrams of type 10.1 are added to the numerator, the term  $N_2$  becomes  $[I] \times [i]$ . By adding terms having up to three particles in a given  $k$  state we can convert  $N_3$  to  $\frac{1}{2}[I] \times [i][j]$ , etc. The denominator can then be canceled against all "disconnected" diagrams, as is done in the GGR and PS methods. The expectation value is given by the sum of all "connected" diagrams, but these now include reducible diagrams such as 10.3 and diagrams like 10.2 which superficially look like "improper" exchange diagrams but have nonzero contributions.

In the simple Jastrow theory the reducible diagrams are canceled by the nonzero "improper" exchange diagrams, and the resulting expansion is irreducible. However, in the presence of operator correlations,

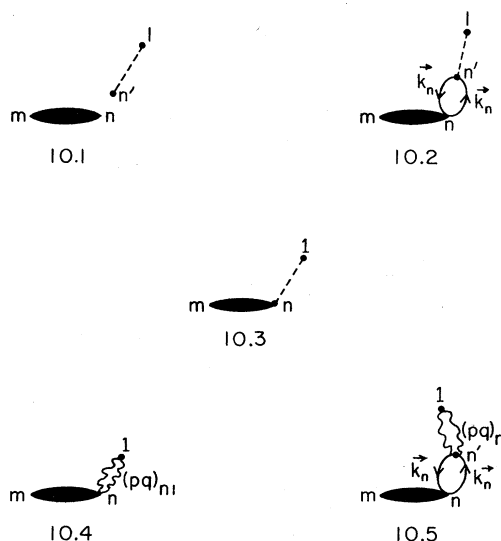


FIG. 10. Cancellation of diagrams violating the exclusion principle.

diagrams 10.4 and 10.5 do not cancel because the  $O_{n1}$  in 10.4 does not commute with  $O_{mn}$  as the  $O_{n'1}$  in 10.5 does. The  $C$  parts of 10.4 and 10.5 are different, and their sum is simply a term in the  $[\bar{A}\bar{a}] - [\bar{A}][\bar{a}]$  of Eq. (4.16).

#### V. CALCULATION OF $C$ PARTS

##### A. Operator diagrams

In this section we review some useful rules for calculating the  $C^i$  of  $\Pi^i O_{ab}^p$ . We give the rules for  $p=1, 6$ , but they are extendible to  $L \cdot S$  or other operators. The rules can be expressed most easily in terms of operator diagrams (OD) in which every particle  $a, b$  involved in the  $\Pi^i O_{ab}^p$  is represented by a point. Every operator  $O_{ab}^p$  is represented by a line  $ab$  labeled  $p$ . The OD corresponding to any regular diagram may be obtained simply by deleting all central correlations and putting in the appropriate number of lines for every operator-dependent leg, e.g., three lines for the interaction line  $f_{mn}^i X_{mn}^j f_{mn}^k$  labeled  $i, j$ , and  $k$ . The OD do not specify the order of operators in  $\Pi^i O_{ab}^p$ ; these must be considered explicitly if necessary.

A sample of the kinds of operator diagrams that we shall evaluate in this work is shown in Fig. 11. Diagram 11.1 is just the operator diagram for the direct two-body interaction, either by itself or with various central dressings added. It is the operator diagram appropriate to the full diagram 9.1. Similarly the OD 11.2 corresponds to diagram 9.2.

For an OD to have a nonzero  $C$  part, at least two operator lines must meet at each point. This is because single operators  $O_{ab}^{p>1}$  are linear in  $\sigma_a$  and/or  $\tau_a$ . If a point is connected to only one operator line, the sum over the spin and isospin coordinates at that point will vanish identically and the OD will give no contribution. If only two operator lines meet at a given point, they must be of the same "type" to give a nonzero  $C$  part. For the operators 2-6 there are only three types,

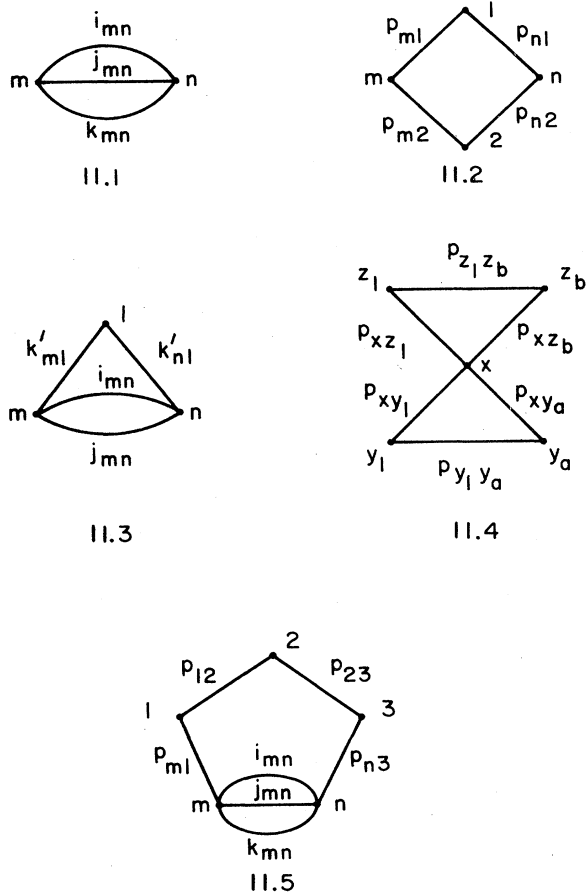


FIG. 11. Examples of operator diagrams.

which we denote as  $\sigma$ ,  $\tau$ , and  $\nu$ . They are linear in the  $\sigma_a$ ,  $\tau_a$ , and  $\sigma_a \tau_a$ , respectively. Obviously  $O^\sigma$  and  $O^i$  are  $\sigma$ -type,  $O^\tau$  is  $\tau$ -type, and  $O^{\sigma\tau}$  and  $O^{i\tau}$  are  $\nu$ -type.

Consider an operator diagram in which two points are joined by a pair of operator lines  $p_{12}, q_{12}$  and no other operator lines are present. This would be the OD corresponding to the separated, noninteracting piece of diagram 9.4. The  $C$  part of the product of these two operators is a simple constant  $A^p$ ,

$$C(O_{12}^p O_{12}^q) = A^p \delta_{pq}, \quad (5.1)$$

where  $A^p = 1, 3, 3, 9, 6, 18$  for  $p = 1, 6$ .

If three or more operator lines meet at a point, as in the OD 11.1, the  $C$  part may be easily evaluated with the  $K^{pq\tau}$  matrix defined as follows:

$$O_{ab}^p O_{ab}^q = \sum_r K^{pq\tau} O_{ab}^r. \quad (5.2)$$

Comparing Eqs. (5.1) and (5.2) we find that  $K^{pq1} = A^p \delta_{pq}$ . The  $C$  part of the OD 11.1 is then easily evaluated:

$$C(O_{mn}^i O_{mn}^j O_{mn}^k) = C\left(\sum_l K^{ijl} O_{mn}^l O_{mn}^k\right) = K^{ijk} A^k. \quad (5.3)$$

The  $K^{ijk}$  is particularly simple for the  $O^{p=1,6}$  because they form a closed set. If  $i, j \leq 6$ , then for  $k > 6$ ,

$K^{ijk} = 0$ . The order of operators in Eq. (5.3) does not matter, and we find trivially that  $K^{ijk} A^k = K^{jik} A^k = K^{kji} A^i$ , etc. This is simply because operators  $O^{p=1,6}$  between the same two points commute with each other. The values of  $K^{ijk}$  for  $i, j, k \leq 6$  are given in Table I.

## B. Single-operator rings

The order of operators in the  $\Pi^i O_{ab}^p$  is also unimportant for determining the  $C$  part if the operators form a single-operator ring (SOR) as in diagram 11.2 of Fig. 11. This case was first discussed by Pandharipande and Wiringa (1976). The ring may be arbitrarily large, but of course to get a nonzero  $C$  part all the operators must be of the same type. That the order is unimportant can be proved simply by noting that

$$C\{O^{(p12)} O^{(p23)} \cdots [O^{(pab)}, O^{(pbc)}] \cdots O^{(p(n-1)n)} O^{(pn1)}\} = 0. \quad (5.4)$$

Here we denote  $O_{ab}^{pab}$  as  $O^{(pab)}$  for convenience. The commutator in Eq. (5.4) will be linear in either  $\sigma_b$  or  $\tau_b$ , thus making the  $C$  part zero. Of course operators with completely different indices commute anyway, i.e.,  $[O_{ab}^p, O_{cd}^q] = 0$ . Thus in practice, if only two operators connect at a point  $b$ , they effectively commute for the purpose of calculating the  $C$  part.

Further, we can use the Pauli identity (4.4) to eliminate completely the operator dependence on point  $b$ . Let  $O_{ab}^p$  and  $O_{bc}^q$  be the only two operators meeting at  $b$ . Summing over spin and isospin states for particle  $b$ , and integrating over the azimuthal angle  $\phi$  of  $\mathbf{r}_{ab}$ , the product of operators  $O_{ab}^p O_{bc}^q$  reduces to a sum over operators  $O_{ac}^r$ :

$$\sum_{\sigma_b, \tau_b} \int d\phi_b O_{ab}^p O_{bc}^q = \sum_r \int d\phi_b \xi_{abc}^{pq\tau} O_{ac}^r. \quad (5.5)$$

The coefficients  $\xi_{abc}^{pq\tau}$  are functions of the inside angles of the triangle  $abc$ , and are zero unless the operators are of the same type:

$$\xi_{abc}^{\sigma\sigma\tau} = \delta_{\sigma\tau}, \quad (5.6)$$

$$\xi_{abc}^{\sigma\tau\tau} = \delta_{\tau\tau} \frac{1}{2} (3 \cos^2 \theta_c - 1), \quad (5.7)$$

$$\xi_{abc}^{\tau\sigma\tau} = \delta_{\tau\tau} \frac{1}{2} (3 \cos^2 \theta_a - 1), \quad (5.8)$$

$$\xi_{abc}^{\tau\tau\tau} = \delta_{\sigma\tau} (3 \cos^2 \theta_b - 1) + \delta_{\tau\tau} \frac{1}{2} [-9 \cos \theta_a \cos \theta_b \cos \theta_c - 3(\cos^2 \theta_a + \cos^2 \theta_b + \cos^2 \theta_c) + 2], \quad (5.9)$$

$$\xi_{abc}^{\tau\tau\tau} = \delta_{\tau\tau}. \quad (5.10)$$

The  $\xi_{abc}^{pq\tau}$  for  $p$  and  $q$  of type  $\nu$  are given by

$$\xi_{abc}^{(p\tau)(q\tau)(r\tau)} = \xi_{abc}^{pq\tau}; \quad p, q, r = \sigma, \tau. \quad (5.11)$$

The ability to thus reduce a product of two operators with a common point to just one operator and some simple radial dependence makes it very easy to calculate the  $C$  part for any SOR. Because the order of operators does not matter, we may simply arrange them in a continuous fashion, e.g.,  $O^{(pab)} O^{(pbc)} O^{(pcd)} \cdots$ , and then successively contract pairs of operators over their common points. Every contraction will give a  $\xi$  function, and eventually we reach the final two operators which must have both points in common. These give a final factor of  $A^p$ .





TABLE II. The matrix  $L^{ijk}$  for  $O^{p=1,6}$ .

$i$	$j$	1	2	3	4	5	6	$i$	$j$	1	2	3	4	5	6
$k=1$	1	1						$k=2$			3				
	2		3							3	6				
	3			3								9			
	4				9							9	18		
	5					6								-6	
	6						18								-18
$k=3$	1			3				$k=4$				9			
	2				9						9	18			
	3	3		6						9		18			
	4		9		18				9	18	18	36			
	5					18								-18	
	6						36							-18	-36
$k=5$	1					6		$k=6$							18
	2					-6									-18
	3						18							18	36
	4						-18							-18	-36
	5	6	-6			12					18	-18			36
	6			18	-18		36		18	-18	36	-36	36	36	72

It can be verified that either Eq. (5.17) or Eq. (5.18) is always true, and if both are true, the  $L^{ijk}$  and  $K^{ijk}$  are both zero. The values of  $L^{ijk}$  are given in Table II. Any diagram having a number of operator lines between two points, plus a single-operator chain (SOC) connecting the same two points, as in diagram 11.5, can have its  $C$  part expressed in terms of the matrices  $A$ ,  $K$ ,  $L$ , and  $\xi$ .

Diagram 11.4 is of interest because of the diagrammatic expansion (4.16). There we found that terms like  $[A\bar{a}] - [A][\bar{a}]$  must be calculated, and the OD 11.4 is representative of any separable diagram which has two SOR touching at the separable point. One ring will contain the interacting particles, one of which could be the common point, and the other will be noninteracting. We label these rings  $Y$  and  $Z$ , respectively, and the common point is  $x$ . The SOR  $Y$  in diagram 11.4 just contains  $x$ ,  $y_1$ , and  $y_a$ , but in general there could be many particles  $y_2, y_3$ , etc., forming a single-operator chain between  $y_1$  and  $y_a$ , or alternatively  $y_1$  and  $y_a$  could be the same point. Similarly, a general SOR for  $Z$  would contain  $x, z_1, \dots, z_b$ .

Although the spatial integrals of  $Y$  and  $Z$  are the same in both the connected ( $[A\bar{a}]$ ) and the separated ( $[A][\bar{a}]$ ) diagrams, the  $C$  parts can be different. For convenience we define the  $C$  part of a separable diagram to be the difference between the  $C$  parts of the connected and separated diagrams.

Let  $C_y$  and  $C_z$  denote the  $C$  parts of  $Y$  and  $Z$  when they are separated:

$$C_y = C \left\{ O^{(p_{xy_1})} \left[ \prod_{j=1, a-1} O^{(p_{y_j y_{j+1}})} \right] O^{(p_{y_a x})} \right\}, \quad (5.19)$$

$$C_z = C \left\{ O^{(p_{xz_1})} \left[ \prod_{j=1, b-1} O^{(p_{z_j z_{j+1}})} \right] O^{(p_{z_b x})} \right\}. \quad (5.20)$$

The  $C$  part of the separated diagram is  $C_y C_z$ . That of the unseparated diagram depends upon the order of the four operators  $O^{(p_{xy_1})}$ ,  $O^{(p_{y_a x})}$ ,  $O^{(p_{xz_1})}$ , and  $O^{(p_{z_b x})}$ , which meet at the common vertex  $x$ . We may successively sum over the spin and isospin of particles  $y_1, y_2, \dots, y_{a-1}$  and reduce the  $O^{(p_{xy_1})} \Pi_{j=1, a-1} O^{(p_{y_j y_{j+1}})}$  to a second operator  $O^{(p_{xy_a})}$  at the position of the operator  $O^{(p_{xy_1})}$ , with a coefficient  $C_y/A^{(p_{xy_a})}$ . [We write  $A^q$  as  $A(q)$  when  $q$  has subscripts.] Doing the reduction for  $Z$  also gives

$$C(\text{unseparated}) = [C_y C_z / A^{(p_{xy_a})} A^{(p_{xz_b})}] \times C[:O^{(p_{xy_a})} O^{(p_{y_a x})} O^{(p_{xz_b})} O^{(p_{z_b x})}:] \quad (5.21)$$

where the four operators between the  $::$  are to be taken in the order in which  $O^{(p_{xy_1})}$ ,  $O^{(p_{y_a x})}$ ,  $O^{(p_{xz_1})}$ , and  $O^{(p_{z_b x})}$  occur in the unseparated diagram.

The  $C[:O^{(p_{xy_a})} O^{(p_{y_a x})} O^{(p_{xz_b})} O^{(p_{z_b x})}:]$  has only two distinct values. The first equals  $A^{(p_{xy_a})} A^{(p_{xz_b})}$  and is obtained in the case of four possible "successive" orders in which two  $O^{(p_{xy_a})}$  and/or  $O^{(p_{xz_b})}$  occur successively and thus can be squared. In the remaining two "alternating" orders of type  $O^{(p_{xy_a})} O^{(p_{xz_b})} O^{(p_{y_a x})} O^{(p_{z_b x})}$  the  $C(:)$  may be expressed simply as a function of the symmetric matrix  $D_{ij}$ ,

$$\sum_{\sigma_c, \tau_c} O_{ac}^i O_{ab}^j O_{ac}^k = \delta_{ik} A^i (1 + D_{ij}) O_{ab}^j. \quad (5.22)$$

In the case of tensor operators the above equation as-

sumes an integration over the angle between  $\mathbf{r}_{ac}$  and  $\mathbf{r}_{ab}$ . The value of  $D_{ij}$  depends only on the types of operators involved:

$$\begin{aligned} D_{\sigma\tau} &= 0, \quad D_{\nu\nu} = -8/9, \\ D_{\sigma\sigma} &= D_{\tau\tau} = D_{\sigma\nu} = D_{\tau\nu} = -4/3. \end{aligned} \quad (5.23)$$

Thus the  $C(:)$  for alternating order equals  $(1 + D_{yz})A(p_{xy})A(p_{xz})$  where  $y$  and  $z$  are the types of operators in the SOR  $Y$  and  $Z$ .

The operators in  $C(:)$  can occur in various orders in the connected diagram. Let  $m$  be the probability of their occurring in the alternating order. The  $C$  part of the separable diagram is then given by  $m D_{yz} C_y C_z$ . For evaluating the expectation value (4.1) with the diagrammatic expansion (4.16), such separable diagrams may be treated as vertex corrections of magnitude

$$m D_{yz} \times \text{contribution of ring } Z, \quad (5.24)$$

to the SOR diagram  $Y$  at its vertex  $x$ .

As an example, we illustrate the calculation of  $m$  for the diagram 9.3 in the case where  $O(mn) = O(mn) = 1$ . The operators  $p_{12}$  and  $q_{12}$  associated with the  $f_{12}^{p>1} f_{12}^{q>1}$  must be identical or the  $C$  part will be zero. One  $O(p12)$  comes from  $\Psi^*$  and the other from  $\Psi$ , while  $O(n1)$  may come from either  $\Psi^*$  or  $\Psi$ . The  $O(p12)$  associated with the exchange occurs at the far left where the  $\Psi^*$  is antisymmetrized, while the interaction operator for particles  $m$  and  $n$ ,  $O(pmn)$ , must come in the middle. The possible operator orders are then obtained from:

$$\begin{aligned} &\frac{1}{2} O(p12) [\frac{1}{2} \{ O(p12), O(n1) \} O(pmn) O(p12) \\ &+ \frac{1}{2} O(p12) O(pmn) \{ O(p12), O(n1) \} ], \end{aligned} \quad (5.25)$$

where the outside factor  $\frac{1}{2}$  compensates for the factor 2 in the definition of  $F(n1)$ , and the other factors of  $\frac{1}{2}$  account for the normalization of SIF. By inspection of Eq. (5.25) the probability of alternating order  $m$  is  $\frac{1}{2}$  in this case.

In general  $m$  depends upon the source of the four operators that meet at the vertex  $x$ . The possible sources are the  $v$ ,  $F$ , and the exchange. The operator from  $v$  defines the center. An operator associated with a single wavy line  $F^{p>1}$  can be on either side of the center with equal probability. The two operators associated with a double wavy line  $f^{p>1} f^{q>1}$  must be on opposite sides of the center. An operator from the exchange must always appear on the extreme left, where  $\Psi^*$  is antisymmetrized.

The possible types of the common vertex  $x$  can be described by four variables,  $x_t$ ,  $x_y$ ,  $x_z$ , and  $x_q$ . The variable  $x_t$  specifies the operator elements of the interacting SOR at the common vertex:  $x_t = I$  if a  $v^t$  is connected at the vertex,  $x_t = f^2$  if a double wavy line  $f^{p>1} f^{q>1}$  connects at the vertex, and  $x_t = P$  otherwise. The variable  $x_q$  specifies the operator elements coming from the passive SOR, and it may be  $f^2$  or  $P$ . The  $m(x_t, x_y, x_z, x_q)$  is symmetric under interchange of  $x_t$  and  $x_q$ , except for the  $x_t = I$  case.

The  $x_y, x_z$  indicate whether exchange operators connected to the common vertex are present in either the  $Y$  or  $Z$  SOR. The possible cases are  $x_y, x_z = d, d$  for no exchange,  $d, e$  for an exchange in  $Z$  connected to the vertex, and  $e, d$  for an exchange in  $Y$ . The case  $x_y, x_z$

$= e, e$  cannot be treated as a vertex correction because the spatial parts do not factorize. There may also be cases where  $x$  is exchanged with some particle that is in neither SOR, for example the exchange between  $n$  and 1 in diagram 9.5 of Fig. 9. This "passive" exchange does not affect the operator order, but it prohibits other exchanges at the common point. For the case where the "passive" exchange is in a hypernet of the  $Y$  SOR, we add the category  $x_y, x_z = e, d$ . We can take care of "passive" exchanges in hypernets of the  $Z$  SOR without considering an  $x_y, x_z = d, e, p$  category explicitly.

The  $m(x_t, x_y, x_z, x_q)$  are given in Table III. There is no  $x_t, x_y = f^2, e$  because  $Y$  would not be an SOR, nor is the combination  $x_z, x_q = e, f^2$  allowed. The  $x_y = e, p$  values are the same as those for  $x_y = d$ , except that no  $x_z = e$  are present, since the "passive" exchanges do not affect the operator order.

For diagrams of the type  $[A \overline{a} b]$ , as in OD 9.5, we may define the  $C$  part to be that of the appropriate expression in curly brackets in Eq. (4.16):

$$\{ [A \overline{a} b] - [A \overline{a}] [b] - [A] [\overline{a} b] + [A] [\overline{a}] [b] \}. \quad (5.26)$$

All the terms in Eq. (5.26) have identical spatial integrals, but again the  $C$  parts vary. Let  $C_A$ ,  $C_a$ , and  $C_b$  be the  $C$  parts of the separated SOR in Eq. (5.26), where we again assume there is only one operator present in the interaction line in  $A$ . Let  $m_{Aa}$ ,  $m_{ab}$  be the appropriate probabilities for alternating order at vertices  $Aa$  and  $ab$ . Then it can be shown that

$$C([A] [\overline{a}] [b]) = C_A C_a C_b, \quad (5.27)$$

$$C([A \overline{a}] [b]) = C_A C_a C_b (1 + m_{Aa} D_{Aa}), \quad (5.28)$$

$$C([A] [\overline{a} b]) = C_A C_a C_b (1 + m_{ab} D_{ab}), \quad (5.29)$$

$$C([A \overline{a} b]) = C_A C_a C_b (1 + m_{Aa} D_{Aa}) (1 + m_{ab} D_{ab}), \quad (5.30)$$

and thus

$$C(5.26) = C_A C_a C_b m_{Aa} m_{ab} D_{Aa} D_{ab}. \quad (5.31)$$

Similarly, the  $C$  part of the diagrams of type  $[Aab]$  can be factorized to  $C_A C_a C_b m_{Aa} m_{Ab} D_{Aa} D_{Ab}$ . These results are valid for SOR in general, irrespective of the nature of the vertex, interacting or passive, and they allow contributions of separable diagrams in which there are only four operators at the articulation point to be treated as vertex corrections. When the articulation point has more than four operator lines present,

TABLE III. The  $m(x_t, x_y, x_z, x_q)$ .

$x_z, x_q =$	$d, f^2$	$d, P$	$e, P$
$m(I, d, x_z, x_q)$	1/2	1/3	1/4
$m(I, e, x_z, x_q)$	1	1/2	
$m(I, e_p, x_z, x_q)$	1/2	1/3	
$m(P, d, x_z, x_q)$	5/12	1/3	1/3
$m(P, e, x_z, x_q)$	1/2	1/3	
$m(P, e_p, x_z, x_q)$	5/12	1/3	
$m(f^2, d, x_z, x_q)$	1/2	5/12	1/2
$m(f^2, e_p, x_z, x_q)$	1/2	5/12	

these relations are no longer exact. Nevertheless the vertex corrections may still be a useful approximation.

## VI. FHNC/SOC EQUATIONS

### A. Single and hypernetted chains in Bose systems

A set of coupled integral equations that sums single chains of operator links and hypernetted chains of central links has been derived by Wiringa and Pandharipande (1978). These equations are a generalization of the FHNC equations of Fantoni and Rosati (1975), which in turn are themselves a generalization of the HNC equation for Bose systems of van Leeuwen *et al.* (1959).

Historically, equations to sum single chains of simple central links were developed first. Consider the diagrams having only  $F^c$  links shown in Fig. 12.1. The contribution of all single chains of  $F^c$  links to the expectation value  $\langle X \rangle$  of Eq. (4.1) can be expressed as

$$\langle X \rangle_{\text{single } F^c \text{ chains}} = \frac{A\rho}{2} \int F_{mn} X_{mn} F_{mn} G_{mn} d^3 r_{mn}, \quad (6.1)$$

$$G_{mn} = \Theta(F_{m1}^c; F_{1n}^c) + \Theta[F_{m1}^c; \Theta(F_{12}^c; F_{2n}^c)] + \Theta[F_{m1}^c; \Theta[F_{12}^c; \Theta(F_{23}^c; F_{3n}^c)]] + \dots, \quad (6.2)$$

$$\Theta(x_{ij}; y_{jk}) = \rho \int x_{ij} y_{jk} d^3 r_j. \quad (6.3)$$

$G_{mn}$  is called a chain function, and  $\Theta$  is an integral operator that connects elements to form chains. Chain functions satisfy the integral equation

$$G_{ik} = \Theta([\text{link}]_{ij}; [\text{link} + G]_{jk}), \quad (6.4)$$

and we can generalize the kind of chain by generalizing the link and the  $\Theta$  operator. For the simple chain approximation in Eq. (6.2), the link is obviously  $F^c$ .

For systems like liquid helium the single-chain (SC)

approximation is not adequate, because  $G^c$  is large, being of order unity at least to the radius of the core. In nuclear matter, however, the SC approximation may be good for the noncentral  $G^{>1}$  because they tend to be quite small ( $<0.1$  in  $v_6$  model throughout their range). For the large central links a better approximation is that of hypernetted chains.

Consider the two-particle distribution function  $g(r)$  defined by

$$g(r) = (1/A\rho) \langle \delta(r - r_{mn}) \rangle; \quad (6.5)$$

$\rho g(r)$  gives the probability of finding a particle at a distance  $r$  from a chosen particle. The diagrams for  $g_{mn}$  can be classified as composite, nodal, and elementary; examples of these are shown in diagrams 12.2, 12.3, and 12.4, respectively, of Fig. 12. Composite diagrams have more than one unconnected path between  $m$  and  $n$ . Nodal diagrams have one or more points through which all paths between  $m$  and  $n$  must pass. By definition all nodal diagrams are chains, and the section between any two nodal points are links, so links cannot contain nodal points. Diagrams that are neither composite nor nodal are elementary, and both composite and elementary diagrams can be links. If we let  $E_{mn}$  denote the sum of all elementary diagrams in the same sense that  $G_{mn}$  is a sum of nodal diagrams, then the exact distribution function  $g(r)$  in Bose fluids with simple central correlations is given by

$$g_{mn} = (f^c)_{mn}^2 \exp(G_{mn} + E_{mn}). \quad (6.6)$$

Expanding the exponential, we have

$$g_{mn}^{-1} = F_{mn}^c + G_{mn} + E_{mn} + F_{mn}^c (G_{mn} + E_{mn}) + \frac{1}{2} (G_{mn} + E_{mn})^2 + \dots = \sum_{\text{all}} (\text{links} + \text{chains})_{mn}. \quad (6.7)$$

Then the sum of all links is obviously just  $g_{mn} - 1 - G_{mn}$ , and substituting into Eq. (6.4) we have the exact relation

$$G_{mn} = \Theta([g - 1 - G]_{m1}; [g - 1]_{1n}), \quad (6.8)$$

in which  $E_{mn}$  is contained indirectly through Eq. (6.6). The  $G$  of Eq. (6.8) is a hypernetted chain, so called because of the many "nets" of correlations generated.

The  $E_{mn}$  in Eq. (6.6) is hard to calculate, and in general must be approximated. The simplest choice is to let  $E_{mn} = 0$ ; this is the HNC or hypernetted chain approximation. All composite and nodal diagrams that do not contain elementary diagrams are summed by HNC. It is thus the zeroth order of an expansion in elementary diagrams. (The HNC/4 approximation mentioned earlier includes the simplest elementary diagram, the four-point diagram in Fig. 12.4.)

### B. Modifications for Fermi systems

The generalization to Fermi systems (FHNC) requires the subdivision of  $G_{ik}$  into parts  $G_{xy, ik}$  in order to keep track of the exchange patterns. The  $xy$  labels indicate the nature of exchanges at the end points  $i$  and  $k$  of the chain;  $xy$  may be  $dd$ ,  $de$ ,  $ed$ ,  $ee$ , or  $cc$ . The subscript  $d$  stands for a "direct" end,  $e$  for an "exchange" end, and  $c$  for a "circular" exchange end.  $G_{dd, ik}$  thus denotes

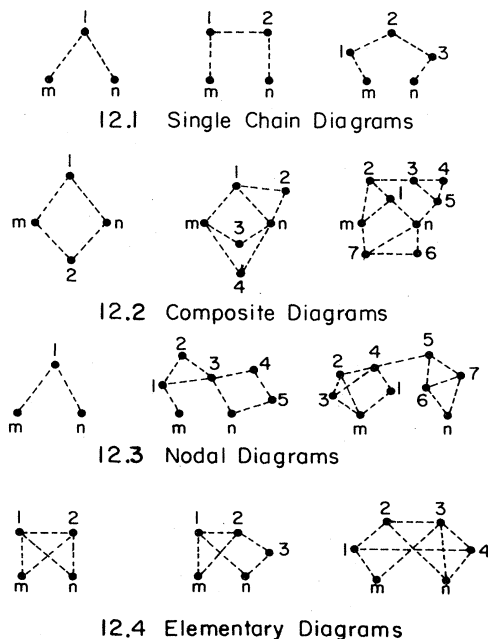
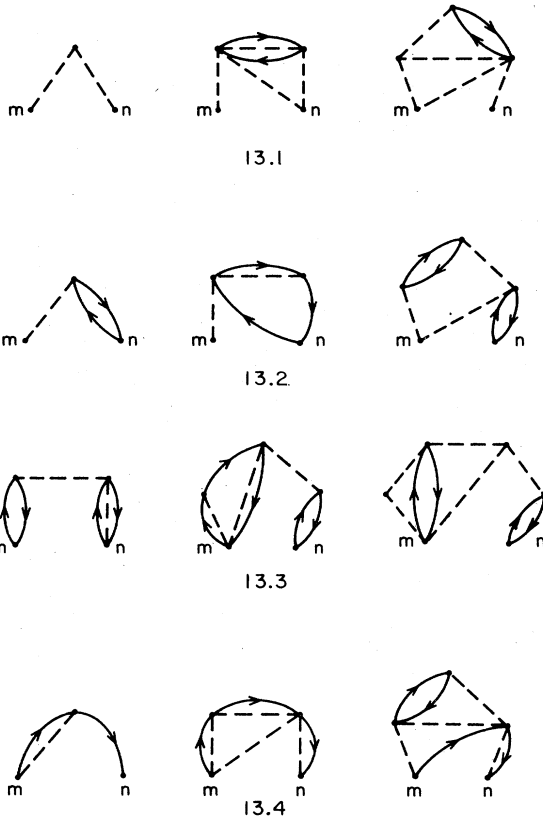


FIG. 12. An illustration of the classification of diagrams with a Bose liquid having Jastrow correlations.


 FIG. 13. Examples of diagrams contributing to the  $G_{xx}^c$ .

the sum of all chains in which neither  $i$  nor  $k$  is exchanged.  $G_{de, ik}$  is the sum of chains in which  $k$  is exchanged with particles in the chain, and  $i$  is not.  $G_{ed, ik}$  just reverses the roles of  $i$  and  $k$  and is numerically equal to  $G_{de, ik}$ . Chains that contribute to  $G_{ee, ik}$  have both  $i$  and  $k$  exchanged in independent exchange loops contained in the chains, while chains with an incomplete exchange loop passing through both  $i$  and  $k$  are included in  $G_{cc, ik}$ . Examples of  $dd$ ,  $de$ ,  $ee$ , and  $cc$  chains are given in Fig. 13, diagrams 13.1–13.4. The generalized links that enter Eq. (6.4) are designated  $X_{xy, ik}$ , and have the same exchange classification. However, since a link can be composite, the  $X_{ee, ik}$  can have both  $i$  and  $k$  exchanged in the same loop, or in two independent loops within the link.

The end points labeled  $d$ ,  $c$ , and  $e$  in chains have zero, one, and two exchange lines, respectively. Since any point in a diagram must have either zero or two exchange lines, we can join  $X_{xx', ij}$  with  $X_{y'y, jk}$  or  $G_{y'y, jk}$  at  $j$  only in the combinations  $x'y' = dd, de, ed, cc$ . For  $xy = dd, de, ee$ , the Fermi chain equations become

$$G_{xy, ik} = \sum_{x', y'} \Theta(X_{xx', ij}; [X + G]_{y'y, jk}), \quad (6.9)$$

where the sum is over  $x'y' = dd, de, ed$ . The links  $X_{xy}$  are given by

$$X_{dd} = f^{c^2} \exp(G_{dd}) - 1 - G_{dd}, \quad (6.10)$$

$$X_{de} = f^{c^2} G_{de} \exp(G_{dd}) - G_{de}, \quad (6.11)$$

$$X_{ee} = f^{c^2} (G_{de}^2 + G_{ee} - L^2/s) \exp(G_{dd}) - G_{ee}, \quad (6.12)$$

where

$$L = -l + sG_{cc}, \quad (6.13)$$

is a generalized Slater function that includes the  $G_{cc}$  chain, and  $s$  is the degeneracy factor ( $s = 4$  for nuclear matter). The  $G_{cc}$  chain equation is

$$G_{cc, ik} = \Theta(X_{cc, ij}; [X_{cc} + L/s]_{jk}), \quad (6.14)$$

$$X_{cc} = f^{c^2} L \exp(G_{dd})/s - L/s. \quad (6.15)$$

The  $X_{xy}$  can be constructed by considering the possible elements  $F^c$  and  $l$  and how they may be joined with the  $G_{xy}$  to form composite diagrams that have the proper exchange character.

The chain equations (6.9) are different, but hopefully more transparent than those given by Fantoni and Rosati. Schmidt (1978) has demonstrated that the two versions are exactly equivalent.

### C. Operator chains

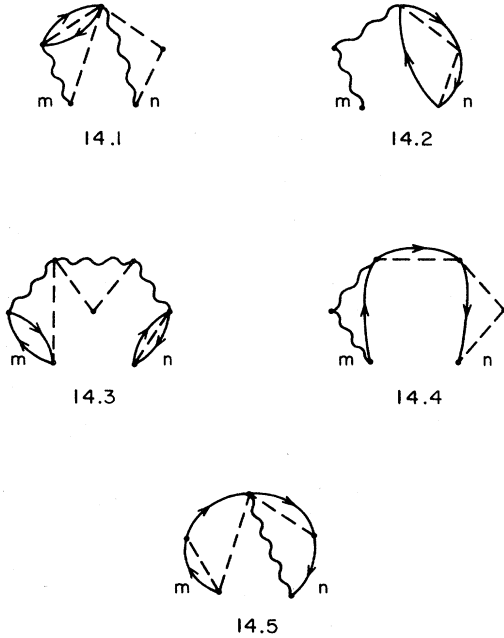
In nuclear matter the chain functions become  $G_{xy, ik}^p$  where  $p$  denotes the operator dependence associated with the chain. The  $G_{xy, ik}^{p>1}$  can be easily calculated in the single-operator chain (SOC) approximation, where each link can contain only one operator element or chain, but may have additional central dressings. (For the remainder of this section,  $p = 2, 6$  unless explicitly stated otherwise.)

Examples of  $G_{dd}^p$ ,  $G_{de}^p$ , and  $G_{ee}^p$  are shown in Fig. 14, diagrams 14.1–14.3. Because all exchange links but one in an exchange loop carry operator dependence, we cannot have any correlation operator links in a closed exchange loop contained within the SOC. For an incomplete circular exchange chain, there is one “gap” in the operator diagram which may be filled with either an  $F^p$  or  $G_{dd}^p$  to obtain an SOC. It is convenient to separate  $G_{cc}^p$  into two parts,  $G_{ca}^p$  and  $G_{cb}^p$  (diagrams 14.4 and 14.5), which have the  $F^p$  or  $G_{dd}^p$  in the first and last links, respectively. A  $G_{cc}^p$  chain with an  $F^p$  or  $G_{dd}^p$  somewhere in the middle is more easily treated as a  $G_{cc}^c$  with an independent SOC in the middle (diagram 16.4).

The contribution of separable diagrams, whose articulation points are at the nodes of the SOC, can be included in the  $G_{xy}^p$  as vertex corrections  $M(t_p, x_t, x_y)$ . The  $t_p$  denotes the chain type,  $x_t$  is  $P$  or  $f^2$  within a chain, and  $x_y$  can be  $d$ ,  $e$ , or  $e_p$ , depending upon the exchange nature of the vertex. The  $M(t_p, x_t, x_y)$  are related to the  $m(x_t, x_y, x_d, x_e)$  of Table III (exact relations are given below), and we find in practice that  $M(t_p, P, e) \approx M(t_p, P, e_p) \approx M(t_p, f^2, e_p)$  generally within 1%. The  $M(t_p, P, d)$  and  $M(t_p, f^2, d)$  differ somewhat more, perhaps 5% from each other and 15% from the  $e, e_p$  cases. It is possible to write chain equations that treat the  $M(t_p, x_t, x_y)$  exactly, but they are far more complicated than necessary. In the equations below we shall simply denote the  $(P, e)$ ,  $(P, e_p)$ , and  $(f^2, e_p)$  vertex corrections by  $M_e^p$  and the  $(P, d)$  and  $(f^2, d)$  by  $M_d^p$ .

Defining the direct functions,

$$h^p = F^p + f^{c^2} G_{dd}^p, \quad (6.16)$$

FIG. 14. Examples of diagrams contributing to the  $G_{xx}^{p=2}$ .

$$h^c = \exp(G_{dd}^c), \quad (6.17)$$

the  $dd$ ,  $de$ , and  $ee$  links are given by

$$X_{dd}^p = h^p h^c - G_{dd}^p, \quad (6.18)$$

$$X_{de}^p = (h^p G_{de}^c + f^c G_{de}^p) h^c - G_{de}^p, \quad (6.19)$$

$$X_{ee}^p = (h^p [G_{de}^c + G_{ee}^c] + f^c [-(L^2/4)\Delta^p + G_{ee}^p + 2G_{de}^p G_{de}^c]) h^c - G_{ee}^p, \quad (6.20)$$

where  $\Delta^p = 1$  for  $p=1, 4$  and zero otherwise. The  $\xi_{ijk}^{pq\tau}$  needed to join operator links can be included in the  $\Theta$  function:

$$\Theta_{ijk}^{pq\tau}(x_{ij}^p; y_{jk}^q) = \rho \int \xi_{ijk}^{pq\tau} x_{ij}^p y_{jk}^q d^3 r_j. \quad (6.21)$$

The SOC equations for  $xy = dd$ ,  $de$ , and  $ee$  are then

$$G_{xy, ik}^r = \sum_{x', y'} \sum_{p, q} \Theta_{ijk}^{pq\tau}(X_{xx', ij}^p; [X + G]_{y', y, jk}^q) M_{x'}^r, \quad (6.22)$$

where the vertex correction subscript  $z = d$  for  $x'y' = dd$ , and  $z = e$  for  $x'y' = de$  or  $ed$ . For the circular exchange chains we need the links

$$X_{cx=aa, b}^p = (h^p M_e^p L/4 + f^c G_{cx}^p) h^c - G_{cx}^p, \quad (6.23)$$

$$X_{cc}^p = (f^c h^c - 1) L/4. \quad (6.24)$$

The  $X_{cx}^p$  can come only at an end specified by  $x = a, b$  in the integral equation, while other links in  $G_{cx}^p$  are given by the  $X_{cc}^p$ . Since there is only one  $F^p$  or  $G_{dd}^p$  link, there is only one point at which the vertex correction should be applied, which is done in Eq. (6.23). We find

$$G_{ca, ik}^r = \sum_{p, q} \Theta_{ijk}^{pq\tau}(X_{ca, ij}^p; \Delta^q [X_{cc}^c + L/4]_{jk}), \quad (6.25)$$

$$G_{cb, ik}^r = \sum_{p, q} \Theta_{ijk}^{pq\tau}(\Delta^p X_{cc}^c; [X + G]_{cb, jk}^q), \quad (6.26)$$

$$G_{cc, ik}^r = G_{ca, ik}^r + G_{cb, ik}^r. \quad (6.27)$$

Every nodal point in  $G_{xy}^p$  is vertex corrected, but not the end points. Terms linear in  $[M(t_p, x_t, x_y) - 1]$  sum once-separable diagrams like 9.3, while quadratic and higher-order terms sum diagrams like 9.6. Diagrams which have three or more SOR touching at the same point, as in 9.7, are neglected. The exact expression for  $M$  is

$$M(t_p, x_t, x_y) = 1 + \sum_{r=2,6} D_{t_p t_r} \times \sum_{x_z, x_q} m(x_t, x_y, x_z, x_q) J^r(x_y, x_z, x_q). \quad (6.28)$$

The  $J^r(x_y, x_z, x_q)$  represent contributions of the passive SOR. If  $x_y = d$ , these SOR can have an exchange at the articulation point, but if  $x_y = e$ , they cannot. Thus we have the classification:

$$J^r(d, d, f^2) = \rho A^r \int d^3 r f^{r^2} h^c \times [(1 + G_{de}^c) M_d^r + (G_{de}^c + G_{de}^{c^2} + G_{ee}^c) M_e^r], \quad (6.29)$$

$$J^r(e, d, f^2) = \rho A^r \int d^3 r f^{r^2} h^c (M_d^r + G_{de}^c M_e^r), \quad (6.30)$$

$$J^r(d, d, P) = \frac{1}{2} \rho A^r \int d^3 r F^r h^c \{ G_{dd}^r [(1 + G_{de}^c) M_d^r + (G_{de}^c + G_{de}^{c^2} + G_{ee}^c) M_e^r] + G_{de}^r (1 + G_{de}^c) M_e^r \}, \quad (6.31)$$

$$J^r(e, d, P) = \frac{1}{2} \rho A^r \int d^3 r F^r h^c \{ G_{dd}^r [M_d^r + G_{de}^c M_e^r] + G_{de}^r M_e^r \}, \quad (6.32)$$

$$J^r(d, e, P) = -\frac{1}{4} \rho A^r \int d^3 r h^r h^c L^2 M_e^r. \quad (6.33)$$

Examples of the  $J^r(x_y, x_z, x_q)$  are shown in Fig. 15, diagrams 15.1, 15.6 with  $(x_y, x_z, x_q) = dd f^2, ed f^2, dd P, ed P$ , and two examples of  $de P$ , respectively. The articulation point is denoted by  $n$ . The  $J^r$  themselves contain vertex corrections (but not at the articulation point) both explicitly and self-consistently through the chain functions in their definitions. Thus diagrams like 9.5 are also summed. Typical values for  $M(t_p, x_t, x_y)$  are given in Table IV.

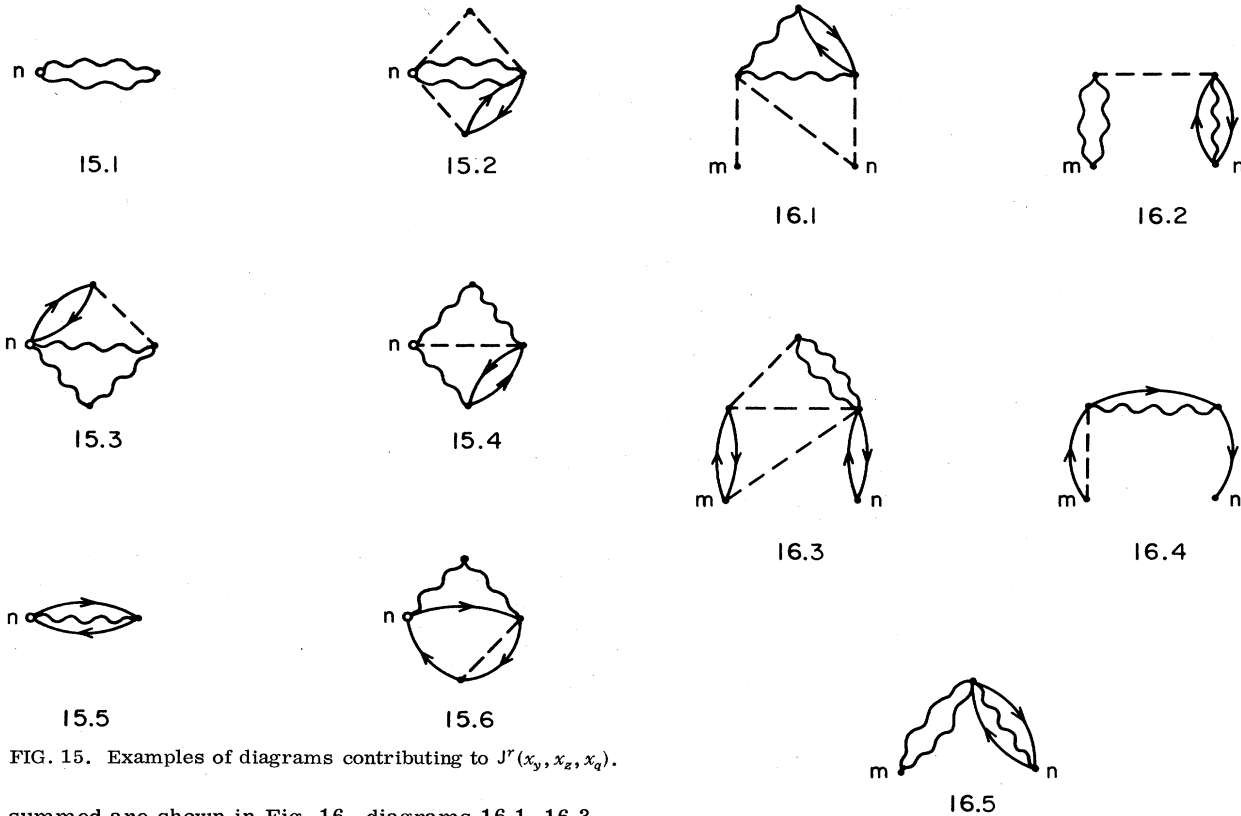
The  $G_{xy, ik}^r$  continue to be calculated in the FHNC approximation, but the links may now contain closed SOR. The  $dd$ ,  $de$ , and  $ee$  links become

$$X_{dd}^c = \left\{ f^{c^2} + \sum_p A^p M_e^{p^2} (f^{p^2} + h^p G_{dd}^p) \right\} h^c - 1 - G_{dd}^c, \quad (6.34)$$

$$X_{de}^c = \left\{ f^{c^2} G_{de}^c + \sum_p A^p M_e^{p^2} [(f^{p^2} + h^p G_{dd}^p) G_{de}^c + h^p G_{de}^p] \right\} h^c - G_{de}^c, \quad (6.35)$$

$$X_{ee}^c = \left\{ f^{c^2} (G_{de}^c + G_{ee}^c - L^2/4) + \sum_p A^p M_e^{p^2} [(f^{p^2} + h^p G_{dd}^p) (G_{de}^c + G_{ee}^c) + h^p (G_{ee}^p + 2G_{de}^p G_{de}^c - L^2 \Delta^p/4) + f^{c^2} (G_{de}^{p^2} - 2G_{cc}^p L \Delta^p/M_e^p)] \right\} h^c - G_{ee}^c, \quad (6.36)$$

and Eq. (6.9) is still used to calculate these chains. Examples of the new diagrams containing SOR that are


 FIG. 15. Examples of diagrams contributing to  $J^r(x_y, x_z, x_q)$ .

summed are shown in Fig. 16, diagrams 16.1–16.3. The circular exchange chains are also modified to include diagrams like 16.4. The  $G_{cc}^c$  equation becomes

$$G_{cc, ik}^c = \Theta \left( X_{cc, ij}^c; \left[ X_{cc}^c + L/4 + \sum_p A^p \Delta^p M_e^p f^{c^2} h^c G_{ca}^p \right]_{jk} \right) + \Theta \left( \left[ \sum_p A^p \Delta^p M_e^p (f^{c^2} h^c - 1) G_{cb}^p \right]_{ij}; \left[ X_{cc}^c + L/4 \right]_{jk} \right). \quad (6.37)$$

Each closed SOR in the links needs two vertex corrections for where the ends of the  $f^p$ ,  $F^p$ , and  $G_{xy}^p$  are joined. They could be either direct or exchange, depending upon how the link is connected to other links. For simplicity, we use  $M_e^p$  throughout, since in practice the chains with exchange links give the largest contribution.

The above  $G_{xy}^c$  equations will generally count diagrams like 16.5, having touching SOR's, with a wrong  $C$  fac-

 TABLE IV. The  $M(t_p, x_t, x_y)$  for the Reid  $v_6$  model at  $k_F = 1.6 \text{ fm}^{-1}$ ,  $d = 2.25 r_0$ ,  $\beta_{\sigma\tau} = 0.4$ ,  $\beta_{t\tau} = 1$ .

$t_p$	$\sigma$	$\tau$	$\nu$
$M(t_p, I, d)$	0.881	0.881	0.909
$M(t_p, I, e)$	0.890	0.893	0.924
$M(t_p, I, e_p)$	0.945	0.947	0.963
$M(t_p, P, d)$	0.870	0.869	0.898
$M(t_p, P, e)$	0.945	0.947	0.963
$M(t_p, P, e_p)$	0.955	0.956	0.969
$M(t_p, f^2, d)$	0.818	0.817	0.856
$M(t_p, f^2, e_p)$	0.946	0.948	0.963

 FIG. 16. Examples of  $G_{xx}^c$  diagrams containing closed SOR's.

tor because the commutators are neglected. The biggest SOR elements, however, turn out to be the exchange ones, such as on the right side of diagram 16.5, and since exchanges are prohibited from touching anyway, the miscounting is probably not serious. The effect of modifying the  $G_{xy}^c$  to include SOR is relatively small ( $< 1 \text{ MeV}$ ).

The most important chains in nuclear matter are the  $\nu$ -type chains,  $G_{xy}^{\sigma\tau}$  and  $G_{xy}^{t\tau}$ . The largest of these are the  $xy = dd$  and  $de$  chains shown in Fig. 17. They appear to be small, but their effect is not because (i) they are often multiplied by  $A^p$ , which is 9 for  $\sigma\tau$  and 18 for  $t\tau$ ; (ii) they are long ranged ( $r^2 G_{xy}^{\nu}$  peaks  $\approx 2 r_0$ ), so their integrals are significant; (iii) the  $\nu^{\sigma\tau}$  and  $\nu^{t\tau}$  dominate the long-range part of the  $NN$  interaction. The chains should therefore be calculated carefully, and truncation of the chain summation at three- or four-body level is not justified because some of the  $G^p$  are of the order of  $F^p$ . However, the small magnitude of the  $F^p$  and  $G^p$  suggest that the SOC approximation is valid. Every multiple-operator chain diagram containing a given number of nodal points is smaller by at least a factor of  $G^p$  or  $F^p$  than a similar SOC diagram.

The central  $G_{xy}^c$  chains are shown in Fig. 18. The necessity of the central correlation hypernets is evident from the large magnitude of  $G_{dd}^c$ , particularly at short distances. The  $G_{dd}^c$  is always exponentiated, and it gives about a 15% boost to two-body functions at  $r \approx r_0$ . It is added to every diagram, since it is purely direct. The  $G_{de}^c$  is also important, being fairly long ranged due to

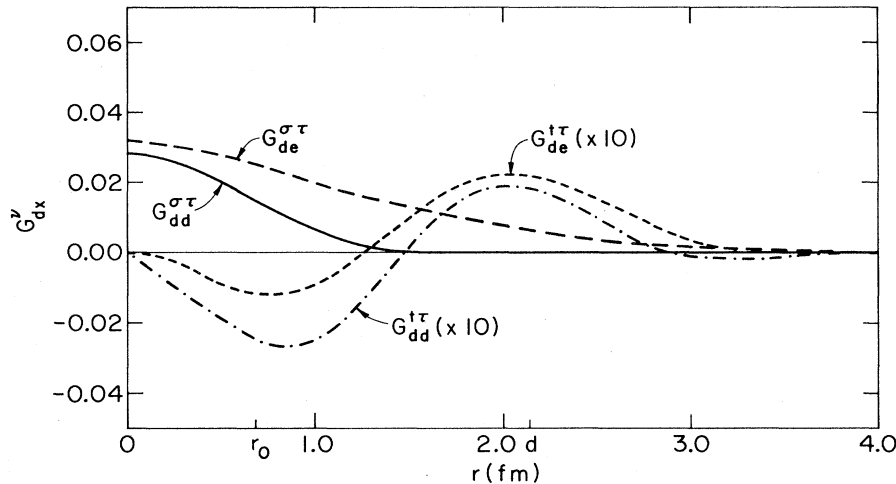


FIG. 17. The functions  $G_{dx}^{\sigma\tau}(r)$  at  $k_F = 1.6 \text{ fm}^{-1}$ ,  $d = 2.25r_0$ ,  $\beta_i = 1$ , in the Reid  $v_8$  model.

the exchange leg. It frequently has an accompanying factor of 2 when it is used (to count both  $de$  and  $ed$  cases) and can make  $>5\%$  contributions out to  $r = d$ . The  $G_{cc}^c$  is also important, despite its apparent small size, because it appears with a factor of 4 in the generalized Slater function  $L$  of Eq. (6.13), and can make a modification of  $\approx 10\%$  to  $l$  out to large distances. Only the  $G_{ee}^c$  is relatively unimportant, which is understandable in view of the fact its leading term is a four-body one, as opposed to three-body terms in the other  $G_{xy}^c$ .

## VII. CALCULATION OF ENERGY

The energy expectation value is expressed as a sum of five terms,

$$E/A = T_F + W + W_F + U + U_F, \quad (7.1)$$

according to the different parts of  $\Psi$  that the Hamiltonian (1.9) acts upon. When  $\nabla_m^2$  operates only on  $\phi_m$  we get the Fermi gas energy  $T_F = 0.3\hbar^2 k_F^2/m$ . The other terms must be evaluated through the diagrammatic cluster expansion. The  $W$  includes the potential energy and kinetic energy terms having  $\nabla_m^2 F_{mn}$ . It is given by the sum of all diagrams having the interaction line, as in diagram 7.5, containing the operator  $H_{mn}$ ,

$$H_{mn}^c = -(\hbar^2/m)\nabla_{mn}^2 + v_{mn}^c, \quad H_{mn}^{p>1} = v_{mn}^p, \quad (7.2)$$

plus two  $F_{mn}$ , with the  $\nabla_{mn}^2$  in  $H_{mn}$  operating only on the  $F_{mn}$ . The  $U$  represents the sum of kinetic energy terms  $\nabla_m F_{mn} \cdot \nabla_m F_{no}$  ( $o \neq n$ ). Its diagrams have two derivative lines of type 7.6–7.8. Kinetic energy terms  $\nabla_m F_{mn} \cdot \nabla_m \phi_m$  are counted in the  $W_F$  and  $U_F$ . As mentioned in Sec. IV, they contribute only when particle  $m$  is exchanged, and thus  $U_F$  or  $W_F$  diagrams have a derivative exchange line and a  $\nabla_m F_{mn}$  line. If the exchange pattern of the diagram is such that a  $\nabla_m l_{mn}$  element appears, the diagram is included in  $W_F$ , whereas those having a  $\nabla_m l_{mo}$  element contribute to  $U_F$ .

### A. Calculation of $W$

The interaction energy  $W$  is the sum of all diagrams with the interaction line  $f_{mn}^i H_{mn}^j f_{mn}^k$ . In the FHNC/SOC approximation it may be subdivided into four parts (Wiringa and Pandharipande, 1979),

$$W = W_0 + W_s + W_c + W_{cs}. \quad (7.3)$$

$W_0$  is the sum of all diagrams that do not have an operator chain connecting points  $m$  and  $n$ . Central correlation chains do not affect the operator algebra, and

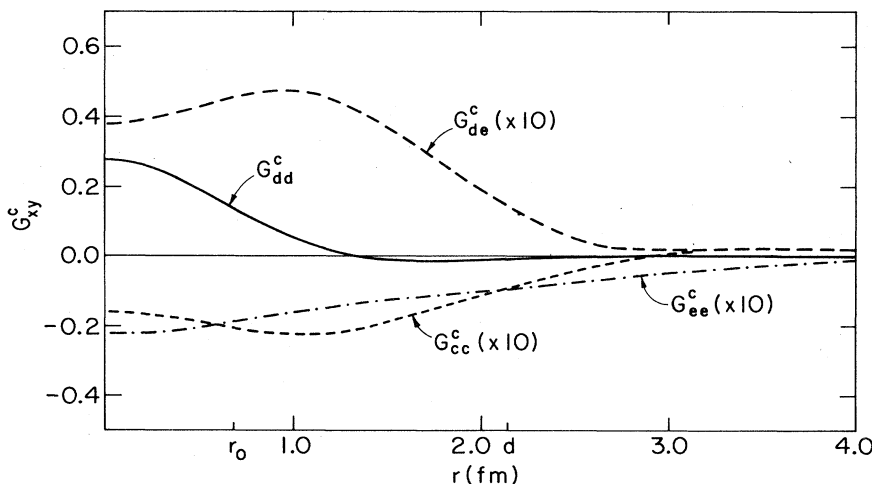


FIG. 18. The functions  $G_{xy}^c(r)$  at  $k_F = 1.6 \text{ fm}^{-1}$ ,  $d = 2.25r_0$ ,  $\beta_i = 1$ , in the Reid  $v_8$  model.



there may be any number of them in a  $W$  diagram of any class.  $W_c$  diagrams have one SOC connecting  $m$  and  $n$  in addition to the interaction line, while  $W_s$  has a reducible SOR at either vertex  $m$  or  $n$ . The  $W_{cs}$  diagrams have both an SOC between  $m$  and  $n$ , and an SOR at  $m$  or  $n$ . This classification is illustrated in Fig. 19, diagrams 19.1–19.4. Diagrams such as 19.5 (19.6) are included in  $W_c$  ( $W_s$ ) through the vertex corrections to the chain functions  $G_{xx'}^{I\Delta 1}$ , as discussed in Sec. VI. Diagrams like 19.7 are also included approximately in the equations for  $W_s$  and  $W_{cs}$ , but diagrams like 19.8 have so far been neglected, along with diagrams with two or more SOC connecting  $m$  and  $n$ .

The expressions for  $W_0$ ,  $W_c$ , and  $W_s$  can be derived easily with the use of the various matrices defined in Sec. V.  $W_{cs}$  is more difficult to calculate, but it is small, and a relatively simple approximation, which is physically reasonable and numerically accurate, may be used to estimate it.

The  $W_0$  is given by

$$W_0 = \frac{\rho}{2} \int d^3r f^i H^j f^k h^c [(1 + G_{de}^c)^2 + G_{ee}^c] K^{ijk} A^k - \frac{\rho}{8} \int d^3r f^i H^j f^k h^c L^2 \Delta^n K^{nim} K^{jkm} A^m. \quad (7.4)$$

We assume a summation over all indices  $i, j, k, m, n, \dots$

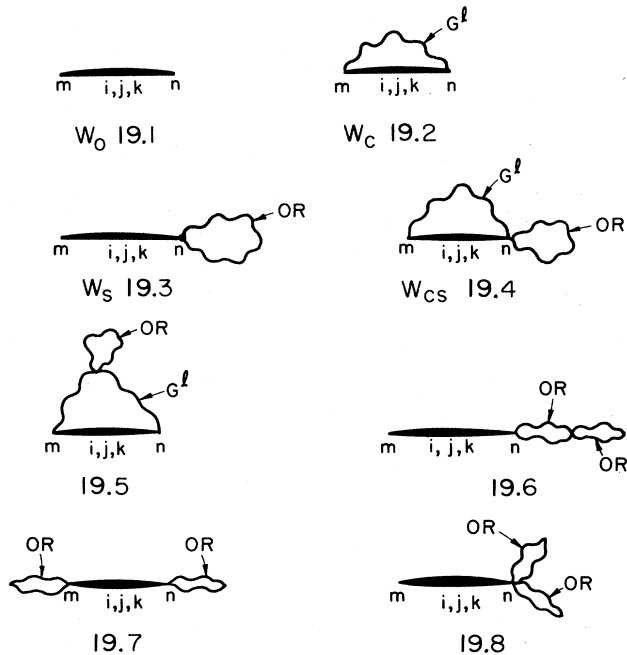


FIG. 19. Classification of  $W$  diagrams. The diagrams may contain any number of hypernetted central correlation chains that are not shown; neither are the exchanges shown explicitly. Only the positions of operator chains,  $G^l$ , and operator rings, OR, are shown.

from 1 to 6 unless otherwise indicated. The first term of Eq. (7.4) includes the interaction line plus all possible central dressings in which the interacting particles are not in a common exchange loop. The second term counts those diagrams in which  $m$  and  $n$  are in the same exchange loop. In the first term there are three operators between the same two points, giving a  $C$  part of  $K^{ijk} A^k$ . In the second term there is an additional operator  $O_{mn}^{n\leq 4}$  from the exchange, and an intermediate summation variable  $m$  is required.

In the calculation of  $W_c$  we have to keep track of the order of operators  $O_{mn}^i$ ,  $O_{mn}^j$ , and  $O_{mn}^k$  from the  $(fHf)_{mn}$ , and  $O_{ma}^i$  and  $O_{nb}^j$  from the SOC  $G_{xx',mn}^{I\Delta 1}$ , and possibly an exchange operator  $O_{mn}^{n\leq 4}$ . The positions of  $O_{ma}^i$  and  $O_{nb}^j$  depend upon whether these operators come from the correlations  $F_{ma}$ ,  $F_{nb}$ , or exchanges  $e_{ma}$ ,  $e_{nb}$ . It is thus necessary to divide  $W_c$  into parts  $W_c(xx')$  which give the contribution of  $G_{xx'}^{I\Delta 1}$  to  $W_c$ .

Let us consider  $W_c(dd)$  and abbreviate the operators  $O_{mn}^i$ ,  $O_{mn}^j$ ,  $\dots$  by  $i, j, \dots$ . The  $W_c(dd)$  diagrams represent terms in  $W_c$  that include  $F_{ma}^{i'} F_{nb}^{j'} f_{mn}^i H_{mn}^j f_{mn}^k$ , and the operators occur in order:

$$\begin{aligned} & \frac{1}{4} \left[ \frac{1}{4} \{i, l'\} j \{k, l''\} + \frac{1}{4} \{i, l''\} j \{k, l'\} \right. \\ & + \frac{1}{6} (\{l', l''\}, i) + l' i l'' + l'' i l' j k \\ & \left. + \frac{1}{6} i j (\{k, l'\}, l'') + l' k l'' + l'' k l' \right]. \end{aligned} \quad (7.5)$$

There is an overall  $1/4$  which compensates for the factor two in the definition of  $F_{ma}^{i'} (= 2f_{ma}^{i'} f_{ma}^c)$  and  $F_{nb}^{j'} (= 2f_{nb}^{j'} f_{nb}^c)$ . The first (second) term in (7.5) has  $f_{ma}^{i'}$  in  $\Psi^*$  ( $\Psi$ ) and  $f_{nb}^{j'}$  in  $\Psi$  ( $\Psi^*$ ); the  $1/4$  in these terms comes from the normalization of symmetrized products  $S(F_{ma} F_{mn})$  and  $S(F_{nb} F_{mn})$ . The third (fourth) term of (7.5) has both  $f_{ma}^{i'}$  and  $f_{nb}^{j'}$  in  $\Psi^*$  ( $\Psi$ ) and the  $1/6$  is the normalization of  $S(F_{ma} F_{nb} F_{mn})$ . All other correlation and exchange operators that occur in the SOC between points  $a$  and  $b$  are omitted from (7.5) because their order is immaterial.

The possible orders of the operators  $i, j, k, l', l''$  in  $W_c(dd)$  diagrams, and the probability of their occurrence are obtained from (7.5) and shown in Table V. It is not necessary to differentiate between orders such as  $il'jkl''$  and  $il''jkl'$  because interchanging the positions of  $l'$  and  $l''$  leaves the  $C$  part invariant. If the interacting particles are exchanged with each other, the  $W_c(dd)$  diagram has an additional  $O_{mn}^{n\leq 4}$  that appears at the extreme left, and is not explicitly shown in the table.

The  $C$  part for any  $W_c$  diagram can be written as a product of the  $\xi$  functions, which are built into the definition of  $G_{xx'}^{I\Delta 1}$  and are independent of the operator order, and a coefficient depending on the order of  $i, j, k, l', l''$  which can be constructed from the  $A$ ,  $K$ , and  $L$  matrices. This coefficient is also exhibited in Table V for each operator order in both direct and exchange cases. The result for  $W_c(dd)$  is

$$\begin{aligned} W_c(dd) = & \frac{\rho}{2} \int d^3r f^i H^j f^k G_{dd}^{I\Delta 1} h^c [(1 + G_{de}^c)^2 + G_{ee}^c] \frac{1}{24} (11K^{ijm} K^{klm} A^m + 5K^{ijm} L^{klm} + 5K^{jkm} L^{ilm} + 3K^{ikm} L^{jlm}) \\ & - \frac{\rho}{8} \int d^3r f^i H^j f^k G_{dd}^{I\Delta 1} h^c L^2 \left[ \frac{1}{8} (K^{jkm} K^{nim'} L^{m'lm} + K^{ijm} K^{mkm'} L^{nim'} + K^{knm} K^{im'} L^{jlm'} + K^{ijm} K^{knm'} L^{m'lm}) \right. \\ & \left. + \frac{1}{12} (4K^{nim} K^{ijm'} K^{mm'} A^k + K^{jkm} K^{mm'} L^{ilm'} + K^{nim} K^{ijm'} L^{klm'}) \right]. \end{aligned} \quad (7.6)$$

TABLE V. Operator orders in  $W_c(dd)$  diagrams.

No.	Operator order	Probability	Direct	Exchange
1	$il'jkl''$	1/8	$K^{ikm}L^{ilm}$	$K^{ikm}K^{nim'}L^{m'lm}$
2	$l'ijkl''$	1/8	$A^mK^{ijm}K^{klm}$	$K^{ijm}K^{mkm'}L^{nlm'}$
3	$il'jl''k$	1/8	$K^{kim}L^{ilm}$	$K^{knm}K^{nim'}L^{jlm'}$
4	$l'ijl''k$	1/8	$K^{ijm}L^{klm}$	$K^{ijm}K^{knm'}L^{m'lm}$
5	$l'l''ijk$	1/12	$A^mK^{ijm}K^{klm}$	$A^kK^{nlm}K^{ijm'}K^{mm'h}$
6	$il'l''jk$	1/12	$A^mK^{ijm}K^{klm}$	$A^kK^{nlm}K^{ijm'}K^{mm'h}$
7	$l'il''jk$	1/12	$K^{ikm}L^{ilm}$	$K^{ikm}K^{nmn'}L^{ilm'}$
8	$ijkl'l''$	1/12	$A^mK^{ijm}K^{klm}$	$A^kK^{nlm}K^{ijm'}K^{mm'h}$
9	$ijl'l''k$	1/12	$A^mK^{ijm}K^{klm}$	$A^kK^{nlm}K^{ijm'}K^{mm'h}$
10	$ijl'kl''$	1/12	$K^{ijm}L^{klm}$	$K^{nim}K^{mjm'}K^{klm'}$

The  $W_c(de)$  and  $W_c(ee)$  may be calculated analogously:

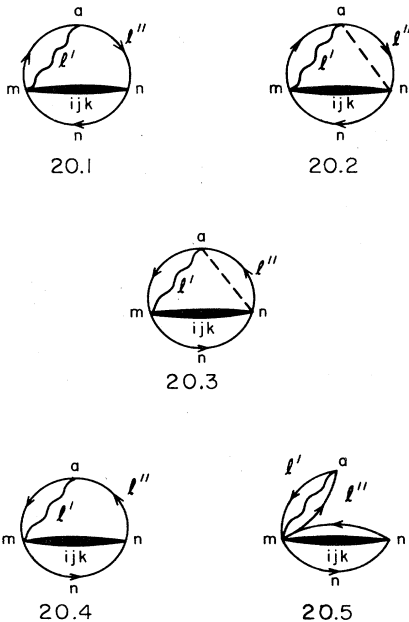
$$W_c(de) = \rho \int d^3r f^i H^j f^k G_{de}^{i>1} h^c (1 + G_{de}) \times \frac{1}{4} (2K^{ijm}K^{klm}A^m + K^{ijm}L^{klm} + K^{jkm}L^{ilm}), \quad (7.7)$$

$$W_c(ee) = \frac{\rho}{2} \int d^3r f^i H^j f^k G_{ee}^{i>1} h^c K^{ijm}K^{klm}A^m. \quad (7.8)$$

The contribution due to  $cc$  chains is slightly more complicated because there is a subset of diagrams that are reducible [see Pandharipande and Bethe (1973)]. For example, diagrams 20.1–20.3 of Fig. 20 are all

$$W_c(cc) = -\frac{\rho}{4} \int d^3r f^i H^j f^k G_{ca}^{i>1} h^c \Delta^n [2K^{ijm}K^{kmm'}(L^{nlm'} + K^{nlm'}A^{m'}) + L^{lmm'}(K^{ijm}K^{nkm'} + K^{jkm}K^{nlm'}) + K^{jnm}(K^{ilmn'}L^{klm'} + K^{kmm'}L^{ilm'})] + \rho \int d^3r f^i H^j f^k (G_{ca}^{i>1} - G_{cb}^{i>1}) h^c L^{ikm}K^{nlm}A^m A^i \Delta^n \Delta^l. \quad (7.9)$$

The diagrams contributing to  $W_s$  are conveniently divided into “direct” and “exchange” categories. Direct  $W_s$  diagrams have no exchange between the interacting particles, while in exchange  $W_s$  diagrams they are in

FIG. 20. The simplest diagrams that contribute to  $W_c(cc)$ .

irreducible, 20.1 and 20.2 being taken care of by  $G_{ca}^i$ , and 20.3 by  $G_{cb}^i$ . However, diagram 20.4 has a reducible counterpart in 20.5, which must be subtracted out according to the cluster expansion. (This is the case  $x_y$ ,  $x_z = e$ ,  $e$  mentioned in Sec. V that cannot be treated as a vertex correction.) The magnitudes of  $G_{cx}^i$  do not depend on the direction of exchange, so in practice we sum diagrams of type 20.1–20.4 by using  $G_{ca}^i$  and summing over both exchange directions. The contribution of diagrams of type 20.5 is proportional to  $G_{ca}^i - G_{cb}^i$ , which is subtracted from the sum to obtain  $W_c(cc)$ :

a common exchange loop. Direct diagrams are constructed using the interaction line, with possible central chains as dressings, and the SOR function  $J^i$  given in Eqs. (6.29)–(6.33) attached at the end points. The appropriate  $J^i(x_y, x_z, x_q)$  is selected so that the common vertex does not participate in more than one exchange. The  $C$  part is easily calculated by keeping track of the possible operator orders as in the  $W_c$  case.

Consider the case where  $J^i(d, d, f^2)$  is the separable SOR, an example of which is shown in diagram 15.1. The  $C$  part of the separable diagram is given by

$$\frac{1}{4} C(\{i, l\}j\{l, k\}) - C(ijk)C(lil) = \frac{1}{4} K^{ijk}A^k A^l (D_{il} + D_{jl} + D_{kl}), \quad (7.10)$$

where the  $D_{pq}$  are given by Eq. (5.23). The  $C$  parts of all  $W_s$  diagrams can be similarly calculated using the matrices  $A$ ,  $K$ , and  $D$ . The total  $W_s$  can be written compactly as

$$W_s = \frac{\rho}{2} \int d^3r f^i H^j f^k h^c K^{ijk} A^k \times [M_{dd}^2 - 1 + 2G_{de}^c (M_{dd} M_{de} - 1) + (G_{de}^c + G_{ee}^c)(M_{de}^2 - 1)] - \frac{\rho}{16} \int d^3r f^i H^j f^k h^c \Delta^n (K^{nlm}K^{jkm} + K^{nkm}K^{ijm}) A^m (M_{ee}^2 - 1). \quad (7.11)$$

The first (second) term is the direct (exchange) part. Terms linear in  $(M_{xx} - 1)$  sum diagrams having only one separable SOR, like 19.3, while those quadratic in

$(M_{xx} - 1)$  give a fair approximation to diagrams like 19.7 having two separable SOR. The  $M_{xx}$  are analogous to the vertex corrections  $M$  discussed in Sec. VI, but depend on all three variables  $i$ ,  $j$ , and  $k$ , as opposed to only one in, for example,  $M(t_j, I, x)$ . The direct  $M_{dx}$  are given by

$$M_{dx} = 1 + \sum_i \left\{ \frac{1}{4} (D_{ii} + D_{ji} + D_{ki}) J^I(x, d, f^2) + \frac{1}{24} (3D_{ji} + 5D_{ii} + 5D_{ki}) J^I(x, d, P) + \delta_{xd} \frac{1}{4} (D_{ii} + D_{ki}) J^I(d, e, P) \right\}. \quad (7.12)$$

The exchange correction  $M_{ee}$  depends in addition on the intermediate summation variable  $m$ :

$$M_{ee} = 1 + \sum_i \left\{ \frac{1}{4} (2D_{mi} + D_{ji} + D_{ni}) J^I(e, d, f^2) + \frac{1}{24} (6D_{mi} + 3D_{ji} + 3D_{ni} + 2D_{ii} + 2D_{ki}) J^I(e, d, P) \right\}. \quad (7.13)$$

The  $W_{cs}$  is very messy, since we need to keep track of the orders of seven to eight operators to calculate it exactly. However, it is small, and of order  $W_c(M^2 - 1)$ , where  $M$  is an appropriate vertex correction. To the extent the  $f^c H^j f^c$  term in  $W_c$  dominates, we can use the interacting vertex corrections  $M(t_j, I, x)$  of Eq. (6.28) to calculate the contribution of  $H^j$  to  $W_{cs}$ . In practice we find that terms containing  $H^j$ ,  $f^j$ , and  $G^j$  dominate the  $W_c$ , and it is probably adequate to calculate the  $W_{cs}$  with  $M(\nu, I, x)$ . Keeping track of exchanges, we have

$$W_{cs} \simeq W_c(dd)_{\text{dir}} [M(\nu, I, d)^2 - 1] + W_c(de) [M(\nu, I, d) M(\nu, I, e) - 1] + [W_c(dd)_{\text{ex}} + W_c(ee) + W_c(cc)] [M(\nu, I, e)^2 - 1], \quad (7.14)$$

where  $W_c(dd)_{\text{dir}}$  and  $W_c(dd)_{\text{ex}}$  are the two terms of Eq. (7.6). The exact vertex corrections for  $W_c(dd)_{\text{dir}}$ ,  $W_c(de)$  (which is the dominant term in  $W_c$ ) and  $W_c(ee)$  have been calculated, and we find numerically that the approximation in Eq. (7.14) is quite good, typically within  $\approx 0.1$  MeV up to  $k_F = 2.0 \text{ fm}^{-1}$ . The exact calculation requires the introduction of new matrices, and has not been done yet for the  $W_c(dd)_{\text{ex}}$  and  $W_c(cc)$ , so it is probably not worthwhile to discuss it here. We believe the above approximation for  $W_{cs}$  is valid to within  $\approx 0.2$  MeV.

## B. Calculation of $U$

The  $U$  diagrams are evaluated up to the SOC level with vertex corrections. They are conveniently divided into four parts

$$U = U_1 + U_2 + U_3 + U_4, \quad (7.15)$$

where  $U_1$  has no operator links and  $U_2$ ,  $U_3$ , and  $U_4$  have one SOR passing through the points  $no$ ,  $mn$  or  $mo$ , and  $mno$ , respectively. Samples of diagrams contributing to  $U_1 - U_4$  are shown in Fig. 21, diagrams 21.1–21.4.

The  $U_i$  can always be expressed as

$$U_i = -\frac{\hbar^2}{8m} \rho^2 \int d^3 r_{mn} d^3 r_{mo} \cos \theta_{mn} u_i(r_{mn}, r_{mo}, r_{no}), \quad (7.16)$$

and in the FHNC/SOC approximation the  $u_i$  contain products of functions of  $r_{mn}$ ,  $r_{mo}$ ,  $r_{no}$ , and  $\xi_{nm}^{pq}$ . The func-

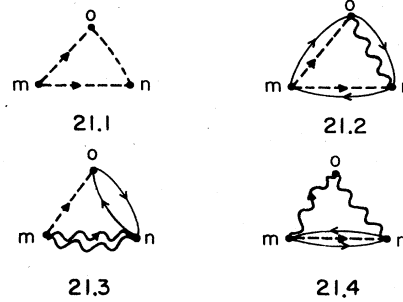


FIG. 21. Examples of  $U$  diagrams.

tions of  $r_{no}$  denoted by  $R_{xx}$ ,  $Y_{xx}$ , and  $Z_{xx}^{p>1}$ , respectively, depict central correlations, closed SOR, and operator links in the  $U$  diagrams.

$$\begin{aligned} R_{dd} &= f^c h^c, \\ R_{de} &= R_{dd} G_{de}^c, \\ R_{ee} &= R_{dd} (G_{de}^c + G_{ee}^c - L^2/4), \\ R_{cc} &= R_{dd} L/4. \end{aligned} \quad (7.17)$$

The  $Y_{xx}$  and  $Z_{xx}^{p>1}$  are multiplied by the vertex corrections  $M_x^p$  discussed in Sec. VI to correct for separable  $U$  diagrams:

$$\begin{aligned} Y_{dd} &= \sum_{p>1} A^p [f^{p^2} + h^p G_{dd}^p] M_d^{p^2} h^c, \\ Y_{ee} &= \sum_{p>1} A^p \{ f^{p^2} (G_{de}^c + G_{ee}^c) + f^c (G_{de}^{p^2} - 2G_{cc}^p L \Delta^p / M_e^p) + h^p [G_{dd}^p (G_{de}^c + G_{ee}^c) + 2G_{de}^p G_{ee}^c + G_{ee}^p - L^2 \Delta^p / 4] \} M_e^{p^2} h^c, \\ Y_{de} &= \sum_{p>1} A^p [f^{p^2} G_{de}^c + h^p (G_{dd}^p G_{de}^c + G_{de}^p)] M_d^p M_e^{p^2} h^c, \\ Y_{cc} &= \sum_{p>1} A^p \Delta^p [\frac{1}{4} h^p L M_e^p + f^c G_{cc}^p] M_e^{p^2} h^c; \\ Z_{dd}^{p>1} &= h^c h^c M_d^{p^2}, \\ Z_{de}^{p>1} &= (h^p G_{de}^c + f^c G_{de}^p) h^c M_d^p M_e^p, \\ Z_{ee}^{p>1} &= [h^p (G_{de}^c + G_{ee}^c) + f^c (G_{ee}^c + 2G_{de}^p G_{de}^c - \Delta^p L^2 / 4)] h^c M_e^{p^2}. \end{aligned} \quad (7.18)$$

There are no  $Z_{cc}^{p>1}$  links in the SOC approximation. The corresponding functions of  $r_{mn}$  and  $r_{mo}$  containing the gradients are denoted by  $\bar{R}_{xx}$ ,  $\bar{Y}_{xx}$ , and  $\bar{Z}_{xx}^{p>1}$ . They are obtained by making the following substitutions in Eqs. (7.17–7.19):

$$\begin{aligned} f^{c^2} &\rightarrow (f^{c^2})', \\ f^{p^2} &\rightarrow (f^{p^2})', \\ h^p &\rightarrow (F^p)' + (f^{c^2})' G_{dd}^p, \end{aligned} \quad (7.20)$$

where the primes represent derivatives with respect to  $r$ . The  $\bar{Z}_{xx}^{t(t\tau)}$  generated by these substitutions contain  $(f^c f^{t(t\tau)})'$  terms. Two new  $\bar{Z}$  links,  $\bar{Z}_{xx}^{t'(t\tau)}$ , are needed to take into account the gradients of the tensor operator. They are obtained from  $Z^{t(t\tau)}$  with the replacements

$$\begin{aligned} h^{t(t\tau)} &\rightarrow F^{t(t\tau)} / r, \\ f^{c^2} &\rightarrow 0. \end{aligned} \quad (7.21)$$

The  $u_i(r_{mn}, r_{mo}, r_{no})$  containing all the twenty-nine possible exchange patterns are given by

$$u_1 = \bar{R}_{dd,mn}(\bar{R}_{dd} + 4\bar{R}_{de} + 2\bar{R}_{ee})_{mo}(R_{dd} + R_{de})_{no} + \bar{R}_{dd,mn}(\bar{R}_{dd} + 2\bar{R}_{de})_{mo}(R_{de} + R_{ee})_{no} \\ + \bar{R}_{de,mn}(3\bar{R}_{de} + 2\bar{R}_{ee})_{mo}R_{dd,no} + 2\bar{R}_{de,mn}\bar{R}_{de,mo}R_{de,no} - 8\bar{R}_{cc,mn}\bar{R}_{cc,mo}R_{cc,no}. \quad (7.22)$$

The  $u_2$  may be obtained by replacing the  $R_{xx',no}$  in  $u_1$  by  $Y_{xx',no}$  while  $u_3$  is the sum of the two terms obtained by replacing the  $\bar{R}_{xx',mn}$  and  $\bar{R}_{xx',mo}$  by  $\bar{Y}_{xx',mn}$  and  $\bar{Y}_{xx',mo}$ , respectively. The  $u_4$  contains a  $\xi_{nm0}^{pqI} A^I$  for the  $C$  part and an  $(M_e^I)^{-3}$  because each  $Z$  or  $\bar{Z}$  link has two vertex corrections.

$$u_4 = \sum_{p,q=2-6, t', t'' \tau} \sum_{l=2-6} \xi_{nm0}^{pqI} A^I / M_d^{p^3} \{ \bar{Z}_{dd,mn}^p (\bar{Z}_{dd}^q + 4\bar{Z}_{de}^q + 2\bar{Z}_{ee}^q)_{mo} (Z_{dd}^I + Z_{de}^I)_{no} \\ + \bar{Z}_{dd,mn}^p (\bar{Z}_{dd}^q + 2\bar{Z}_{de}^q)_{mo} (Z_{de}^I + Z_{ee}^I)_{no} + \bar{Z}_{de,mn}^p (3\bar{Z}_{de}^q + 2\bar{Z}_{ee}^q)_{mo} Z_{dd,no}^I + 2\bar{Z}_{de,mn}^p \bar{Z}_{de,mo}^q Z_{de,no}^I \}. \quad (7.23)$$

The  $\xi_{nm0}^{pqI}$  having  $p$  or  $q = t'(t''\tau)$  give the  $C$  parts of SOR containing gradients of tensor operators. Those with non-zero values are found to be

$$\xi_{nm0}^{t't\sigma} = \xi_{nm0}^{t't\sigma} \tau\tau = -3 \left( \frac{\cos\theta_n \cos\theta_o}{\cos\theta_m} + \cos^2\theta_n \right), \quad (7.24)$$

$$\xi_{nm0}^{t'tk} = \xi_{nm0}^{t'tk} \tau\tau = 6(1 - \cos^2\theta_m) \delta_{kt} + \left[ 9 \cos\theta_m \cos\theta_n \cos\theta_o + \frac{9}{2} \cos^2\theta_o + 3(\cos^2\theta_m + \cos^2\theta_n) - \frac{3}{2} \frac{\cos\theta_n \cos\theta_o}{\cos\theta_m} - 3 \right] \delta_{kt}, \quad (7.25)$$

$$\xi_{nm0}^{t'tk} = \xi_{nm0}^{t'tk} \tau\tau = 12 \cos^2\theta_m \delta_{kt} + \left[ -18 \cos\theta_m \cos\theta_n \cos\theta_o - 6 \cos^2\theta_m - 9(\cos^2\theta_n + \cos^2\theta_o) - \frac{9}{2} \frac{\cos\theta_n \cos\theta_o}{\cos\theta_m} + \frac{9}{2} \right] \delta_{kt}. \quad (7.26)$$

### C. Calculation of $W_F$ and $U_F$

The  $W_F$  diagrams can conveniently be broken down like  $W$  into parts,  $W_{F0}$ ,  $W_{Fc}$ ,  $W_{Fs}$ , and  $W_{Fcs}$ . The  $W_{F0}$  and  $W_{Fs}$  are given by

$$W_{F0} + W_{Fs} = -\frac{\hbar^2}{8m} \rho \int d^3r (f^i f^k) l^i l^k h^c \Delta^j K^{ij} A^k M_{de}^2. \quad (7.27)$$

In the operator algebra the exchange operator  $j$  in  $W_{Fs}$  diagrams plays the role of the  $j$  operator associated with  $H^j$  in direct  $W_s$  diagrams, so the vertex correction in Eq. (7.27) is identical to the  $M_{de}$  of Eq. (7.12). At present the  $W_{Fc}$  and  $W_{Fcs}$  are calculated in strictly the single-operator ring approximation:

$$W_{Fc} + W_{Fcs} = -\frac{\hbar^2}{4m} \rho \int d^3r f^c f^c l^i l^i h^c \Delta^n A^n (G_{dd}^n M_e^2 L + 4G_{cc}^n M_e^n). \quad (7.28)$$

The  $U_F$  is treated like  $U$ , its diagrams being grouped into five classes which, respectively, have no SOR connecting  $m$ ,  $n$ , and one, SOR passing through either  $n$  and  $o$ ,  $m$  and  $n$ ,  $m$  and  $o$ , or  $m$ ,  $n$ , and  $o$ . The  $mn$  and  $mo$  links are symmetric in  $U$ , but not in  $U_F$ , hence the extra class. The  $U_F$  may be written as

$$U_{Fi} = -\frac{\hbar^2}{2m} \rho^2 \int d^3r_{mn} d^3r_{mo} \cos\theta_m u_{Fi}(r_{mn}, r_{mo}, r_{ro}). \quad (7.29)$$

The  $u_{Fi}$  contain  $(R, Y, \text{ or } Z)_{no}$ ,  $(\bar{R}, \bar{Y}, \text{ or } \bar{Z})_{mn}$ , and new functions  $(\bar{R}, \bar{Y}, \text{ or } \bar{Z})_{mo}$  containing the  $l'_{mo}$ :

$$\bar{R}_{ee} = f^c h^c l' / 4, \\ \bar{R}_{cc} = (f^c h^c - 1) l', \\ \bar{Y}_{ee} = \sum_{p>1} A^p [h^c h^p M_e^{p^2} L / 4 + (f^c h^c - 1) G_{cc}^p M_e^p] l' \Delta^p, \\ \bar{Y}_{cc} = \sum_{p>1} A^p \Delta^p h^c h^p M_e^{p^2} l', \\ \bar{Z}_{ee}^{p>1} = \Delta^p \bar{R}_{ee} M_e^{p^2}. \quad (7.30)$$

The  $u_{F1}$  is given by

$$u_{F1} = \bar{R}_{dd,mn} \bar{R}_{ee,mo} (R_{dd} + R_{de})_{no} + \bar{R}_{de,mn} \bar{R}_{ee,mo} R_{dd,no} \\ + \bar{R}_{cc,mn} \bar{R}_{cc,mo} R_{cc,no}, \quad (7.31)$$

while the  $u_{F2}$ ,  $u_{F3}$ , and  $u_{F4}$  are obtained by, respectively, substituting the  $R_{xx'}$  by  $Y_{xx'}$ , the  $\bar{R}_{xx'}$  by  $\bar{Y}_{xx'}$ , and the  $\bar{R}_{xx'}$  by  $\bar{Y}_{xx'}$  in  $u_{F1}$ . The  $u_{F5}$  is given by

$$u_{F5} = \sum_{p=2-6, t', t'' \tau} \sum_{q, l=2-6} \xi_{nm0}^{pqI} A^I / M_d^{p^3} \\ \times [\bar{Z}_{dd,mn}^p \bar{Z}_{ee,mo}^q (Z_{dd}^I + Z_{de}^I)_{no} + \bar{Z}_{de,mn}^p \bar{Z}_{ee,mo}^q Z_{de,no}^I]. \quad (7.32)$$

## VIII. FURTHER VARIATIONS OF THE THEME

### A. Hypernetted operator chain equations

Fantoni and Rosati (1978) have developed a set of integral equations that approximately sums hypernetted operator chains (HOC) by neglecting a number of commutators. Consider the HOC diagram 22.1 of Fig. 22, and assume for simplicity that all the operator links are  $\tau$  type. The seven  $\tau_a \cdot \tau_b$  operators in the diagram occur in various orders labeled  $i$  with weights  $w^i$ ; however, we could rearrange them and express

$$\sum_i w^i \prod_i O_{ab}^i = \tau_m \cdot \tau_1 (\tau_1 \cdot \tau_4 \tau_4 \cdot \tau_2) (\tau_1 \cdot \tau_3 \tau_3 \cdot \tau_2) \tau_1 \cdot \tau_2 \tau_2 \cdot \tau_n \\ + \text{terms having commutators.} \quad (8.1)$$

On summing over  $\tau_3$  and  $\tau_4$  we get

$$\sum_{\tau_3, \tau_4, i} w^i \prod_i O_{ab} = \tau_m \cdot \tau_1 (\tau_1 \cdot \tau_2)^3 \tau_2 \cdot \tau_n + \text{commutator terms.} \quad (8.2)$$

Since

$$(\tau_1 \cdot \tau_2)^3 = -6 + 7\tau_1 \cdot \tau_2, \quad (8.3)$$

the 1-2 link in the first term of Eq. (8.2) is effectively a single-operator link and may simply be included in

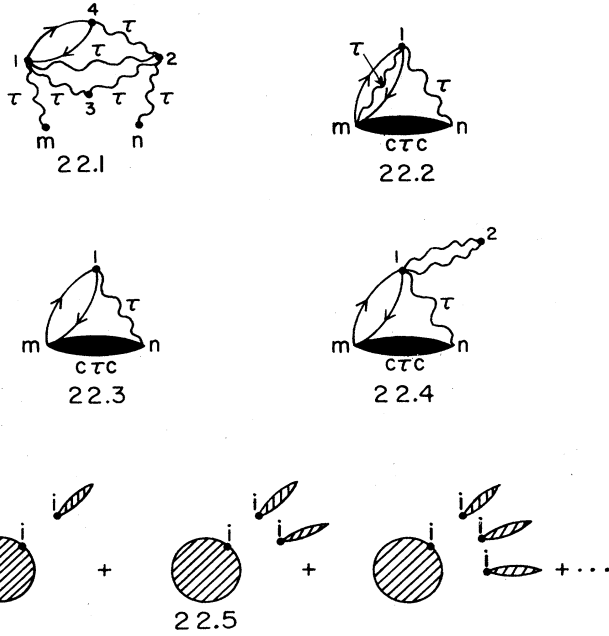


FIG. 22. Diagrams 22.1 and 22.2 are typical of chain diagrams having multiple-operator links, while 22.3 is the SOC diagram corresponding to 22.2, and 22.4 is a correction to 22.3. Diagrams 22.5 illustrate the simple structure of typical diagrams that are summed analytically to obtain vertex corrections in Owen's method.

the links  $X^p O^p$  of the chain equation (6.22). The commutator terms in (8.2) are much more difficult to sum.

The HOC equations neglect all commutator terms, and have the same form as Eq. (6.22) with the vertex corrections  $M_x^p$  set to unity. The links  $X_{xx}^p$ , however, include all operator hypernets, such as the one in diagram 22.1, treated approximately in the manner illustrated above. The  $X_{dd}^p$ , for example, is given by the operator equation

$$\sum_{p=1,6} X_{dd}^p O^p = \left( \sum_{p'} f^{p'} O^{p'} \right)^2 \exp \left( \sum_{p'} G_{dd}^{p'} O^{p'} \right) - 1 - \sum_p G_{dd}^p O^p, \quad (8.4)$$

which is a direct generalization of the link equation (6.10) of FHNC. Fantoni and Rosati have introduced a very useful set of projection operators  $P^i$  to calculate the exponential in Eq. (8.4). The  $P^i$  are linear combinations of  $O^i$ ,

$$P^{i=1,6} = P^1 \pi^1, Q \pi^1, (1-Q) P^3 \pi^1, P^1 \pi^3, Q \pi^3, (1-Q) P^3 \pi^3, \quad (8.5)$$

where  $P$  and  $\pi$  are standard spin, isospin projection operators:

$$P^1 = \frac{1}{4}(1 - \sigma_1 \cdot \sigma_2), \quad P^3 = \frac{1}{4}(3 + \sigma_1 \cdot \sigma_2), \\ \pi^1 = \frac{1}{4}(1 - \tau_1 \cdot \tau_2), \quad \pi^3 = \frac{1}{4}(3 + \tau_1 \cdot \tau_2), \quad (8.6)$$

and

$$Q = \frac{1}{6}(3 + \sigma_1 \cdot \sigma_2 + S_{12}). \quad (8.7)$$

The  $P^p$  satisfies equations of projection operators,

$$P^p P^q = \delta_{pq} P^p, \quad (8.8)$$

and the exponentiation is carried out by defining new chain functions  $\hat{G}^p$  such that

$$\sum_{p=1,6} \hat{G}_{dd}^p P^p = \sum_{p=1,6} G_{dd}^p O^p, \quad (8.9)$$

$$\exp \left( \sum_{p=1,6} \hat{G}_{dd}^p P^p \right) = 1 + \sum_{p=1,6} [\exp(\hat{G}_{dd}^p) - 1] P^p. \quad (8.10)$$

If the commutator terms were indeed small, the HOC equations would constitute a substantial improvement over the FHNC/SOC equations. However, there is no reason for the commutator terms in Eq. (8.2) to be small. Consider the multiple-operator diagram 22.2. Its contribution in the HOC approximation is easily calculated by taking the  $O_{m1}^p$  next to the exchange operator  $e_{m1}$  and neglecting the commutators. It is found to be

$$+ \frac{3}{4} \rho^2 \int d^3 r_{mn} d^3 r_{m1} l_{m1}^2 f_{mn}^c v_{mn}^T f_{mn}^c F_{m1}^T F_{m1}^T. \quad (8.11)$$

The contribution of this rather simple diagram may be calculated exactly by treating all the operator orders. It is found to be zero; the commutator terms of Eq. (8.2) just cancel the first term in this case.

In the FHNC/SOC summation the multiple-operator diagram 22.2 is viewed as a correction to the SOC diagram 22.3. It will be a small correction when the  $F^{p>1}$  and  $G^{p>1}$  are  $\ll 1$ , as is the case in nuclear matter. Further, the SOC diagram 22.3 has other commutator corrections, such as 22.4, which the present HOC equations neglect. These vertex corrections can be significant when the  $f^{p>1}$  have a long range.

## B. Calculations with independent-pair wave function

Owen (1979a) has developed a very promising variational theory based on the wave function  $\Psi_{IP}$  given by Eqs. (2.25) and (2.26). He has recently (1979b) applied it to the  $v_6$  model of nuclear matter. The  $f^p(r_{ij}, d, \beta_p)$  of Sec. III are used to calculate the  $u_{ij}$ , and so his method also has the same variational parameters  $d$  and  $\beta_p$ . In the low-density limit the  $\Psi_{IP}$  and the "symmetrized product"  $\Psi_{SP}$  [Eq. (2.19)] become identical.

The diagrammatic cluster expansion of expectation values with  $\Psi_{IP}$  has been carried out by Owen (1979a) by a generalization of the method of Gaudin, Gillespie, and Ripka (1971). However, the application of the method described in Sec. IV gives the same results, and we shall continue to use the diagrammatic notation of Sec. IV, which is only superficially different from Owen's, to describe his method.

The diagrams depicting expectation values with  $\Psi_{IP}$  are formed with the elements 1–9 of Fig. 7; however, the wavy lines must be labeled either  $L$  or  $R$  to specify whether they come from the expansion of the left-hand  $\Psi_{IP}^*$  or the right-hand  $\Psi_{IP}$ . The  $\Psi_{IP}$  has no terms of type  $u_{ij} u_{jk}$  in which two or more  $u$ 's have a common particle. This restriction of  $\Psi_{IP}$  is simply incorporated by an additional diagram rule stating that no two wavy  $L$  lines or  $R$  lines touch. A consequence of this rule is that we cannot have diagrams in which three or more wavy lines touch at a point.

The wavy lines must also carry the operator label  $p$ . In the previous theory a wavy line labeled  $p$  represented  $2f^c f^p O^p$ , and the operator  $O^p$  could be on the left or right side of the Hamiltonian  $H$  with a probability of  $1/2$ . The wavy lines  $pL(pR)$  represent  $f^c f^p O^p$  with the operator on the left (right) of  $H$ . The double wavy line (element 3 of Fig. 7) must now be labeled  $pL, qR$ , and it represents  $f^p f^q O^p O^q$ , the operators  $O^p$  and  $O^q$  being on the left and right side of  $H$ , respectively.

In building chains with the  $\Psi_{IP}$  we have to be careful to avoid connecting links  $X_{xx',ij}^p$  to  $X_{yy',jk}^q$  or  $G_{yy',jk}^q$  [Eq. (6.22)] when both contain wavy  $L$  lines or  $R$  lines ending in the nodal point  $j$ . This requires a more elaborate classification of chains  $G_{xx',kj}^p$  and links  $X_{xx',ij}^p$ . The subscript  $x$  referring to the end  $i$  must now specify both the exchange pattern and the occurrence of wavy  $L$  and  $R$  lines at  $i$ . Thus the number of chains is much larger. For example, the four parts  $G_{dLaR,ij}^p$ ,  $G_{dLaL,ij}^p$ ,  $G_{dRaL,ij}^p$ , and  $G_{dRaR,ij}^p$  of the single operator  $G_{da,ij}^p$  have to be considered explicitly. Symmetry under the exchange of  $L$  with  $R$  can, however, be used to reduce the number of required chain functions. Owen writes the chain equation (6.22) in a matrix form

$$G_{xy,ij}^r = \Theta \frac{pqr}{ijk} (X_{xx',ij}^p M_{x'y'}^{pq}; [X+G]_{yy',jk}^q), \quad (8.12)$$

and puts all the restrictions and vertex corrections in his coupling matrix  $M_{x'y'}^{pq}$ . The elements such as  $M_{dLaL}^p$  or  $M_{dLaR}^p$  would obviously need to be zero because such couplings build wrong diagrams. The elements such as  $M_{dLaR}^p$  which build allowed chains equal the vertex correction at the vertex  $j$  in the chain built.

The somewhat larger number of chain functions does not seem to pose a significant problem. The main advantage of the method is that it is much simpler to go beyond the SOC approximation. Complicated operator hypernets such as that in diagram 22.1 do not exist in this method. The maximum number of operators at a nodal point in a chain can be four, two from wavy lines and two from exchange. These generate very few multiple-operator links, such as diagram 22.2, which can be easily calculated.

Separable diagrams such as 9.3, 9.5–9.7 do not exist. In the typical case, for example when  $i$  is a  $dL$  vertex in both the irreducible and the separated parts, only the separated diagrams illustrated in diagram 22.5 exist. These form a simple geometric series which can be summed analytically. In the previous method the calculation of separable diagrams having many operator rings with a common articulation point becomes very tedious. Thus Owen's method, though a little more complicated at the SOC level of computation, has enormous advantages in computing multiple-operator diagrams.

It is interesting to ask whether  $\Psi_{IP}$  or  $\Psi_{SP}$  is a better variational wave function. Such a question can always be settled by computing numerically the energy expectation value with both  $\Psi_{IP}$  and  $\Psi_{SP}$ , but simpler arguments could be more illuminating. The central correlations in  $\Psi_{IP}$  [Eq. (2.26)] are treated in the Jastrow (or equivalently SP) approximation, but in principle we could also treat them in the independent-pair approximation. Let

$$f^c = 1 + u^c. \quad (8.13)$$

Then the IP analogue of the  $\Psi_J$  will become

$$\Psi_{IP}^c = \left( 1 + \sum_{i<j} u_{ij}^c + \sum_{\substack{i<j,k \\ k<l}} u_{ij}^c u_{kl}^c + \cdots \right) \Phi. \quad (8.14)$$

This  $\Psi_{IP}^c$  is not a very good wave function; for example, it gives only half of the correlation energy of Bose liquids interacting with nuclear-type Yukawa potentials (Owen, 1978). One understands the deficiency of  $\Psi_{IP}^c$  by noting that when the potential has a strong repulsive core  $f^c(r \rightarrow 0) \rightarrow 0$ , and  $\Psi_J \rightarrow 0$  as any  $r_{ij} \rightarrow 0$ ; but the  $\Psi_{IP}$  does not vanish when  $r_{ij} \rightarrow 0$ . However, such a simple criterion for deciding between Owen's  $\Psi_{IP}$  and  $\Psi_{SP}$  is not yet available.

The  $\Psi_{SP}$  has additional terms of the type  $f_{ij}^p f_{jk}^q \{O_{ij}^p, O_{jk}^q\}$ , absent in the  $\Psi_{IP}$ . They contribute to many different separable and chain diagrams, and *a priori* it is difficult to estimate their net contribution. As a matter of fact, the current results in nuclear matter indicate that  $\Psi_{SP}$  and  $\Psi_{IP}$  give very comparable energies. The  $\Psi_{SP}$  has a formal advantage which can be easily seen by considering a spin-one-half fermion fluid having central  $v^c$  and spin-spin  $v^s$  parts in its two-body potential. If we completely spin-polarize the liquid, its variational wave function may be expected to go over to a Jastrow wave function for fermions interacting with an effective central potential  $v^c + v^s$ . The  $\Psi_{SP}$  has this property while the  $\Psi_{IP}$  does not.

## IX. RESULTS

In this section we summarize the results obtained by the variational methods using correlation operators, as discussed in the preceding sections, and compare them with results obtained by other methods.

### A. Neutron matter model $v_3$

The  $v_3$  model interaction is of the form  $v_{ij}^c + v_{ij}^s(\sigma_i \cdot \sigma_j)$ ; the  $v_{ij}^c$  and  $v_{ij}^s$  are given by Owen (1979a) and are based on the potentials of Bethe and Johnson (BJ) (1974). The  $F$  operator has the form  $f_{ij}^c + \beta_0 f_{ij}^s(\sigma_i \cdot \sigma_j)$ , and has been used in both the  $\Psi_{SP}$  [Eq. (2.19)] and  $\Psi_{IP}$  [Eq. (2.26)] wave functions. The calculation with  $\Psi_{SP}$  (Lagaris *et al.*, 1978) uses the FHNC/SOC approximation, while that with the  $\Psi_{IP}$  (Owen, 1979) sums all hypernetted operator chains. The results of both calculations are summarized in Table VI. Owen gives results for both the PB and JF kinetic energy prescriptions (Zabolitzky, 1977), while the  $\Psi_{SP}$  calculation uses the PB form only. Also listed are energies obtained with the Jastrow wave function without any  $f^s$  correlation; both  $\Psi_{IP}$  and  $\Psi_{SP}$  reduce to the same  $\Psi_J$  in the limit  $\beta_0 \rightarrow 0$ .

The  $f^s$  has a very small effect on the  $E(\rho)$  of the  $v_3$

TABLE VI. The  $E(\rho)$  in MeV of the  $v_3$ -model of neutron matter.

$\rho$	$E(\Psi_{IP}, JF)$	$E(\Psi_{IP}, PB)$	$E(\Psi_J, PB)$	$E(\Psi_J, PB)$
0.17	17.2	17.0	17.4	17.8
0.3	29.1	28.2	28.8	29.2
0.4	41.1	38.8	39.9	40.3

model due to very large cancellations. The  $W_0$  and  $W_F$  decrease, while  $W_c$  increases, as  $\beta_\sigma$  is increased keeping the total energy almost constant. For example, at  $d = 2.3r_0$ , the  $E(\Psi_{SP}, PB)$  and  $W_c$  are, respectively, 29.2 and 0.0 MeV for  $\beta_\sigma = 0$ , and 28.8 and 7.4 MeV for  $\beta_\sigma = 0.5$ . Thus it is very difficult to calculate the energy gain due to the  $f^\sigma$  correlation in this model. However, it is encouraging to note that the SOC approximation used to calculate the large  $W_c$  contributions seems to be reasonably accurate in this case. Owen also does a calculation which he calls "SOC" using the  $\Psi_{IP}$ . He fails to obtain a minimum in  $E(d)$  in this calculation, but his "SOC" calculation is significantly different from the single-operator chain approximation which is presented here, and used in the  $\Psi_{SP}$  calculations.

### B. Nuclear matter $v_6$ models

The Reid  $v_{6,8}$  and BJ-II  $v_{6,8}$  models are obtained by expressing the  $^1S_0$ ,  $^3S_1 - ^3D_1$ ,  $^1P_1$ , and  $^3P_2 - ^3F_2$  potentials in the Reid (1968) and Bethe-Johnson-II (1974) interaction models as  $\sum_i v_i(r) O_i^{1,2,3}$ . The  $v_{i=7,8}$  potentials are neglected in the  $v_6$  models. The HJ  $v_6$  model is obtained by neglecting the  $(L \cdot S)$  and quadratic spin-orbit terms in the Hamada-Johnston (1962) potential, while the GT-5200 potential of Gammel and Thaler (1960) is itself of a  $v_6$  form.

The  $\sigma\tau$  and  $t\tau$  correlations and chains are most important in nuclear matter, and the energy is more sensitive to  $\beta_{t\tau}$  and  $d$  than to  $\beta_{\sigma\tau}$ . It is very insensitive to  $\beta_\sigma$ ,  $\beta_\tau$ , and  $\beta_t$ . In the calculations based on the FHNC/SOC equations the equilibrium value of  $\beta_{t\tau}$  is generally close to unity, but that of  $\beta_{\sigma\tau}$  is generally  $<1$ . The contributions to  $E(k_F, d, \beta_i)$  for the Reid (BJ-II)  $v_6$  model at its minimum are given in Table VII(VIII). The  $f^\sigma$ ,  $f^\tau$ , and  $f^{\sigma\tau}$  lower the energy by 2(5) MeV. As in the  $v_3$  model of neutron matter, there is a very large cancellation between the two-body and the  $W_c$  contributions due to  $f^\sigma$ ,  $f^\tau$ , and  $f^{\sigma\tau}$ . The largest contribution of  $f^t$  and  $f^{t\tau}$  from many-body clusters is via the  $W_s$  term. The contributions to  $E(k_F = 1.3 \text{ fm}^{-1})$  of the Reid, BJ-II, HJ, and GT-5200  $v_6$  models in FHNC/SOC calculations are compared in Table IX.

The  $E(k_F)$  of the  $v_6$  and  $v_8$  models, as obtained in various calculations, is shown in Figs. 23–26. A brief description of the various calculations along with their references is given in Table X. An estimate of the errors in SOC calculations is discussed in the next section. The error in the energy expectation value of the Reid and BJ-II  $v_6$  models is  $\sim \pm 1$  MeV at  $k_F = 1.6 \text{ fm}^{-1}$ . However, the variational wave function neglects the explicit  $k$ -dependent terms in the correlation operator  $F$ . From Fig. 4 we may expect these to lower the energy in the  $k_F = 1.6 \text{ fm}^{-1}$  region by  $\sim 1$  MeV. Thus the estimated error in the SOC energies in the equilibrium region is  $+0$  to  $-2$  MeV. The errors in SOC calculations of the HJ and GT-5200 models have not been analyzed in such detail, but we may expect them to be similar.

The energies with  $\Psi_{IP}$  (Figs. 23 and 24) have been calculated with the Jackson-Feenberg (JF) kinetic energy expression, and at all  $\beta_i = 1$ . The JF energies were found to be higher by an MeV in the  $v_3$  model, and we may also expect some lowering of the  $\Psi_{IP}$  energies

TABLE VII. Reid  $v_6$   $E(k_F = 1.6 \text{ fm}^{-1}, d = 2.5r_0)$  in MeV.

$\beta_i \geq 2$	$\beta_i = 1$	$\beta_i = 5, 6 = 1$ $\beta_{i=2,4} = 0.4$	$\beta_i = 5, 6 = 1$ $\beta_{i=2,4} = 0$	$\beta_i = 0$
$T_F$	31.85	31.85	31.85	31.85
2-body	-65.76	-59.16	-52.75	-10.75
$W_0(\text{MB})$	-6.91	-6.30	-5.28	1.97
$W_c$	13.02	6.46	0.77	0.0
$W_s$	18.30	12.21	10.35	0.0
$W_{cs}$	-2.97	-1.01	0.05	0.0
$W_F(\text{MB}) + U_F$	-1.07	-0.20	0.48	0.18
$U$	-0.91	-0.80	-0.60	1.93
$E$	-14.45	-16.95	-15.13	25.18

by varying the  $\beta_i$ . So the error in the preliminary IP curves is probably  $-1$  to  $-4$  MeV in the range  $k_F = 1.4$ – $1.8 \text{ fm}^{-1}$ . The IP energies may be very reliable upper bounds. Owen's method is capable of giving more accurate energies and error estimates, which we hope will soon be available. From the present results it appears that  $\Psi_{IP}$  and  $\Psi_{SP}$  may give similar  $E(\rho)$  in Reid  $v_6$  and GT-5200 models, the  $\Psi_{IP}$  being a little better at low densities, and  $\Psi_{SP}$  a little better at high densities.

Typically the LOBT approximation gives too high energies; however, the three- and four-body cluster contributions lower the BBG energy of the Reid  $v_6$  model below the variational SOC and IP energies. The estimated error in BBG energies in the Reid  $v_6$  model is  $\sim \pm 0.5$  to  $\pm 3$  MeV over  $k_F = 1.4$  to  $1.8 \text{ fm}^{-1}$ . The BHF equilibrium density for the HJ and GT-5200  $v_6$  models is  $\sim 30\%$  lower than that given by SOC calculations, while the RBHF calculations, if carried to higher densities, might give equilibrium densities closer to the variational results. The RBHF  $E(\rho)$  is probably too low in the HJ  $v_6$  model.

At low densities the CBPT energies are in excellent agreement with the SOC energies, but at large densities they are much lower. The cluster expansion is truncated rather severely at the three-body level, and only the second-order correlated basis perturbation term is included in the present CBPT calculations. A higher-order calculation in the CBPT approach will probably give higher energies at high  $\rho$ . The failure of the present CBPT calculations to obtain a minimum in the  $E(\rho)$  of the GT-5200 model also indicates that they overestimate the binding at high  $\rho$ .

The present HOC results should be taken with some

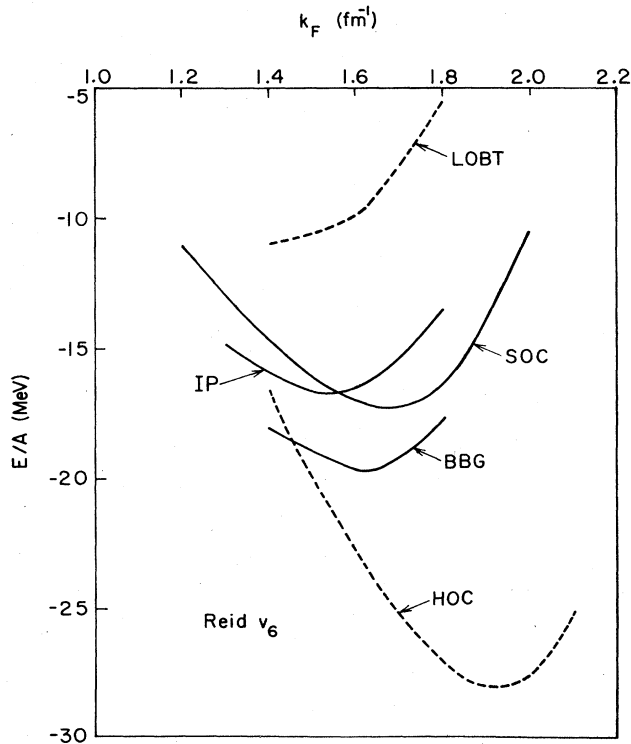
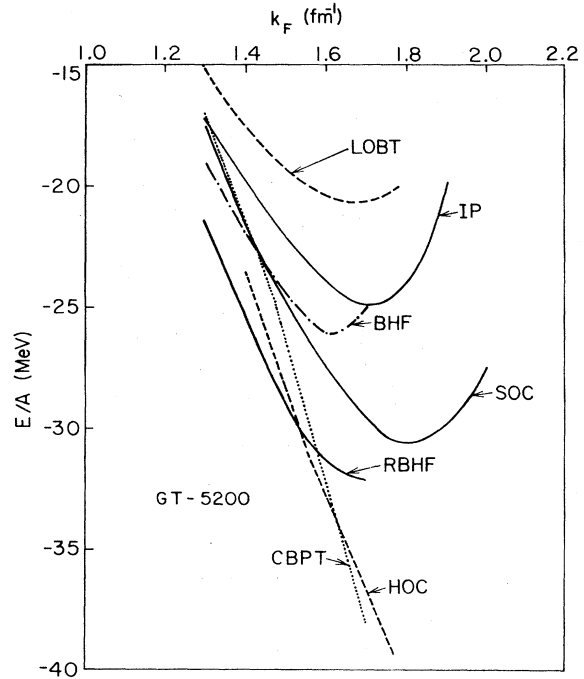
TABLE VIII. BJ-II  $v_6$   $E(k_F = 1.2 \text{ fm}^{-1}, d = 2.25r_0)$  in MeV.

$\beta_i \geq 2$	$\beta_i = 1$	$\beta_i = 5, 6 = 1.1$ $\beta_{i=2,4} = 0.6$	$\beta_i = 5, 6 = 1.1$ $\beta_{i=2,4} = 0$	$\beta_i = 0$
$T_F$	17.92	17.92	17.92	17.92
2-body	-39.70	-35.48	-24.17	-8.40
$W_0(\text{MB})$	-0.82	-0.98	-0.80	-0.12
$W_c$	3.43	1.85	0.58	0.0
$W_s$	14.68	10.73	6.79	0.0
$W_{cs}$	-1.03	-0.56	0.25	0.0
$W_F(\text{MB}) + U_F$	0.62	0.42	0.12	-0.01
$U$	-0.19	-0.54	-0.78	0.45
$E$	-5.09	-6.64	-1.25	9.83

TABLE IX.  $E_{\min}(k_F=1.3 \text{ fm}^{-1})$  for various potentials in MeV.

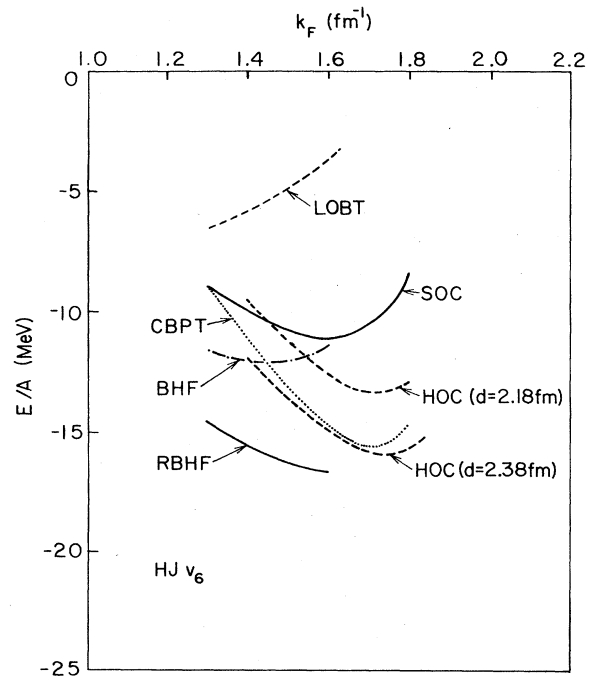
Model	Reid $v_6$	BJ-II $v_6$	HJ $v_6$	GT-5200
$d/r_0$	2.25	2.25	2.35	2.42
$\beta_{i=2,4}$	0.4	0.6	0.5	0.75
$\beta_{i=5,6}$	1.0	1.1	1.0	1.0
$T_F$	21.03	21.03	21.03	21.03
2-body	-42.28	-37.55	-37.04	-50.28
$W_0(\text{MB})$	-0.21	-3.96	-0.15	1.77
$W_c$	2.79	4.01	2.31	3.43
$W_s$	6.44	11.71	5.19	6.83
$W_{cs}$	-0.42	-0.87	-0.35	-0.66
$W_F(\text{MB}) + U_F$	0.26	-0.17	0.23	0.69
$U$	-0.59	-0.76	-0.23	-0.32
$E$	-12.98	-6.56	-9.01	-17.51

caution because the calculated energies do not exhibit a minimum with respect to variations in the correlation range  $d$ . The CBPT calculations also have this problem to some extent at high  $\rho$ . The HOC energies are quite sensitive to  $d$  (Fig. 25) and thus very uncertain. The present HOC calculations neglect all commutator terms, including those of the separable type. The  $W_s$  is quite large, and hopefully the HOC calculations will exhibit minima when the separable and other commutator terms are included. It was noted by Wiringa and Pandharipande (1978) that the variational energies in the FHNC/SOC scheme decrease rapidly with  $d$ , without exhibiting a minimum when the commutator terms are neglected.

FIG. 23. The  $E(k_F)$  for nuclear matter in the Reid  $v_6$  model in various calculations, as described in Table X.FIG. 24. The  $E(k_F)$  for nuclear matter with the Gammel-Thaler 5200 potential in various calculations, as described in Table X.

### C. Convergence of FHNC/SOC calculations

There are two major approximations involved in the FHNC/SOC summations. First is the assumption that the major contribution of passive noncentral correla-

FIG. 25. The  $E(k_F)$  for nuclear matter in the Hamada-Johnston  $v_6$  model in various calculations, as described in Table X.



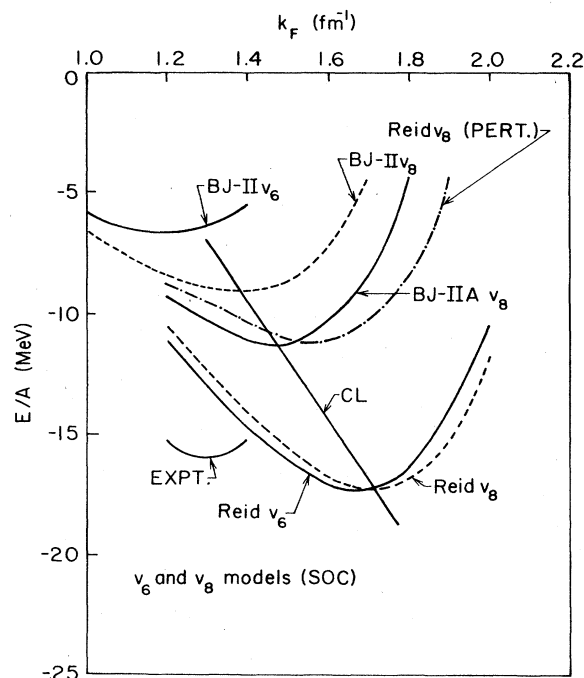


FIG. 26. The  $E(k_F)$  for nuclear matter in Reid models  $v_6$  and  $v_8$ , Bethe-Johnson II (BJ-II) models  $v_6$  and  $v_8$ , and BJ-IIA model  $v_8$ , calculated in the SOC approach, and Reid model  $v_8$  calculated with a simple perturbation method (PERT). The solid line CL denotes the "Coester line" passing through the equilibrium points of the phase-equivalent  $v_8$  models. The curve labeled EXPT has a compressibility of 250 MeV and the empirical equilibrium point.

tions can be taken into account with single-operator chains. Second is that separable diagrams having many operator rings at a common articulation point are smaller than those having only two. These two approximations have been recently studied by Wiringa (1979)

by calculating the leading corrections. The corrections are found to be quite small ( $\sim 1/10$ ) compared to the leading terms. Moreover they tend to cancel out, and the net change in the energy-density curve of the Reid and BJ-II  $v_6$  models is negligible.

The SOC approximation may be tested by looking at corrections to  $W_c$  (diagram 19.2), which gives the contribution of diagrams with one SOC. The bulk of  $W_c$  comes from the  $G_{de}^p$  chain, whose leading contributor is the three-body diagram 27.1 of Fig. 27 we have discussed so often. The importance of this diagram was also stressed by Brueckner (1976), who finds that it represents the bulk of Pauli exclusion effects in variational theory. At  $k_F = 1.6 \text{ fm}^{-1}$  it gives a total contribution of  $\sim 9.5 \text{ MeV}$ , where the total  $W_c$  is  $\sim 6.5 \text{ MeV}$ . The leading multiple-operator correction to diagram 27.1 is 27.2, which is found to be  $\sim -1/7$  of 27.1 over a wide density range. The other possible corrections, such as diagram 27.3, should be even smaller. For example, in going from 27.1 to 27.2 an  $f_{m1}^c$  is replaced by  $2f_{m1}^{c\phi_1}$ , while the  $2f_m^c$  in diagram 27.1 goes to  $f_m^{c\phi_1}$  in 27.3.

Terms with more than one SOC have also been examined. The diagram 27.4 with two  $G_{de}$  chains is typically much less than  $1/20$ th of the  $W_c$ , which is understandable since the  $G^p$ 's are  $< 0.1$  (Fig. 17).

All once-separable diagrams having passive SOR, plus some twice- and more-separable diagrams like 19.6, are included in the basic FHNC/SOC calculation, in an exact self-consistent manner. Diagrams like 19.7 are approximated and those like 19.8 are neglected. The diagrams 19.7 and 19.8 are now calculated; the results are given in Table XI. The total  $W_0$  is  $-64.4 \text{ MeV}$  at the parameters in Table XI. But the part of the  $W_0$  (diagram 19.1) having  $(f^c H^c f^c)_{mn}$  does not contribute to separable diagrams. The first line of Table XI gives the operator ring parts of  $W_0$  which can form separable diagrams. It is clear that the addition of a separable ring reduces the diagram by  $\sim 0.1$ . The consistent solution of SOC equations sums many important diagrams,

TABLE X. Index to calculations shown in Figs. 23–26.

LOBT:	Lowest-order Brueckner theory; two-body cluster calculation with standard choice [ $U(k > k_F) = 0$ ] of spectrum; Day (1978b); Lejeune and Mahaux (1979).
BBG:	Brueckner-Bethe-Goldstone; two-, three-, and estimates of four-body cluster contributions with standard choice of spectrum; Day (1978b).
BHF:	Brueckner-Hartree-Fock; two-body cluster contribution with continuous choice [ $U(k > k_F) \neq 0$ ] of spectrum; Lejeune and Mahaux (1979).
RBHF:	Renormalized Brueckner-Hartree-Fock; two- and parts of four-body clusters with continuous choice of spectrum; Lejeune and Mahaux (1979).
CBPT:	Correlated basis perturbation theory; two- and three-body contributions to variational energy expectation value plus two-body second-order perturbation correction; Kürten, Ristig, and Clark (1979).
SOC:	Single-operator chain (with commutators): Variational energy for symmetrized product wave function calculated with FHNC/SOC method; Lagaris, Pandharipande, and Wiringa (1978).
HOC:	Hypernetted operator chain (without commutators): Variational energy for symmetrized product wave function with a fixed correlation range calculated with HOC method; Benhar, Ciofi degli Atti, Fantoni, and Rosati (1978).
IP:	Independent pair; variational energy calculation with independent-pair wave function; includes hypernetted operator chain and commutator contributions; Owen (1979).

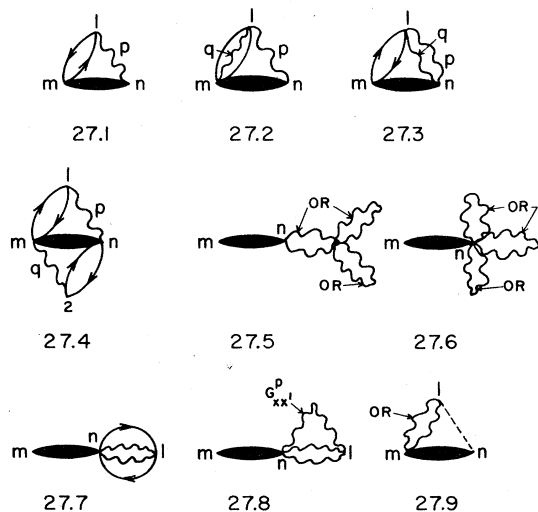


FIG. 27. Diagrams illustrating the leading corrections to the basic FHNC/SOC calculation.

such as 19.6 and 19.7. The remaining diagram 19.8 is  $\sim -1/10$  of 19.3. The vertex correction in 19.8 must be iterated self-consistently to sum diagrams of type 27.5. The net correction from these diagrams is 10% ( $\sim -1.5$  MeV at  $k_f = 1.65 \text{ fm}^{-1}$ ) to the total  $W_s$ . These solutions still do not sum diagrams like 27.6, which would give  $\sim 1\%$  of  $W_s$ .

The basic equations also neglect separable diagrams of the type 27.7, 27.8, which have passive multiple operator rings. Of these, 27.7 could be significant, while the rest should be much smaller than 27.7. The vertex correction in diagram 27.7 is the largest correction to the basic FHNC/SOC calculation. It increases the  $W_s$  by  $\sim 15\%$  ( $\sim +2.5$  MeV at  $k_f = 1.65 \text{ fm}^{-1}$ ). Curiously enough this repulsive correction just about cancels the attractive contributions of diagrams 27.2 and 19.7.

Diagrams of type 27.9 superficially appear to be corrections to the large separable diagrams in  $W_s$ , but in fact they are much smaller. The  $W_s$  is large because of the long range of  $f^{p>1}$ ; however, at large  $r_m$  the  $n1$  link in diagram 27.9 is practically zero. These diagrams are incorrectly treated in the basic scheme as SOR in the central chains  $G_{xx}^c$ , [Eqs. (6.34)–(6.37)]. A modification of the FHNC equations by Wiringa (1979) allows one to sum all central chains with nontouching SOR in the middle, and no SOR at either end. Diagrams like 27.9 can then be added explicitly and exactly. They give a contribution of  $\sim -1$  MeV, which largely compensates the change in  $W_0$  from cleaning up the touching SOR's in the  $G_{xx}^c$ .

TABLE XI. Contribution of separable diagrams  $W_s$  in MeV in Reid  $v_8$  model at  $k_F = 1.65 \text{ fm}^{-1}$ ,  $d = 2.6r_0$ ,  $\beta_0 = \beta_\tau = \beta_{\sigma\tau} = 0.5$  and  $\beta_t = \beta_{t\tau} = 0.95$ .

Description	Diagram No.	Contribution
Irreducible OR		-92.0
Once-separable	19.3	+18.1
Twice-separable	19.6	-1.8
Twice-separable	19.7	-1.2
Twice-separable	19.8	-1.9

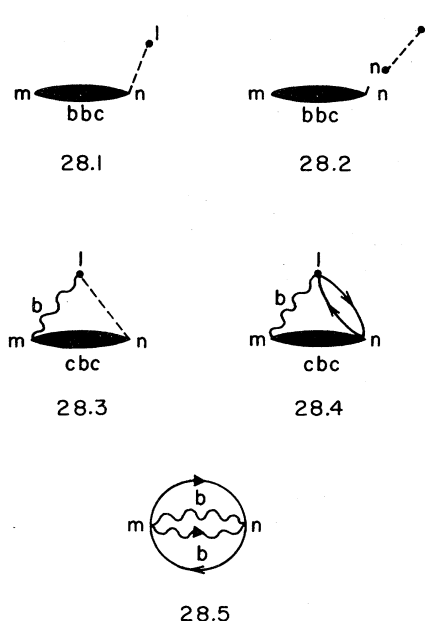


FIG. 28. Diagrams 28.1–28.3 occur only in the  $v_8$  models; they give zero contribution in  $v_6$  models. The leading  $G_{de}^{b(br)}$  and  $BW_F$  terms are shown by diagrams 28.4 and 28.5.

In view of the cancellations among all these higher-order corrections, the energy minima for the Reid and BJ-II  $v_6$  models calculated by the FHNC/SOC prescription are probably accurate within  $\pm 1$  MeV. This cancellation may not persist in other systems or at very high densities. Hence it is advisable to supplement the FHNC/SOC calculation with diagrams of type 19.8, 27.2, 27.7, and 27.9 and the corrected  $G_{xx}^c$  equation.

#### D. The $v_8$ problem

There are two striking differences between the  $v_6$  and the  $v_8$  problems. First, the C parts of a product of  $v_6$  operators is a number or a function of  $\mathbf{r}_i$ , the particle coordinates, but that of a product of  $v_8$  operators is in general an operator because of the  $\nabla$  in the angular momentum operator  $\mathbf{L}$ . So we have a number of new terms; for example the separable diagram 28.1 of Fig. 28 now contributes because the  $\nabla$ 's in  $b_{mn}$  operators (the  $\mathbf{L} \cdot \mathbf{S}$  is denoted by  $b$ ) can operate on the  $f_{m1}$  in the connected diagram 28.1, but not in the separated diagram 28.2. Second, the eight  $v_8$  operators do not form a closed set. Lagaris and Pandharipande (1979) find that the set of operators needed to treat the  $v_8$  problem includes twenty-two operators: 1,  $\sigma$ ,  $\tau$ ,  $\sigma\tau$ ,  $\alpha(\mathbf{A}, \mathbf{B})$ ,  $\alpha(\mathbf{A}, \mathbf{B})\tau$ ,  $\beta(\mathbf{A})$ , and  $\beta(\mathbf{A})\tau$ . Here  $\mathbf{A}$  and  $\mathbf{B}$  are the vector operators  $\mathbf{r}$ ,  $\nabla$ , and  $\mathbf{L}$ ;  $\alpha(\mathbf{A}, \mathbf{B})$  are generalizations of the tensor operator:

$$\alpha(\mathbf{A}, \mathbf{B}) = \frac{3}{2}(\sigma_1 \cdot \mathbf{A} \sigma_2 \cdot \mathbf{B} + \sigma_2 \cdot \mathbf{A} \sigma_1 \cdot \mathbf{B}) - \sigma_1 \cdot \sigma_2 \mathbf{A} \cdot \mathbf{B}; \quad (9.1)$$

and  $\beta(\mathbf{A})$  that of the spin-orbit operator:

$$\beta(\mathbf{A}) = \frac{1}{2}(\sigma_1 + \sigma_2) \cdot \mathbf{A}. \quad (9.2)$$

The vector operators  $\mathbf{A}$  do not commute, but it may be verified that

$$\alpha(\mathbf{A}, \mathbf{B}) = \alpha(\mathbf{B}, \mathbf{A}). \quad (9.3)$$

The  $\alpha$  and  $\beta$  operators retain the useful property

$$\sigma_1 \cdot \sigma_2 \alpha(A, B) = \alpha(A, B) \sigma_1 \cdot \sigma_2 = \alpha(A, B), \quad (9.4)$$

$$\sigma_1 \cdot \sigma_2 \beta(A) = \beta(A) \sigma_1 \cdot \sigma_2 = \beta(A), \quad (9.5)$$

of the tensor and spin-orbit operators.

The spin-orbit interaction cannot be treated as a weak perturbation. The first-order shift

$$\Delta E = \langle \Psi_6 | \Delta H | \Psi_6 \rangle / \langle \Psi_6 | \Psi_6 \rangle, \quad (9.6)$$

where

$$\Delta H = \sum_{i < j} v^b(r_{ij}) O_{ij}^b + v^{b\tau}(r_{ij}) O_{ij}^{b\tau} \quad (9.7)$$

and  $\Psi_6$  is the variational wave function for the ground state of the  $v_6$  model is quite large and positive. The Reid  $v_8$  energies obtained by a first-order perturbation treatment of the spin-orbit interaction are shown in Fig. 26. The  $W$  diagrams containing  $f_{mn}^{t(t\tau)} v_{mn}^{b(b\tau)} f_{mn}^{t(t\tau)}$  give the dominant contribution to  $\Delta E$ .

As shown in Figs. 5 and 6, the spin-orbit forces generate significant spin-orbit correlations and also have an effect on the  $f^{b\leq 6}$ . An interesting quantity is the expectation value of the  $v_6$  Hamiltonian with the  $f^{b\leq 6}$  of the  $v_8$  correlation operator. This quantity, called "E6" in Table XII, can be calculated easily with the FHNC/SOC method. It corresponds to the sum of all energy diagrams of the  $v_8$  model that do not contain the  $v^{b(b\tau)}$  or  $f^{b(b\tau)}$ . The E6 is generally 2–3 MeV higher than the ground-state energy of the  $v_6$  model shown in Fig. 26.

Lagaris and Pandharipande (1979) calculate the  $v_8$  model energies by adding the contribution of selected diagrams having  $v^{b(b\tau)}$  and  $f^{b(b\tau)}$  to E6. These extra contributions are prefixed by a letter  $B$  in Table XII. For example the  $B2$ -body gives the contribution of two-body diagrams having spin-orbit potential and/or correlations. It is negative, since the contribution from terms having  $f^c v^{b(b\tau)} f^{b(b\tau)}$  overcomes the positive contribution of the  $f^{t(t\tau)} v^{b(b\tau)} f^{t(t\tau)}$  terms. It is also much smaller than the two-body contribution contained in E6. The order of magnitudes of the contributions in E6 can be obtained from Tables VII and VIII.

The many-body contributions to  $BW_0$  are calculated with the  $G_{xx}^c$ , and found to be rather small, while  $BW_c$  containing  $G_{xx}^{p=2,6}$  is estimated to be  $< 0.5$  MeV and neg-

lected. Separable diagrams having  $b$  operators in the interacting ring only ( $BIW_s$ ) and the passive ring only ( $BPW_s$ ) are large but tend to cancel. It is necessary to calculate these separable diagrams correctly to obtain a reasonable minimum with respect to variation in  $\beta_{b(b\tau)}$ . The  $BIW_s$  has large negative contributions that are linear in  $\beta_{b(b\tau)}$ . These come from the  $L$  operators in  $v_{mn}^b$  and  $f_{mn}^b$  operating on the  $F_{mi}$ . The  $BPW_s$  is totally quadratic in  $\beta_{b(b\tau)}$  and repulsive.

Unlike the  $O_{ij}^{p=1,6}$ , which are either linear in both  $\sigma_i$  and  $\sigma_j$  or independent of  $\sigma_i$  and  $\sigma_j$ , the  $O_{ij}^{b(b\tau)}$  have two terms, one linear in  $\sigma_i$ , the other in  $\sigma_j$ . Hence operator rings having single  $b(b\tau)$  links do not contribute. The simplest many-body rings containing two  $b(b\tau)$  links are shown in Fig. 28, diagrams 28.3 and 28.4. These give rather small contributions, labeled  $BIC$  in Table XII, indicating that the effect of  $f^{b(b\tau)}$  in chains may not be very important. The diagrams containing derivative  $b(b\tau)$  lines also appear to be small. The two-body  $W_F$  diagram 28.5, which is generally the largest, is itself quite small. In Reid  $v_8$  it is  $-0.23$  MeV at  $k_F = 1.7 \text{ fm}^{-1}$ , while in BJ-II  $v_8$  it is  $-0.17$  MeV at  $k_F = 1.4 \text{ fm}^{-1}$ ; it is included in the  $B2$ -body of Table XII. The many-body  $BW_F$ ,  $BU_F$ , and  $BU$  are neglected. The  $BTOT$  of Table XII gives the estimated contribution of all diagrams containing  $v^{b(b\tau)}$  and/or  $f^{b(b\tau)}$ , and  $E(v_8)$  gives the total energy.

The  $E(k_F)$  of Reid  $v_6$  and  $v_8$  models is quite similar; however, this is due to chance cancellations. The intrinsic effect of the  $L \cdot S$  correlations is better described by the difference between Reid  $v_8$  (perturbation method) and  $v_8$  (SOC method) curves. The  $L \cdot S$  potentials are much stronger in the BJ-II model ( $\sim$  three times those in the Reid model), and they have a more visible effect on the BJ-II  $E(k_F)$ .

Earlier estimates (Wiringa and Pandharipande, 1979) of the effect of  $L \cdot S$  potentials on the  $E(k_F)$  were much too large, mostly because the repulsive  $BPW_s$  diagrams were not calculated in these calculations. We note that in the present density range ( $k_F < 2.5 \text{ fm}^{-1}$ ) the  $v_8$  variational calculations do not exhibit instability towards collapse as predicted by Calogero and Simonov (1970) at very high densities.

We have also shown in Fig. 26 the  $E(k_F)$  of a BJ-IIA  $v_8$  model calculated similarly. The interaction in the  $TS = 10, 11$ , and  $00$  states of this model is the same as that in BJ-II, but it has the  $^3S_1 - ^3D_1$  potential "5.595" in the  $TS = 01$  states, where BJ-II uses the potential "6.55." The BJ  $^3S_1 - ^3D_1$  potentials are labeled by the percentage of  $D$  state in the deuteron. Thus the BJ-IIA has a slightly weaker tensor potential and it gives a little more binding.

## X. OUTLOOK

The three  $v_8$  models (Reid, BJ-II, and BJ-IIA) are phase equivalent; they all fit the  $^1S_0$ ,  $^3S_1 - ^3D_1$ ,  $^1P_1$ , and  $^3P_2 - ^3F_2$  phase shifts. The equilibrium points predicted by these models form a "Coester line" shown in Fig. 26. It misses the empirical point by a significant margin. This clearly indicates deficiencies in the considered model Hamiltonians for nuclear matter and/or the many-body calculation. We first discuss possible improvements in the many-body theory; much of the

TABLE XII. Contributions to the energy of Reid and BJ-II  $v_8$  models.

	Reid	BJ-II
$k_F(\text{fm}^{-1})$	1.7	1.4
$\beta_0 = \beta_\tau = \beta_{0\tau}$	0.83	0.9
$\beta_t = \beta_{t\tau}$	1.1	1.1
$\beta_b = \beta_{b\tau}$	0.65	0.7
E6 (MeV)	-14.09	-3.79
B2-Body	-3.11	-4.82
$BW_0$ (MB)	0.23	-0.03
$BIW_s$	-2.98	-3.51
$BPW_s$	+2.44	+3.05
$BIC$	+0.32	+0.14
$BTOT$	-3.09	-5.17
$E(v_8)$	-17.18	-8.95

work reviewed here is meant to eliminate the uncertainties in the many-body calculation. The discussion of errors in the preceding section suggests that we can currently calculate the equilibrium energy of Reid type models with a  $\sim 2$  MeV accuracy, and the equilibrium  $k_F$  within  $\sim .2 \text{ fm}^{-1}$ .

### A. Variational method

In the past few years significant advances were made in the variational theory of helium liquids to remove inherent restrictions in the variational wave function  $\Psi_v$ . Euler–Langrange equations were developed, by minimizing the energy expectation value, to find the optimized  $f_J$  without any external constraints such as the range  $d$  (Lantto and Siemens, 1977). Much of this work has been reviewed recently by Ripka (1979), and it could be possible to extend it and obtain Euler–Langrange equations for the  $f^p$  of the correlation operator. These would eliminate the need for external parameters such as  $d$  and  $\beta_p$ . The leading part of the momentum dependence of the  $F$  operator, and a three-body correlation, were included in the variational wave function by Schmidt and Pandharipande (1979a), thus eliminating other restrictions in the traditional  $\Psi_J$ . It would be quite possible to calculate nuclear matter energy with momentum-dependent correlations, which are in fact no more difficult than the spin-orbit correlations. It would also be possible to include a simple  $f_3(\mathbf{r}_i, \mathbf{r}_j, \mathbf{r}_k)$  in the  $\Psi_v$ . However, comparison of the energies obtained for the  $v_6$  models with the IP and SP wave functions suggests that we examine the effects of three-body spin-dependent correlations in nuclear matter. This comparison could be premature at present, for other differences such as those in  $\beta_p$  and the kinetic energy prescriptions also contribute to the difference between the available SP and IP energies. Nevertheless, the  $\Psi_{SP}$  contains three-particle correlations of the type  $f^p(r_{ij})f^q(r_{ik})\{O_{ij}^p, O_{ik}^q\}$  absent in  $\Psi_{IP}$ . This extra correlation appears to increase the energy at small  $\rho$ . The results displayed in Fig. 23 definitely indicate that the  $\Psi_{SP}$  energies are too high by  $\sim 2$  MeV in the Reid  $v_6$  model at  $k_F = 1.4 \text{ fm}^{-1}$ . If the  $\Psi_{IP}$  energies continue to remain above the  $\Psi_{SP}$  energies at high  $\rho$ , even after varying  $\beta_p$  and kinetic energy prescriptions, then we have a more complex problem.

In studies of helium liquids it was necessary to improve upon the calculation of the energy expectation value when more general  $\Psi_v$  were introduced. The PB kinetic energy prescription, which works quite well with the short-ranged  $f_J(d, r)$ ,  $d \sim 2r_0$ , can give arbitrarily low energies when more general  $f_J$  allowed. So most calculations use the JF kinetic energy prescription when optimum  $f_J$  are used. However, the JF energy is too high in the HNC approximation, and it converges rather slowly. Smith *et al.* (1978) had to calculate diagrams up to HNC/6 to obtain reasonable energies for liquid  $^4\text{He}$  with the optimum  $f_J$ . Schmidt and Pandharipande (1979b) find it convenient to generalize the HNC scheme to three point functions which represent contributions of hypernetted cloth (rather than chain) with three ends. Such generalizations were considered in

statistical mechanics by Wertheim (1967), and may be used to calculate leading HNC/5, 6... diagrams by integral equations.

The energy of nuclear matter is much more difficult to calculate because of the spin operators. The FHNC/SOC method may be useful only when  $f^{p>1}$  and  $G^{p>1}$  are  $\ll 1$ . The  $\Psi_{IP}$  offers many advantages in this respect. It will probably be necessary to incorporate the commutator terms in Fantoni and Rosati's HOC equations if it becomes necessary to calculate the energies with  $\Psi_{SP}$ 's containing stronger  $f^{p>1}$ . The most accurate energy evaluations are done with the Monte Carlo method. Development of techniques to perform Monte Carlo simulations of spin-isospin correlated nuclear matter on computers will significantly reduce the uncertainties in the many-body calculation. Further, it should be much simpler to treat finite nuclei with the Monte Carlo method. The chain summation techniques become much more complex in a finite system (Fantoni and Rosati, 1979).

### B. Brueckner–Bethe–Goldstone expansion

The results of BBG calculations stress the need to go beyond two-body cluster contributions to obtain a reasonable  $E(\rho)$  in the region of equilibrium density. Rajaraman and Bethe's (1967) work indicated that the three-hole line graphs that correspond to bubble insertions in particle line, three-body rings, and three-body ladders have contributions of order  $\kappa W_2$ , and Day's (1978a) results for Reid  $v_6$  models, summarized in Table XIII, confirm this. We note that in all  $v_6$  models  $\kappa > 0.25$  at equilibrium density (Lejeune and Mahaux, 1978), and  $\kappa W_2$  is of the order of 10 MeV.

All lowest-order calculations, LOBT, BHF, or RBHF, can have errors of order  $\kappa W$ . Their inadequacy can be most clearly seen in the results obtained for the  $v_1$  model of nuclear matter and summarized in Table XIV. The  $v_1$  model has only a central interaction, and has been studied by Zabolitzky (1976) with a Jastrow wave function, and by Lagaris (1979) with a symmetrized product wave function. The backflow has little effect, and the Jastrow wave function is a very good approximation in this model.

Grange and Lejeune (1979) have studied the  $v_1$  model with the standard  $[U(k > k_F) = 0]$  and continuous  $[U(k > k_F) \neq 0]$  choices of particle spectrum. In this simple model it is seen that the LOBT energies are too high, BHF energies are low, and RBHF much too low. At the (two + three)-body level the  $U(k > k_F) = 0$  and  $U(k > k_F) \neq 0$  energies become rather similar and are only  $\sim 5\%$  above the variational results.

Detailed calculations of the four-body cluster contri-

TABLE XIII. The details of three-hole line contributions in BBG theory with Reid  $v_6$  potential.

$k_F$	Bubble in particle line	Three-body ring	Three-body ladder	Hole-hole
1.4	+3.3	-5.7	-4.0	-0.4
1.6	+9.5	-10.9	-8.5	-0.6
1.8	+22.2	-18.6	-17.1	-0.9

TABLE XIV. Nuclear matter model  $v_1$ .

Method	$U(k > k_F)$	$k_F = 1.6 \text{ fm}^{-1}$	$k_F = 1.8 \text{ fm}^{-1}$
Brueckner theory $E(k_F)$ in MeV.			
LOBT (2-body)	0	-83.6	-120.3
BHF (2-body)	$\neq 0$	-108.4	-164.1
RBHF (2 + parts of 4)-body	$\neq 0$	-115.2	-180.1
(2 + 3)-body	0	-88.6	-127.4
(2 + 3)-body	$\neq 0$	-89.3	-133.5
(2 + 3 + estimate of 4)-body	0	-89.1	-128.7
(2 + 3 + estimate of 4)-body	$\neq 0$	-96.9	-137.0
Brueckner theory $\kappa_2$			
LOBT	0	0.06	0.07
BHF	$\neq 0$	0.22	0.28
Variational $E(k_F)$			
Jastrow FHNC		-95.1	-141.2
(Symmetrized product FHNC/SOC)		-96.9	-143.1

bution are not yet available. Their estimates, however, seem to be rather different for the two choices. The present results indicate that the  $U(k > k_F) = 0$  energies converge rather rapidly to a value higher than the variational result, while  $U(k > k_F) \neq 0$  energies have a poorer convergence, but they may converge to the variational result. The general trend of cluster contributions with the  $U(k > k_F) \neq 0$  choice is quite similar to that in variational calculations; the two-body is too low, the (two+three)-body too high, and the four-body substantially attractive.

The two-body contribution  $\kappa_2$  to the  $\kappa$  is quite different with the two choices, indicating that many-body cluster contributions to  $\kappa$  are significant in either or both choices of  $U(k > k_F)$ . The possibility of the energy calculated with Brueckner-Bethe-Goldstone theory being dependent on choice of  $U(k > k_F)$  was discussed earlier by Baker and co-workers (see Baker, 1978, and references therein). Arguments in favor of a continuous choice for the  $U(k)$  have been recently discussed by Lejeune and Mahaux (1978). The  $U(k)$  in the  $v_1$  model can be very large ( $> 100$  MeV), and thus it is suitable for such studies. Accurate calculations of the four-body cluster contributions of the  $v_1$  model would be very interesting.

### C. The nuclear Hamiltonian

Of the three  $v_8$  models, BJ-II is probably the most promising. In the FHNC/SOC approximation it gives equilibrium  $k_F = 1.4 \text{ fm}^{-1}$  against the empirical  $1.3 \text{ fm}^{-1}$ . However, from Fig. 23 it appears that the FHNC/SOC calculation may overestimate the equilibrium  $k_F$ ; thus it is possible that BJ-II  $v_8$  gives the experimental density. It, however, underestimates the binding by more than 5 MeV. The BJ-IIA has a weaker tensor force, giving a 5.5%  $D$  state in the deuteron, while BJ-II gives 6.5%. The BJ-IIA gives more binding, but the  $\rho_0$  is already too high. The Reid  $v_8$  and BJ-II  $v_8$  have similar tensor forces, but the  $L \cdot S$  potential and the core in the  $T, S = 1, 1$  state in Reid are both weaker than in BJ-II. The Reid  $v_8$  gives more than enough binding but too high density.

It is well known that the interaction in the  $^1D_2$  state is

not as attractive as that in the  $^1S_0$  state. This difference indicates the presence of quadratic spin-orbit or just plain repulsive  $L^2$  terms in the nuclear Hamiltonian. The  $v_8$  models are not very realistic, and a study of  $v_{10}$  models which include  $L^2$  terms is necessary.

A significant part of the attraction between nucleons comes from the coupling of the  $N$ - $N$  channel to  $N$ - $\Delta$  and  $\Delta$ - $\Delta$  channels in two-pion exchange processes, much as the  $r^{-6}$  attraction in the interatomic Lennard-Jones potentials comes from the coupling to  $1^-$  dipole states in two-photon exchange processes. However, the  $N$ - $\Delta$  mass difference ( $\sim 300$  MeV) is not enormous compared to typical energies ( $\sim 50$  MeV) involved in nuclear matter, and it has been suggested that the  $N$ - $\Delta$  and  $\Delta$ - $\Delta$  channels must be treated explicitly in nuclear matter. The coupling is produced by the four operators  $(\sigma_1 \cdot S_{t,2})(\tau_1 \cdot T_{t,2})$ ,  $S_{12}^I(\tau_1 \cdot T_{t,2})$ ,  $(S_{t,1} \cdot S_{t,2})(T_{t,1} \cdot T_{t,2})$ , and  $S_{12}^{II}(T_{t,1} \cdot T_{t,2})$  in the nuclear Hamiltonian. The  $S_t, T_t$  are transition spins and isospins that convert nucleons into  $\Delta$ 's, and  $S_{12}^I$  and  $S_{12}^{II}$  are tensor operators that contain transition spins  $S_t$  (see the review by Green 1976). Nucleon-nucleon phase shifts in the  $S$  and  $P$  states can be fitted by static potentials containing twelve operators, eight of the  $v_8$  model and the above four (Smith and Pandharipande, 1976). Probably two more quadratic  $L^2$  terms are needed to obtain reasonable phases in the  $D$  waves.

The  $N$ - $\Delta$  and  $\Delta$ - $\Delta$  components in the nuclear matter wave function can be produced via correlation operators containing transition spin and isospin. An explicit treatment of these channels is expected to reduce both the equilibrium density and binding energy of nuclear matter. In LOBT the equilibrium  $\rho_0$  and  $E_0$  with the Reid potential are found to be  $\approx 0.2 \text{ fm}^{-3}$  and  $-11.6$  MeV, and these reduce to  $\approx 0.14 \text{ fm}^{-3}$  and  $-7.9$  MeV if the  $N$ - $\Delta$  channel in the  $^1S_0$  interaction is treated in the LOBT approximation (Day and Coester, 1976). This effect has also been studied by lowest-order constrained-variational (LOCV) methods (Howes *et al.*, 1978; Modares and Irvine, 1979). In this approximation the equilibrium with Reid potential occurs at  $\approx 0.29 \text{ fm}^{-3}$  and  $-23$  MeV, and it shifts to  $\approx 0.25 \text{ fm}^{-3}$  and  $-16$  MeV when the  $N$ - $\Delta$  channel in the  $^1S_0$  interaction is treated explicitly. So it appears that to be reasonably realistic

we may have to consider a  $v_{14}$  problem in which the interaction is a sum of 14 operators.

A complete variational calculation with the transition spin operators  $S_t$  and  $T_t$  in the Hamiltonian and the correlation operator will include a variety of chain and separable diagrams formed with "transition" correlations. The algebra of transition spin operators is quite similar to that of Pauli spins. We have the basic relations:

$$T_t^\dagger \cdot T_t = 2 \quad (10.1)$$

$$T_t^\dagger \times T_t = -\frac{2}{3} i \tau \quad (10.2)$$

$$(T_t^\dagger \cdot A)(T_t \cdot B) = \frac{2}{3} A \cdot B - \frac{1}{3} i \tau \cdot (A \times B) \quad (10.3)$$

which are also valid for  $S_t$ . The  $C$  parts of products of transition spin operators can be calculated easily.

The three-body force illustrated by the Feynman diagram 29.1 of Fig. 29 is often included in nuclear matter. Contributions of this force will form a part of the SOR diagrams of type 29.2, and they are attractive. However, the presently available results suggest that the repulsive contributions from diagrams such as 29.3 and 29.4 may be dominant. For example, the contribution of the three-body force, in units of MeV and fm, is estimated to be  $\sim -0.34 k_F^{5/6}$ , while that of the dispersion and Pauli correction due to transition potentials is estimated from the LOBT (and LOCV) calculations to be  $\sim +0.7 k_F^{5/9}$  (Niskanen, 1977).

The  $N$ - $N$  interaction in high partial waves is relatively unknown, but it seems to have a significant influence on the equilibrium density. In Day's calculations the leading contribution of the interaction in  $l \geq 3$  states is via the three-hole line cluster energy. It is  $-5.3$  MeV at  $k_F = 1.8 \text{ fm}^{-1}$  in the Reid  $v_6$  model, and can influence the  $\rho_0$  by 20–30%. These states are relatively unimportant in determining the two-body cluster energy because of the small momenta of hole states. Thus a reasonable treatment of the interaction in  $l \geq 3$

states seems necessary to calculate the many-body cluster contributions. The  $N$ - $N$  scattering data are very inadequate for determining the potential in high partial waves. There have been substantial improvements in our understanding of the  $N$ - $N$  interaction from the meson exchange point of view (Brown and Jackson, 1976) which may be useful in choosing the potential in  $l \geq 3$  states. The recent meson-theoretic potentials are strongly momentum dependent, and Maxwell and Smith (1979) have attempted to extend the variational method to treat them.

In the search for a better nuclear Hamiltonian we may also take into account some of the failures of the Reid and HJ models in very light nuclei. For example, the  $d(\gamma, p)$  measurements of Hughes *et al.* (1976) and calculations of Arenhovel and Fabian (1977) indicate that the  $D$ -state percentage  $P_D$  in the deuteron should be  $\sim 4\%$  instead of the 5.5%–7% in the Reid and BJ models.

Recent measurements of the charge form factors of  $^3\text{He}$  and  $^4\text{He}$  nuclei (Arnold *et al.*, 1978) suggest that the point proton densities  $\rho_p$  in these nuclei have a substantial hole. In  $^3\text{He}$ , for example, the estimated  $\rho_p$  is  $\sim 0.08 \text{ fm}^{-3}$  at the center, and it rises to a maximum of  $\sim 0.13 \text{ fm}^{-3}$  at 0.7 fm away from center (Sick, 1978). The  $\rho_p$  obtained for  $^3\text{He}$  by Faddeev calculations with the Reid model, however, peaks at  $\sim 0.13 \text{ fm}^{-3}$  at the center and falls off monotonically.

Thus we must conclude that a suitable nuclear Hamiltonian has not yet been found. The many-body theory for nuclear matter (as well as other strongly interacting quantum systems) has made considerable progress in recent years, and we hope that it will prove to be useful in the search for the nuclear Hamiltonian.

## ACKNOWLEDGMENTS

The authors wish to thank O. Benhar, H. A. Bethe, J. W. Clark, B. D. Day, S. Fantoni, I. E. Lagaris, L. J. Lantto, C. Mahaux, J. C. Owen, G. Ripka, K. E. Schmidt, P. J. Siemens, and R. Smith for clarifying discussions. A number of new results included in this review were communicated to the authors at the Trieste (October 1978) meeting, and special thanks are due to the organizers: C. Ciofi degli Atti, A. Kallio, and S. Rosati. Parts of this review were prepared for the Nordic workshop in Copenhagen (May 1978), and it is a pleasure to thank its organizer, G. E. Brown. We also wish to thank D. Hunter for suggesting the title, and the medium energy physics division of the Los Alamos Scientific Laboratory for partial support.

## REFERENCES

- Arenhovel, H., and W. Fabian, 1977, Nucl. Phys. A **282**, 397.
- Arnold, R. G., B. T. Chertok, S. Rock, W. Schutz, Z. M. Szalata, D. Day, J. S. McCarthy, F. Martin, B. A. Mecking, I. Sick, and G. Tamas, 1978, Phys. Rev. Lett. **40**, 1429.
- Baker, G., 1978, Phys. Rev. C **17**, 1253.
- Bäckman, S.-O., J. W. Clark, W. J. Ter Louw, D. A. Chakalakal, and M. L. Ristig, 1972, Phys. Lett. B **41**, 247.
- Bäckman, S.-O., O. Sjöberg, and A. D. Jackson, 1979, preprint.
- Benhar, O., C. Ciofi degli Atti, S. Fantoni, and S. Rosati, 1977, Phys. Lett. B **70**, 1.
- Benhar, O., C. Ciofi degli Atti, S. Fantoni, and S. Rosati, 1978, to be published in Nucl. Phys.

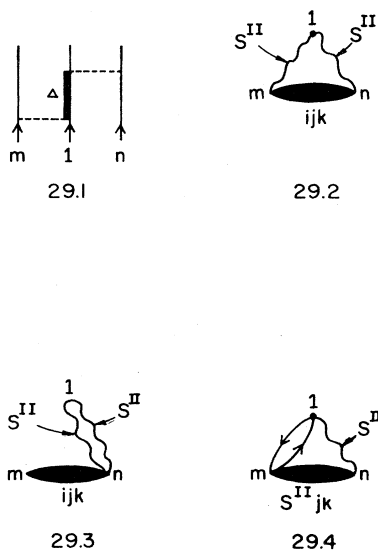
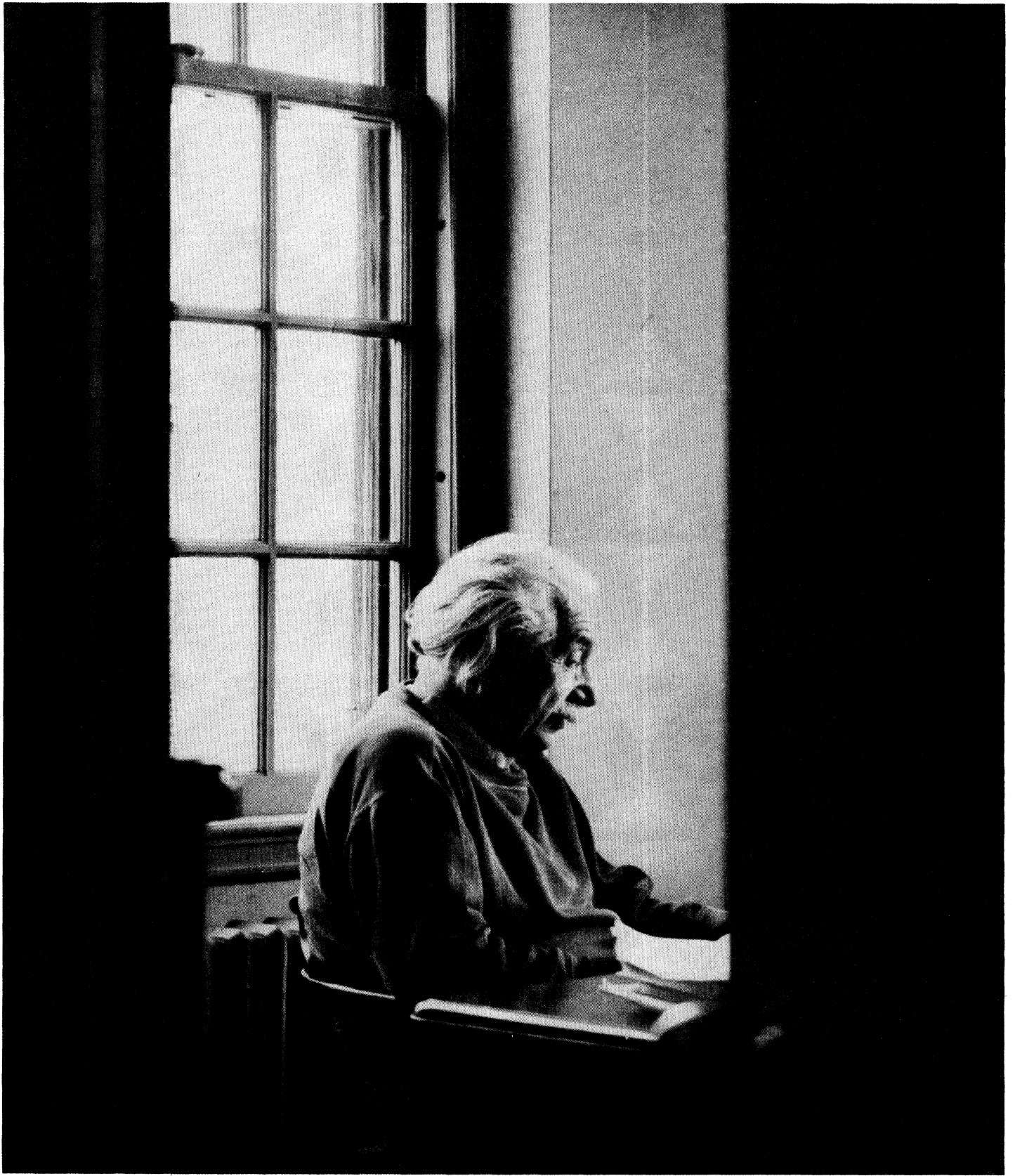


FIG. 29. The Feynman diagram 29.1 generates a "three-body" force between nucleons. The cluster expansion diagrams 29.2–29.4 illustrate various new terms generated by the transition potentials and correlations.

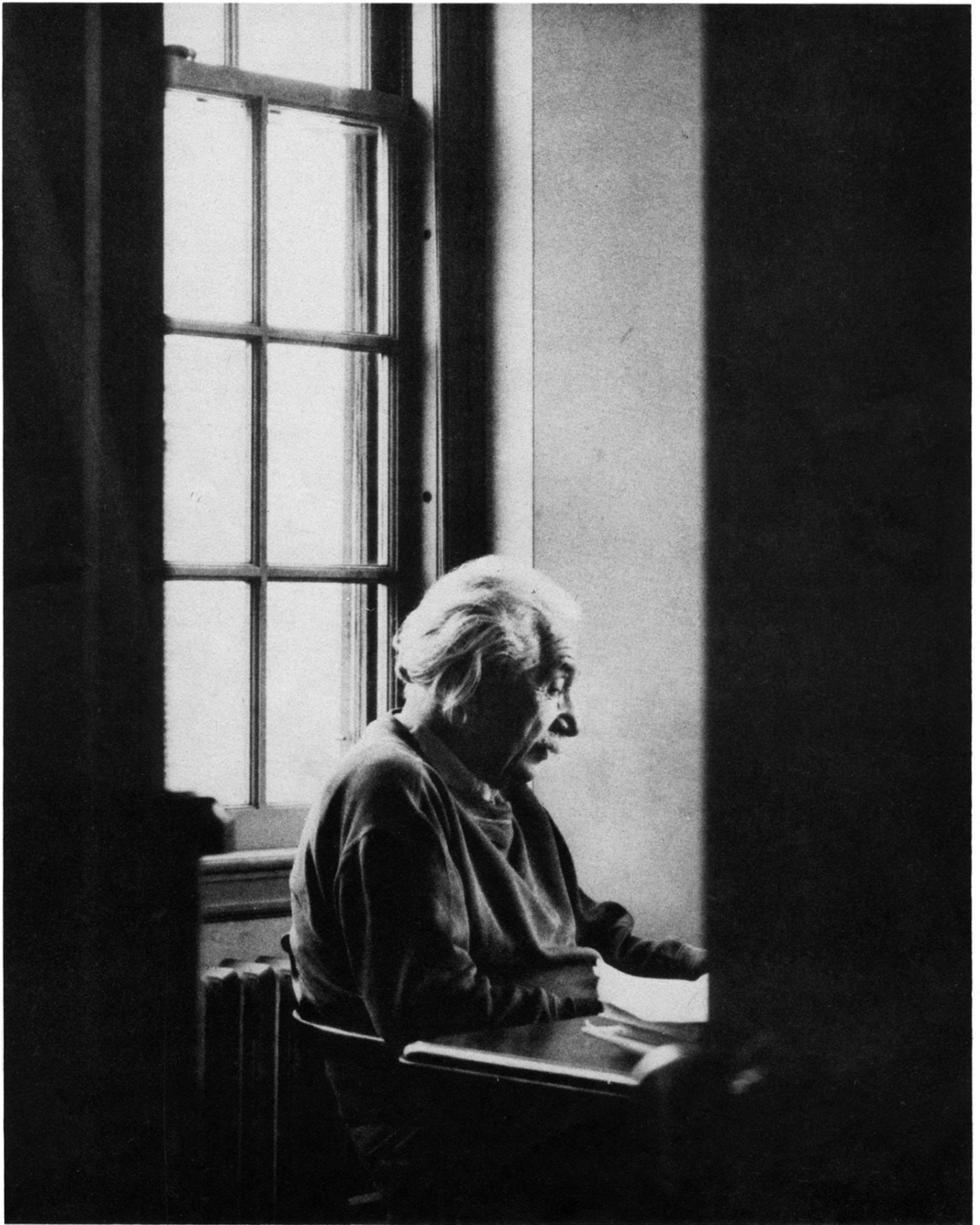
- Bethe, H. A., 1956, Phys. Rev. **103**, 1353.
- Bethe, H. A., 1971, Annu. Rev. Nucl. Sci. **21**, 93.
- Bethe, H. A., 1977, invited talk at Workshop on Nuclear and Dense Matter, Urbana, unpublished.
- Bethe, H. A., and R. F. Bacher, 1936, Rev. Mod. Phys. **8**, 82.
- Bethe, H. A., and M. B. Johnson, 1974, Nucl. Phys. A **230**, 1.
- Blaizot, J. P., D. Cogny, and B. Grammaticos, 1976, Nucl. Phys. A **265**, 315.
- Brandow, B. H., 1966, Phys. Rev. **152**, 863.
- Brown, G. E., 1971, Rev. Mod. Phys. **43**, 1.
- Brown, G. E., and A. D. Jackson, 1976, *The Nucleon-Nucleon Interaction* (North-Holland, Amsterdam).
- Brueckner, K. A., 1954, Phys. Rev. **96**, 908.
- Brueckner, K. A., 1976, Phys. Rev. C **14**, 1999.
- Brueckner, K. A., and C. A. Levinson, 1955, Phys. Rev. **97**, 1344.
- Calogero, F., and Yu. A. Simonov, 1970, Phys. Rev. Lett. **25**, 881.
- Ceperley, D. M., G. V. Chester, and M. H. Kalos, 1977, Phys. Rev. B **16**, 3081.
- Ceperley, D. M., and M. H. Kalos, 1978, in *Monte Carlo Methods in Statistical Physics*, edited by K. Binder (Springer, Berlin).
- Chang, C. C., and C. E. Campbell, 1977, Phys. Rev. B **15**, 4238.
- Clark, J. W., 1978, *Progress in Particle and Nuclear Physics*, in press.
- Day, B. D., 1967, Rev. Mod. Phys. **39**, 719.
- Day, B. D., 1978a, Rev. Mod. Phys. **50**, 495.
- Day, B. D., 1978b, invited talk at Conference on Recent Progress in Many-Body Theories, Trieste, to be published in Nucl. Phys.
- Day, B. D., and F. Coester, 1976, Phys. Rev. C **13**, 1720.
- de Boer, J., and A. Michaels, 1938, Physica (Utrecht) **5**, 945.
- Euler, H., 1937, Z. Phys. **105**, 553.
- Fantoni, S., and S. Rosati, 1975, Nuovo Cimento A **25**, 593.
- Fantoni, S., and S. Rosati, 1978, Nuovo Cimento A **43**, 413.
- Fantoni, S., and S. Rosati, 1979, to be published in Nucl. Phys.
- Feenberg, E., 1969, *Theory of Quantum Fluids* (Academic, New York).
- Feynman, R. P., and M. Cohen, 1956, Phys. Rev. **102**, 1189.
- Friman, B. L., and E. M. Nyman, 1978, Nucl. Phys. A **302**, 365.
- Gammel, J. L., and R. M. Thaler, 1960, in *Progress in Elementary Particle and Cosmic Ray Physics*, edited by J. G. Wilson and S. A. Wouthuysen (North-Holland, Amsterdam), Vol. V.
- Gaudin, M., J. Gillespie, and G. Ripka, 1971, Nucl. Phys. A **176**, 237.
- Goldstone, J., 1957, Proc. R. Soc. London, Ser. A **239**, 267.
- Grangé, P., and A. Lejeune, 1979, to be published in Nucl. Phys.
- Green, A. M., 1976, Rep. Prog. Phys. **39**, 1109.
- Hamada, T., and I. D. Johnston, 1962, Nucl. Phys. **34**, 382.
- Howes, C., R. F. Bishop, and J. M. Irvine, 1978, J. Phys. G; Nucl. Phys. **4**, L123.
- Hughes, R. J., A. Zieger, H. Waffler, and B. Ziegler, 1976, Nucl. Phys. A **267**, 329.
- Iwanato, F., and M. Yamada, 1957, Prog. Theor. Phys. **18**, 543.
- Jastrow, R., 1955, Phys. Rev. **98**, 1479.
- Jeukenne, J.-P., A. Lejeune, and C. Mahaux, 1975, Nucl. Phys. A **245**, 411.
- Kalos, M. H., 1970, Phys. Rev. A **2**, 250.
- Kalos, M. H., 1977, invited talk at Workshop on Nuclear and Dense Matter, Urbana, unpublished.
- Kalos, M. H., D. Levesque, and L. Verlet, 1974, Phys. Rev. A **9**, 2178.
- Kurten, K. E., M. L. Ristig, and J. W. Clark, 1978, Phys. Lett. B **74**, 153.
- Kurten, K. E., M. L. Ristig, and J. W. Clark, 1979, Nucl. Phys. A **317**, 87.
- Lagaris, I. E., 1979, private communication.
- Lagaris, I. E., V. R. Pandharipande, and R. B. Wiringa, 1978, to be published in Nucl. Phys.
- Lagaris, I. E., and V. R. Pandharipande, 1979, to be published.
- Lanto, L. J., and P. J. Siemens, 1977, Phys. Lett. B **68**, 308.
- Lanto, L. J., and P. J. Siemens, 1979, Nucl. Phys. A **317**, 55.
- Lejeune, A., and C. Mahaux, 1978, Nucl. Phys. A **295**, 189.
- Lejeune, A., and C. Mahaux, 1979, Nucl. Phys. A **317**, 37.
- Maxwell, O., and R. A. Smith, 1979, preprint.
- Moddare, M., and J. M. Irvine, 1979, J. Phys. G; Nucl. Phys. **5**, 511.
- Niskanen, J. A., 1977, Ph.D. Thesis, University of Helsinki, ISBN 951-99140-1-3.
- Owen, J. C., 1978, Phys. Lett. B **77**, 9.
- Owen, J. C., 1979a, Ann. Phys. (New York) **118**, 373.
- Owen, J. C., 1979b, private communication.
- Pandharipande, V. R., 1971, Nucl. Phys. A **174**, 641.
- Pandharipande, V. R., 1972, Nucl. Phys. A **181**, 33.
- Pandharipande, V. R., 1978, Phys. Rev. B **18**, 218.
- Pandharipande, V. R., and H. A. Bethe, 1973, Phys. Rev. C **7**, 1312.
- Pandharipande, V. R., and Naoki Itoh, 1973, Phys. Rev. A **8**, 2564.
- Pandharipande, V. R., and K. E. Schmidt, 1977, Phys. Rev. A **15**, 2488.
- Pandharipande, V. R., and R. B. Wiringa, 1976, Nucl. Phys. A **266**, 269.
- Pandharipande, V. R., R. B. Wiringa, and B. D. Day, 1975, Phys. Lett. B **59**, 205.
- Rajaraman, R., H. A. Bethe, 1967, Rev. Mod. Phys. **39**, 745.
- Reid, R. V., 1968, Ann. Phys. (N.Y.) **50**, 411.
- Ripka, G., 1979, preprint.
- Schmidt, K. E., 1978, private communication.
- Schmidt, K. E., and V. R. Pandharipande, 1978, Nucl. Phys., in press.
- Schmidt, K. E., and V. R. Pandharipande, 1979a, Phys. Rev. B, **19**, 2504.
- Schmidt, K. E., and V. R. Pandharipande, 1979b, private communication.
- Sick, I., 1978, Invited talk, International Conference on Few Body Problems and Nuclear Forces, Graz, unpublished.
- Smith, R. A., and V. R. Pandharipande, 1976, Nucl. Phys. A **256**, 327.
- Smith, R. A., A. Kallio, M. Puoskari, and P. Toropainen, 1978, preprint.
- Speth, J., E. Werner, and W. Wild, 1977, Phys. Rep. **33C**, 129.
- van Kampen, N. G., 1961, Physica (Utrecht) **27**, 783.
- van Leeuwen, J. M. J., J. Groeneveld, and J. de Boer, 1959, Physica (Utrecht) **25**, 792.
- von Weizsacker, C. F., 1935, Z. Phys. **96**, 431.
- Wertheim, M. S., 1967, J. Math. Phys. **8**, 927.
- Wiringa, R. B., 1979, to be published.
- Wiringa, R. B., and V. R. Pandharipande, 1978, Nucl. Phys. A **299**, 1.
- Wiringa, R. B., and V. R. Pandharipande, 1979, Nucl. Phys. A **317**, 1.
- Youngblood, D. H., 1978, Bull. Am. Phys. Soc. **23**, 42.
- Youngblood, D. H., C. M. Rozsa, J. M. Moss, D. R. Brown, and J. D. Bronson, 1977, Phys. Rev. Lett. **39**, 1188.
- Zabolitzky, J. G., 1976, Phys. Lett. B **64**, 233.
- Zabolitzky, J. G., 1977, Phys. Rev. A **16**, 1258.





Photographed by Alfred Eisenstaedt, Life Magazine, Copyright © 1947, Time Inc.





Photographed by Alfred Eisenstaedt, Life Magazine, Copyright © 1947, Time Inc.